UNIVERSITY OF SOUTHAMPTON

FACULTY OF PHYSICAL SCIENCES AND ENGINEERING

Electronics and Computer Science

Study of Surface Discharge Behaviour at the Oil-pressboard Interface

by

Hidayat Zainuddin

Thesis for the degree of Doctor of Philosophy

November 2013

UNIVERSITY OF SOUTHAMPTON

ABSTRACT

FACULTY OF PHYSICAL SCIENCES AND ENGINEERING

ELECTRONICS AND COMPUTER SCIENCE

Doctor of Philosophy

STUDY OF SURFACE DISCHARGE BEHAVIOUR AT THE OIL-PRESSBOARD INTERFACE

by Hidayat Zainuddin

This thesis is concerned with the surface discharge behaviour at the oil-pressboard interface. For large transformers this is classified as a serious failure mode because it can lead to catastrophic failure under normal AC voltage operating conditions. To increase understanding on this failure mode, a surface discharge experiment at the oil-pressboard interface has been conducted on different moisture levels in pressboard by applying a long period of AC voltage stress. The processes in the surface discharge at the oil-pressboard interface until the appearance of a first full discharge have been recognised and correlated with the measured data. The results show that the different moisture levels within the pressboard play an important role on the partial discharge (PD) activity of certain processes. The decreasing trend in the PD data during the surface discharges cannot be treated as a reliable condition monitoring measure of health because it is the key indicator of white marks propagation toward the earth point. The characteristics of full discharge events have been analysed to develop knowledge for condition monitoring of surface discharge at the oil-pressboard interface. Full discharges are corona-like events in which their random occurrences are dominated by accumulated charges on the pressboard surface along the white marks rather than the polarity of applied AC voltage. A 2-D axial symmetry surface discharge model has also been developed using COMSOL Multiphysics, a finite element analysis (FEA) software package. The model considers the pressboard region near the interface (a transition region) as porous, whilst in the bulk region of pressboard as a perfect insulator. The model is developed using continuity equations and coupled with the Poisson's equation to study the problem in terms of charge transport mechanisms and electric field distributions. The thermal conduction equation is included to study the thermal effects of surface discharge activity at the oil-pressboard interface. The behaviour of surface discharge is studied by validating the simulated surface discharge current pulse with the measured current. The simulation results show that a field dependent molecular ionisation mechanism plays an important role in the streamer propagation during the period of the rising front of the current pulse, whilst during the period of decaying tail of the current pulse, the contribution of an electron attachment process is dominant. The modelling results suggest that degradation marks (white and black marks) are due to high energy over long periods of partial discharge events that lead to thermal degradation at the oil-pressboard interface.

Contents

List of Figures

List of Tables

Declaration of Authorship

I, Hidayat Zainuddin, declare that this thesis entitled:

"Study of Surface Discharge Behaviour at the Oil-pressboard Interface"

and the work presented in it are my own and has been generated by me as the result of my own original research. I confirm that:

1. This work was done wholly or mainly while in candidature for a research degree at this University;
2. Where any part of this thesis has previously been submitted for a degree or any other qualification at this University or any other institution, this has been clearly stated;
3. Where I have consulted the published work of others, this is always clearly attributed;
4. Where I have quoted from the work of others, the source is always given. With the exception of such quotations, this thesis is entirely my own work;
5. I have acknowledged all main sources of help;
6. Where the thesis is based on work done by myself jointly with others, I have made clear exactly what was done by others and what I have contributed myself;
7. Parts of this work have been published as detailed in Appendix C.

Signed: ……

Date: ……

Acknowledgements

First and foremost, I would like to express my deepest gratitude to Allah s.w.t for giving me the deen, the iman, the health and strength to finish this thesis successfully. Without His permission, I will not be able to reach this stage. I bare witness that there is no God but Allah and Muhammad is the messenger of Allah.

Secondly, I would like to convey my honest appreciation to my supervisor, Professor Paul Lewin and my former second supervisor Dr. Peter Mark Mitchinson for their valuable suggestions, guidance and encouragement that have substantially helped in my work. It has been a great honor to work with and learn something worthwhile from these amazing people.

Next, I would like to acknowledge the Malaysian Government and Universiti Teknikal Malaysia Melaka (UTeM) for giving me the opportunity to pursue my doctoral study as well as the financial sponsorship. Also, thanks to the Tony Davies High Voltage Laboratory for funding me during the remaining six month period of my study.

A big thank you to all the technical supports provided by the Tony Davies High Voltage Laboratory technical team (Neil Palmer, Mike Smith and Brian Rogers). Their kind assistance had helped me a lot during my years of study.

I am also greatly thankful to my colleagues, Dr. Linh Hoang Truong, Muhamad Safwan Abd. Rahman, Dr. Abdul Rahim Abdullah (UTeM) and others who I could not possibly mention here for meaningful helps, discussions, and opinions while performing the work in this research. Also, a huge thanks to all my friends especially the Malaysian Community in Southampton for the sincere pray, overwhelming helpfulness and enjoyable moments throughout the period of my study.

Exceptional gratitude goes to my beloved wife, Intan Suhana for her unconditional love and prays while patiently standing beside me bearing the hardship together along the journey. To my 3 wonderful children, Alham, Najah and Amni, your smiles and playful actions always brighten my gloomy days. For that, I could not thank you enough for being understanding on those weekends we did not spend the time together. Last but not least, special devotion to my parents, parents-in-law and the rest of my family for their endless affection and prays as well as continuous supports and motivations that inspiring my days until the end of the study.

Symbols and Abbreviations

Symbols

Δ	Molecular ionisation energy (J)
ε_0	Permittivity of vacuum or free space (8.854×10^{-12} F·m^{-1})
ε_r	Relative permittivity of a material
μ	Mobility of charge carrier (m^2·s^{-1}·V^{-1})
ρ	Mass density (kg·m^{-3})
σ	Electric conductivity (S·m^{-1})
τ_a	Electron attachment time constant (s)
a	Molecular separation distance (m)
C_P	Specific heat capacity of a material (J·kg^{-1}·K^{-1})
D	Diffusion coefficient (m^2·s^{-1})
$\vec{D}$	Electric displacement field vector (C·m^{-2})
$\vec{E}$	Electric field vector (V·m^{-1})
EA	Electron attachment rate (mol·m^{-3}·s^{-1})
$f(\lvert\vec{E}\rvert)$	Electric field dependent function
$\vec{F}$	Total flux density vector (mol·m^{-2}·s^{-1})
G	Generation rate term of particles (mol·m^{-3}·s^{-1})
$G(\lvert\vec{E}\rvert)$	Generation rate term of particles that electric field dependent (mol·m^{-3}·s^{-1})
h	Planck's constant (6.626×10^{-34} J·s)
I	Electric Current (A)
I_1	Modified Bessel function of the first kind
$\overrightarrow{J_c}$	Conduction current density vector in a volume (mol·m^{-2}·s^{-1}) or on surface (mol·m^{-1}·s^{-1})
$\overrightarrow{J_d}$	Displacement current density vector (C·m^{-2}·s^{-1})
k	Boltzmann's constant (1.38×10^{-23} J·K^{-1})
k_T	Thermal conductivity of a material (W·m^{-1}·K^{-1})
K_d^0	Zero field dissociation rate constant (s^{-1})
K_d	Dissociation rate constant (s^{-1})
K_r	Recombination rate constant (m^3·mol^{-1}·s^{-1})

m^*	Effective electron mass (kg)
$\hat{n}$	Unit vector normal to the boundary
N	Density of particles in a volume ($mol \cdot m^{-3}$) or on surface ($mol \cdot m^{-2}$)
N_A	Avogadro's number (6.023×10^{23} mol^{-1})
q	Elementary charge (1.6022×10^{-19} C)
Q	Electrical power dissipation in a volume ($W \cdot m^{-3}$) or on surface ($W \cdot m^{-2}$)
R	Recombination rate term of particles ($mol \cdot m^{-3} \cdot s^{-1}$)
t	Time (s)
T	Absolute temperature (K)
$\vec{u}$	Velocity vector of a fluid ($m \cdot s^{-1}$)
v_i	Velocity of each charge carrier ($m \cdot s^{-1}$)
X	Relative mass density

Abbreviations

AC	Alternating current
BS	British Standards
CIGRE	International Council on Large Electric Systems
CIGRE WG	International Council on Large Electric Systems Working Group
CSN	Chain scission number
CTI	Comparative tracking index
DC	Direct current
DGA	Dissolved gas analysis
DP	Depolymerisation
EDL	Electric double layer
EHD	Electro-hydrodynamic
EPRI	Electric Power Research Institute, United States
FEA	Finite element analysis
FFT	Fast Fourier Transform
GSU	Generator step-up (transformer)
HV	High voltage
IEC	International Electrotechnical Commission
IEEE	Institute of Electrical and Electronics Engineers
OLTC	On-Load Tap Charger
PD	Partial discharge
PDIV	Partial discharge inception voltage

PMT	Photomultiplier tube
ppm	Parts per million
PRPD	Phase resolved partial discharge
RFCT	Radio frequency current transformer
RMS	Root mean square

Chapter 1

Introduction

1.1 High Voltage Transformers

Transformers are one of the basic elements of a power system. They are connected to a large number of customers via power transmission and distribution systems. When it comes to reliability, large power transformers are a major concern to any electricity utility. Failures of a power transformer may cause long interruptions of power supply and have extremely high financial impact either due to replacement of unreliable units or major maintenance procedures. A major repair may involve reprocessing under factory conditions [1]. Statistics have shown that a fairly high proportion of transformer failures (up to 50%) are linked to failure of insulation systems [1, 2, 3]. Failures of insulation systems can cause danger to personnel, i.e. can lead to injury and death. Therefore, a lot of research into dielectric breakdown mechanisms of transformer insulation systems has been undertaken in order to reduce the number of catastrophic failures of transformers due to insulation failure.

The insulation system is the heart of a transformer particularly in high voltage (HV) applications. It plays an important role in the reliability of a transformer. With reference to Figure 1.1, the insulation system for a large power transformer is basically a composite of cellulose-based solid insulation and oil which can be categorised into major insulation and minor insulation [2, 4]. The major insulation consists of insulation at the region between different windings, between windings and the core limb/yoke and between leads and ground. For example, a form of pressboard-oil sandwich, i.e. a number of oil ducts created from suitably spaced pressboard barriers between windings.

On the other hand, the minor insulation consists of internal insulation within the windings, i.e. insulation at the inter-turn and inter-disc level.

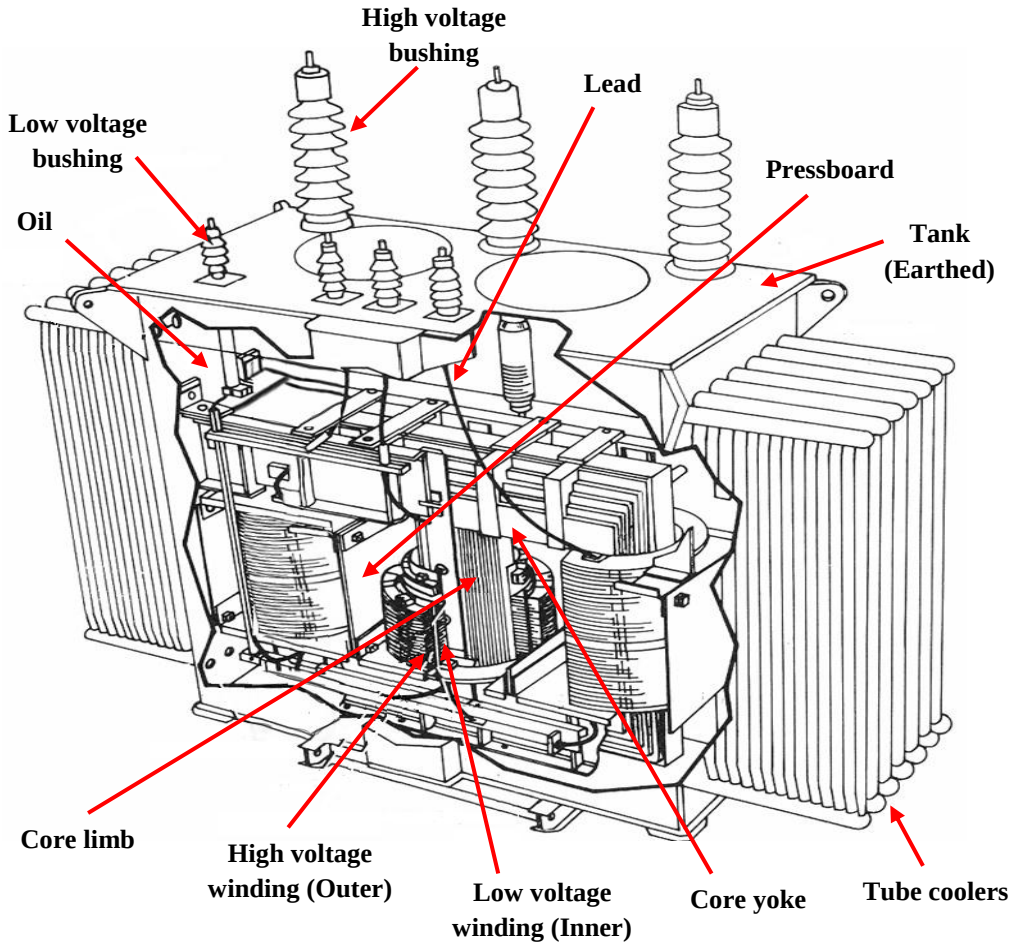

Figure 1.1: Oil-filled power transformer arrangement (amended from [5])

In a large oil-immersed power transformer, the use of cellulose-based pressboard for electrical insulation is required in the gap between phase windings. Pressboard barriers that have higher dielectric strength compared to the mineral oil are important in dealing with the pre-breakdown events by increasing the partial discharge (PD) inception voltage level and performing its barrier function against electrical streamers developing into breakdown of the insulation system between phases [4]. Considering a HV transformer without pressboard barriers at the inter-phase region, the dielectric strength would be strongly dependent on the oil. This will lead to a lower breakdown voltage if the same distance of inter-phase windings is applied, or require a larger distance between inter-phase windings to increase the breakdown voltage level. Thus, the use of pressboard offers design benefits such as reduced overall size and cost. The barriers

also help to prevent agglomeration of impurities in the oil by breaking the oil path into smaller sections [4].

1.2 Motivation and Problem Statement

1.2.1 Failure Analysis of Insulation System

A paper [3] by Sokolov has summarised six surveys (i.e. by CIGRE, IEEE, EPRI, Australia-New Zealand, India Power Grid and China) on transformer failure statistics according to nine faulty components as shown in Table 1.1. Three of the components which may be associated with failure due to problems in internal insulation systems of power transformers are tank and dielectric liquid, windings and dielectric issues. This does not mean faulty on-load tap chargers (OLTCs) are not associated with transformer insulation failures because CIGRE WG 12-18 [6] has suggested failure modes of OLTCs may also involve contamination and degradation agents in the insulation system. However, their failures are usually associated with mechanical failure as a result of frequent switching operations [7], thus, by classifying failure statistics based on faulty components, it can assist in identifying the main factors that contribute to failure. Bushings, on the other hand, are a component that is outside of the transformer tank, thus, can be classified as an outdoor insulation.

Based on Table 1.1, the term of dielectric issues has been used by EPRI in their survey on generator step-up (GSU) transformers in the US to directly categorise faults related to insulation systems. However, this can be either major or minor insulation systems in a power transformer. Thus, the information is insufficient to differentiate between failures due to major insulation or minor insulation. It was highlighted that 21% of 45 failure transformers were related to the dielectric issues category. On the other hand, an earlier survey conducted by CIGRE Working Group Study Committee 12 on 47000 transformers from 13 countries over a 10 year period (1968-1978) reported 13% of over 1000 failed transformers were linked to the tank and dielectric liquid and 29% were due to winding failures. A failure report by IEEE shows that out of 164 failure events, 3% of them were related to the tank and dielectric liquid, while 41% were linked to winding failures. Another survey conducted by a Chinese utility reported among 176 failures observed, approximately 9% were attributed to the tank and dielectric liquid as the

faulty component whilst 12% related to windings. Meanwhile, surveys in Australia-New Zealand and India found 30% and 73.3% respectively were due to winding failures. Both surveys have no report on failures that involved the tank and dielectric liquid. All the surveys except by EPRI suggested that between both components, i.e. (windings and tank and dielectric fluid), failures of windings are more dominant in transformer failures. However, it is unclear whether the failures were related to minor (turn and coil) insulation failure or winding distortion. On top of that, although failures related to the tank and dielectric liquid could represent major insulation failure, nevertheless, it is unsure whether pressboard failure is counted or not. Hence, the surveys did not provide sufficient information about particular insulation systems as defective components.

Table 1.1: Summary of failure surveys by a few organisations based on faulty components [3]

Faulty component	CIGRE Survey 1983 (%)	IEEE 1986 (%)	EPRI GSU US (%)	Australia-New Zealand 1985-95 (%)	India Power Grid (%)	China 220kV (Numbers)
Windings/insulation	29	41		30	73.3*	21
Dielectric issues			21			
Mechanical			11			
Magnetic circuit	11	10				4
Terminals	29	9	5			
OLTC	13			25		15
Bushing	5	13	30	19	13.3	45
Tank and dielectric liquid	13	3				16
Cooling and others		17	12		13.3	22
Total failure observed	>1000	164	45	498	15	176

* Including 2 cases due to water entry through bushing

There are also surveys performed by two consulting companies in the field of service and condition monitoring of power apparatus, i.e. ZTZ-Service and Doble Client been considered in failure analysis given by Sokolov [2, 3]. The surveys categorised major and minor insulation as defective components to associate failures of transformer caused by insulation system impairment. In addition, winding distortion was regarded as mechanical defect. Hence, this is rather straight forward to link the failures with insulation system defect such as ageing and contamination when compared with surveys that have been discussed previously. In general, the earlier surveys [2] by both companies over the period 1996-1997 recorded a quite high rate with about 30% of the failures were attributed to impairment of major and minor insulation in transformers serviced for more than 20 years. The insulation failures were linked to insulation degradation due to particle contamination and ingress of moisture. The updated surveys (Doble Client in period 1996-1998 and ZTZ-Service in period 2000-2005) [3] recorded the majority (30%-50%) of the transformer failures were associated with major and minor insulation. The ZTZ-Service update reported that out of 45 failures of GSU transformers, 11.2% were found due to major insulation failure and 37.8% associated to minor insulation. This latest survey also discovered that majority of 63 failures of transmission transformers were related to major insulation defects with a total percentage of 17.3%. This figure was followed by minor insulation failures of 14.3%. Meanwhile, the Doble Client survey found 13.4% of 52 transformer failures were linked to major insulation and 23% related to minor insulation. There is an agreement in the updated surveys by both companies that insulation weaknesses were the main factor for transformer failures. The surveys also found that the average age of the failed transformers was between 20-22 years.

While some surveys relate the insulation failure mode with the degradation mechanism in aged transformers, Lapworth and Wilson [8], on the other hand, have documented some evidence from cases in the UK where failures of 30-40 year old transformers associated with dielectric failure may not necessarily be due to insulation degradation. Instead, they experienced dangerous internal over-voltages as a result of switching operations, a failure mode also highlighted earlier by Allen and White [1] as one of the causes of transformer failure. There was no clear evidence from the test data of any forthcoming failure on the transformers. In fact, there was a catastrophic failure case as a result of tracking fault along the barrier pressboard in which the test data history of contamination level showed a consistently falling trend. Thus, for this case, an

important question may come into mind, what is actually the main cause of the failure? Is it true that internal over-voltages cause the failure or are the defect and faulty conditions in the insulation that ultimately stimulate the insulation breakdown not clearly identified through condition-based monitoring?

1.2.2 Defects and Failure Mode in Composite Insulation Systems

Cellulose-based paper/pressboard and oil are the main insulation materials used in power transformers. Cellulose-based materials immersed in oil form a complex composite insulation system. The dielectric breakdown mechanism even after many years of research is not clearly understood. The breakdown mechanism has to be based on certain possible progression of defective and faulty conditions [2, 6]. The defective condition such as surface contamination, oil contamination and excessive moisture is an abnormal state that attributes to reversible changes of the physical of insulation material. This condition has no significant impact on short term reliability, but asset life may be compromised in long term unless remedial action is carried out [6]. In contrast, an equipment with a faulty condition can remain in service, but short term reliability is likely to be reduced [6]. Fault condition attributes to irreversible processes that can be characterised in terms of gassing or bubble generation and destructive partial discharge activities. Damage created by these partial discharge activities usually results in carbonised tracks at the oil-pressboard interface and it may not be possible to improve the condition by remedial action. This research focusses on the failure mode that creates this particular damage pattern, i.e. surface discharge and creeping discharge; and is a continuation of a previous work of PhD research by Mitchinson [9] undertaken at the Tony Davies High Voltage Laboratory, University of Southampton.

Sokolov classified creeping discharge as the most dangerous fault condition in composite insulation as it results in catastrophic failure under normal operating conditions [2]. It depends substantially on the configuration of electrical field whereby it is stimulated by the presence of high tangential component of electric field intensity across the pressboard surface [9, 10]. Sokolov describes the phenomenon of creeping discharge occurs in four progression steps [2], but later combines the final two steps to give three steps of progression [11]. The steps begin with partial breakdown of an oil gap between the winding and the nearest pressboard barrier. This followed by surface

discharges in the oil across a barrier surface. Over time, the surface discharges result in creeping path (tracking) which is expected due to the drying out of the pressboard (forcing oil and water out of the pressboard pores) and the carbonisation of the oil and cellulose.

Mitchinson has experimentally studied and explained the mechanism of the second and third step using a model system [9]. In brief, the results suggested that the surface discharge and creeping discharge are two aspects of the same phenomenon, i.e. creeping discharge is the appearance of surface discharge growing along the interface. It is characterised by the formation of white marks from the discharge source towards the earth bar electrode which is believed to be associated with the drying out processes that occur at the pressboard. Mitchinson's experiments involved using a high voltage needle electrode to provide a high local electric field on the pressboard surface [9, 12]. It has been recognized that the development of surface tracking is also accompanied by corona-like activity around the needle tip upon increasing the voltage level into the sustained PD region [9, 12]. The corona-like glow is a sign that ionisation and secondary avalanches are taking place [13, 14]. Surface discharges can be sustained for long periods without surface flashover or breakdown as long as surface breakdown voltage is not exceeded [9, 15]. After long periods of surface discharge, additional discharges seen as a full discharge event may occur across the pressboard surface from the needle tip to the earth without resulting in complete electrical breakdown [15]. The full discharge event may lead to a leakage current flowing to earth that was found unlikely to trip the protection systems used in the experimental work. It should be highlighted that creeping discharge can continue from minutes to months or even years under normal AC voltage operation until the creeping conductive path becomes an essential part of a powerful arc [16]. It has been experimentally demonstrated by Mitchinson [9] that besides the voltage level, the degree of damage due to the surface tracking increases with duration of electrical stress. This is likely showing that creeping discharge is a "silent killer" of transformer useful life. Moreover, the condition-based monitoring programme has classified the detection of this failure mode using typical test methods, i.e. the dissolved gas analysis (DGA) and PD measurement are at a "fair level" (stage 4 out of 6) [6]. Thus, it does make sense to classify creeping discharge as the most dangerous faulty condition in composite insulation. From this point, it may be possible to link creeping and surface discharges as the cause of catastrophic failures that

result in the tracking faults along the barrier pressboard as reported by Lapworth and Wilson [8].

Sokolov identified seven possible scenarios involving typical defective and faulty conditions in composite insulation system that lead to breakdown or flashover based on historical cases analysis for over 200 failures [2]. In general, these seven scenarios can be divided into two categories of defective condition. The first category is a physicochemical-related defect which encompasses five scenarios that involve degradation agents such as water and surface contamination. The second category associates with mechanical error which consists of two scenarios that occur due to winding distortion. Creeping discharge and surface discharge may occur as sequential element in both categories. However, it has been highlighted that the typical failure scenario for an initially defect-free insulation always begins with contamination [6]. Thus, the physicochemical-related defect is the major concern when associating failure scenarios with creeping and surface discharges.

1.2.3 Characterising the Defective and Faulty Conditions

The presence of defects and faults can be detected by monitoring and diagnostic tests. However, despite advances in monitoring technologies in recent years, one still cannot avoid unexpected faults and failures occurring in the insulation system. This may be due to the use of alerting method in condition-base monitoring, i.e. "caution level" and "alarm level" that are usually defined in terms of test data quantities, e.g., gas concentration, water content, etc [17]. The rising trend in quantities of these parameters is normally treated as giving a good indication of serious problems or at least something to be further investigated. On the other hand, the decreasing trend or the absence of an increasing trend is regarded as a healthy condition although this is not a necessary condition as reported in [6, 8]. The transformer may be suffering from an unexpected failure that could be triggered by an abnormal event. This issue has been highlighted by Lapworth and Wilson [8] by documenting some cases where there was no evidence of problems or there was a falling trend from the monitoring data history. This includes the case of flashover failure along the inter-phase pressboard as shown in Figure 1.2. Although Lapworth and Wilson [8] have suggested that the transformer failed due to internal over-voltages caused by remote energisation, it appears that this is still

debatable due to the fairly low sensitivity in detecting surface discharge activity that suggested by CIGRE WG 18.12 [6]. It is possible that in addition to the internal over-voltages caused by remote energisation, there is also surface discharge activity at the oil-presboard interface. Hence, the damage caused by surface discharge activity at the oil-pressboard interface might have induced the failure as a result of remote energisation.

Figure 1.2: Flashover failure along barrier board [8]

Characterising the defective and faulty conditions in insulation of a transformer is very important for the development of effective condition-based monitoring programmes for a transformer. The characteristics may provide useful information about degradation processes within a transformer. An approach that may be more appropriate has been proposed by CIGRE WG 18.12 [6]. This approach quantifies the defective condition in terms of degradation of the transformer withstand strength rather than only based on the trend of test data quantities as mentioned previously. This is because the defective condition involves substantial reduction in the safety margin which reduces the initial withstand strength and unexpected failure may occur under the effect of abnormal event such as a lightning strike or remote energisation. Through this approach, the "caution level" would suggest a defective stage that has possibility of reduction of dielectric margin by 10% or more with respect to specified stresses. Meanwhile, the "alarm level" is used to describe the defective condition where there is possibility of occurrence of critical partial discharge at rated voltage. This approach still needs to be further studied as all diagnostic procedures need significant diagnostic experience in order to derive the appropriate decision. The investigations should be able to correlate between particular test results and defective condition. For that reason, a lot of site data

and laboratory works are needed. Some works have been documented in condition-based ranking method with the aim to classify the transformer population from the sites in terms of its reliability and usability [17].

As for laboratory work, it should be emphasised that the effect of defective conditions as the variable parameters on the faulty conditions need to be studied. Therefore, this research has considered the effect of moisture content in the pressboard on the degradation process at the oil-pressboard interface through surface discharge experiment. Appropriate measurement schemes are required to investigate the characteristics of faulty conditions that are useful for condition monitoring purposes. In addition, it should also be noted that a depth of understanding about the physical process of defective and faulty conditions that lead to the insulation breakdown is very important. Hence, a model of surface discharge at the oil-pressboard interface has been developed by considering its dynamic process from the perspective of charge transportation.

1.3 Research Objectives and Contributions

The main objective of this research is to study the behaviour of surface discharge at the oil-pressboard interface. The research has involved experimental and computer simulation studies. A series of surface discharge experiments at the oil-pressboard interface have been conducted in an oil bath experimental setup under a long duration AC electrical stress as such modelling surface discharge activity within a power transformer without a loading current and assuming the discharge started at the interface. Throughout the experiment, surface discharge activities are observed and measured for analysis purposes. A computer simulation model has been developed in the COMSOL Multiphysics environment, a finite element analysis (FEA) software package to study the surface discharge mechanism by validating the simulated result with the experiment. With respect to all these, the following contributions have been identified:

1. The process of surface discharge until the occurrence of a first full discharge event has been recognised for systematic study of surface discharge phenomenon at the oil-pressboard interface. In this research, full discharge is defined as a rare discharge event (usually visible in the form of arcs) that temporarily bridges the HV

electrode and the earth at the oil-pressboard without resulting in a complete electrical breakdown. The significant activities from surface discharge process have been correlated with the measured PD data to provide a mechanism for early detection of inter-phase barrier board creep stress failure.

2. The effects of different moisture levels in pressboard on the surface discharge behaviour have been recorded and analysed for condition monitoring and failure prognostic purposes.

3. The experimental work has recognised a decreasing trend in PD data at some point of surface discharge activity suggesting that such traditional evaluation is not a reliable condition monitoring method as a measure of asset health.

4. The characteristics of full discharge events have been explained to provide some value added information for condition monitoring programmes designed to detect surface discharge at the oil-pressboard interface.

5. A mathematical model has been developed and validated using experimental results to study the mechanism of surface discharge at the oil-pressboard interface. The model was developed by considering the pressboard as a porous material at a region called the 'transition region', a region near the pressboard surface. The model is able to describe the mechanisms of some physical features of degradation on the pressboard surface as a result of surface discharge activity at the oil-pressboard.

1.4 Thesis Structure

Chapter 1 discusses the problems within large transformers associated with the oil-pressboard interface that motivates this research. Challenges in detecting the defective and faulty conditions within a transformer are also discussed. The research objectives and contributions have been outlined.

Chapter 2 contains a literature review related to this research. The literature review covers the properties of oil and pressboard as a major insulation system within a large transformer. The presence of oil-impregnated pressboard has become a concern in terms of contamination, degradation mechanism and creepage stress. Experimental results on the effect of oil-pressboard interface to the streamer propagation to

breakdown are discussed. Recent findings on the effect moisture content in pressboard to the creeping discharge phenomena in terms of surface flashover and PD inception voltages are highlighted. In addition, computational modelling approaches by some authors related to problems at the oil-pressboard interface are discussed for consideration in this thesis.

Chapter 3 describes the surface discharge experiment conducted throughout the research. The chronological process for the occurrence of a first full discharge event during surface discharges at the oil pressboard interface has been highlighted. The characteristics of significant PD activities from the chronological process are explained based on the measured data. This chapter also discusses the effect of different moisture levels in pressboard.

Chapter 4 particularly explains the characteristics of full discharge events observed during surface discharges at the oil-pressboard interface in terms time and frequency domain analysis. Correlation between leakage current measurements and PD monitoring data from different full discharge events are discussed to provide useful knowledge for the development of a condition monitoring programme to detect surface discharging in a large transformer. This chapter also compares the full discharge at the oil-pressboard interface with the dry band arcing at the air-solid interface of the outdoor insulation.

Chapter 5 describes the surface discharge model developed in this research that considers the porosity of pressboard. This includes the governing equations, assumptions for parameter determination and appropriate consideration for boundary condition setting. The validation of the model using experimental results is discussed. In terms of simulation results, the role of electric field dependent molecular ionisation on the streamer development is explained. In addition, the roles of electron attachment mechanism and other recombination processes (ion-ion and ion-electron) for the extinction of partial discharge activity are also discussed. The mechanisms behind the physical features of degradation (formation of white and black marks) observed due the surface discharge activity at the oil-pressboard interface are also explained.

Finally, Chapter 6 details the conclusions and recommendations for further work of this research.

Chapter 2

The Oil-pressboard Interface

This chapter presents a review of the literature that is directly relevant to both the experimental work and physical model development that has been undertaken as part of this thesis. Initially, the insulation materials are discussed and then this is followed by a review of the electrical breakdown phenomena. Considerations when modelling the interface are then detailed.

2.1 Mineral Oil

Mineral oil has traditionally been used as an insulating system for electrical equipment including transformers, circuit breakers and cables. In power transformers, the widespread use of mineral oil offers dual functions, i.e. as a coolant and an insulator [18, 19]. As a cooling system for a power transformer, mineral oil (also called transformer oil) serves as a dissipater of heat due to its ability to transfer heat by means of conduction and convection. In terms of insulation, the use of transformer oil makes an important contribution to insulate different parts within the transformer and to the efficiency of cellulose-based solid insulation materials, i.e. paper and pressboard. This is based on its ability to conform to complex geometries by filling spaces and penetrating into materials through impregnation process.

Mineral oils are obtained from crude petroleum extracted from the earth. The blend of complex mixtures of many hydrocarbon molecules which have a variety of structures and a distribution of molecular sizes and weights is dependent on the source of the crude oil and the refining process [18, 19]. There are three main groups of hydrocarbon molecules in transformer oil, which are paraffinic ($C_{2n}H_{2n+2}$), naphthenic ($C_{2n}H_{2n}$) and

aromatic (C_nH_n) [18, 19]. Examples of molecular structures for each hydrocarbon group are shown in Figure 2.1. The paraffinic hydrocarbons are composed of straight and branched chains of carbon and hydrogen atoms, whilst the naphthenes have a saturated ring-like structure. The aromatics also have ring-like structure which is unsaturated that can be identified by double bonds (double lines in Figure 2.1) between some of the carbon atoms. In general, these mixtures determine the physical properties of transformer oil that make it an excellent electrical insulator and cooling medium such as high resistivity, high dielectric strength, high specific heat and thermal conductivity along with low viscosity and pour point as well as low density. The other important parameter for most transformer oils is the relative permittivity ε_{oil}, that typically has a value of 2.2.

The paraffins and naphthenes are present in larger amounts compared to the aromatic hydrocarbons in which many physical characteristics of a transformer oil reflect their presence, although these characteristics are also influenced greatly by the aromatic content [19]. Paraffinic compounds are important in lowering the density of the transformer oil. However, their drawbacks compared to the naphthenic compounds are their tendency to increase the viscosity at low temperature and the pour point. Pour point of a fluid determines the lowest temperature at which the fluid is capable of any observable flow. Low viscosity allows better oil impregnation of cellulose-based materials to eliminate void and gas pockets and assist in the circulation for cooling purpose preventing local overheating [18, 19]. Hence, proper percentages between both the paraffin and naphthene compounds are necessary to obtain desirable physical properties for the transformer oil. Transformer oil is normally categorised as paraffinic or naphthenic oils dependent on the percentage of both compound types in the oil [18, 19]. However, in some cases, for naphthenic oils, the paraffin compounds still exceed the naphthene compounds but with lower ratio between both compounds compared to the paraffinic oils.

The aromatic hydrocarbons, particularly the polyaromatic (two or more rings) ones, are more reactive than saturated hydrocarbons so they dominate the chemical behaviour of a transformer oil [19]. They act as weak dipoles which contribute to the values of dissipation factor at lower temperature. The presence of aromatic components also lowers the resistivity of the mineral oil. This is probably due to a conduction mechanism available to all unsaturated molecules as a result of the intermolecular

transfer of electrons due to weak bonds within the molecules. However, positively, they act as a natural oxidation inhibitor for oxidation stability of transformer oil. They are also important to maintain gas absorbing capability particularly hydrogen due to bubbles formed by partial discharges. The bubbles can be a result of localised vaporisation processes when the boiling points of water (373 K) and transformer oil (in the range of 500-800 K) are reached. Therefore, a low amount of aromatic constituents are beneficial up to a certain level.

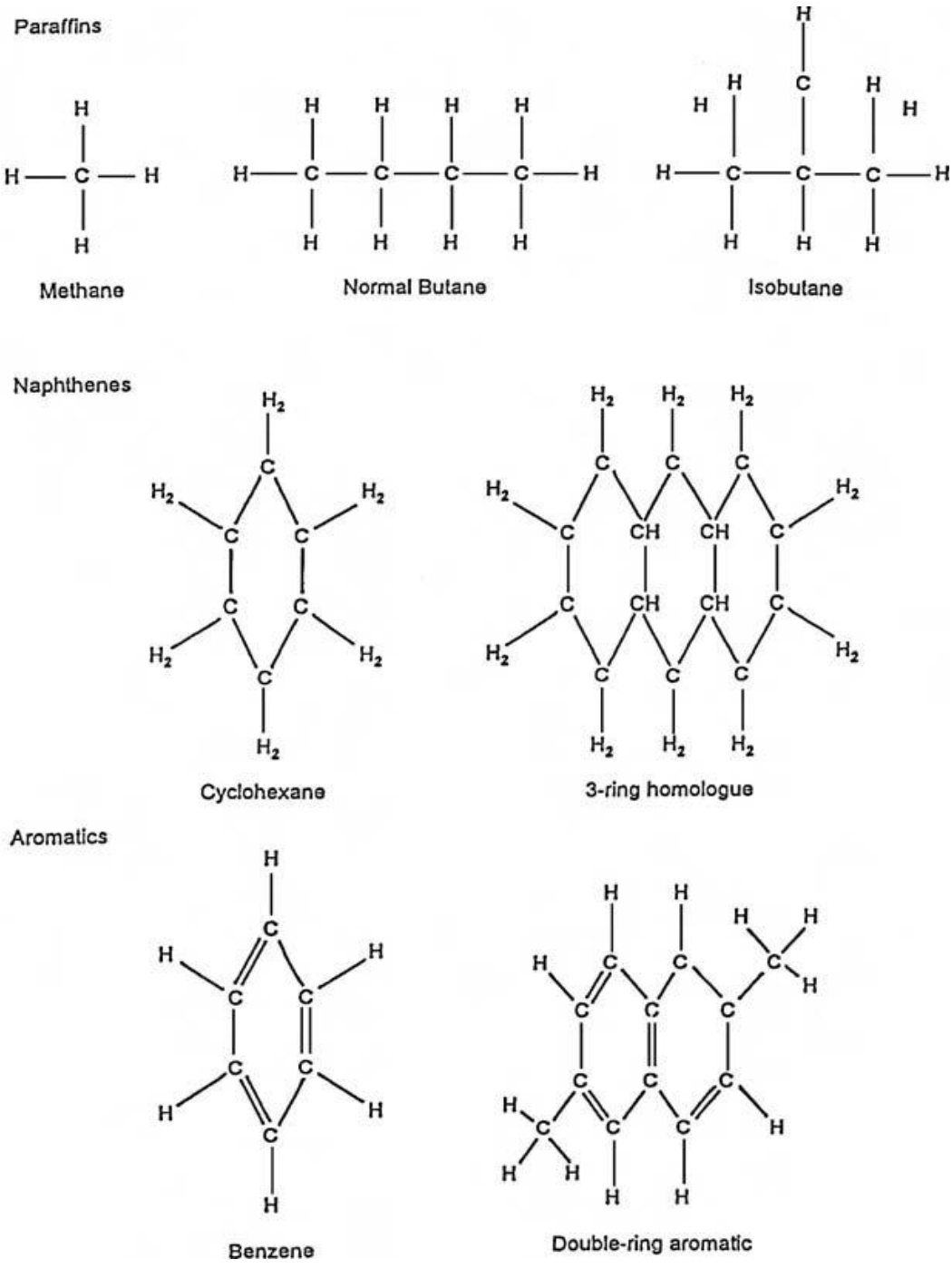

Figure 2.1: Molecular structures of hydrocarbon groups [18]

2.2 Cellulose-based Pressboard

The inter-phase region of a HV transformer comprises of composite insulation of oil and cellulose-based pressboard barrier. Pressboard is a solid material with porous and non-homogenous surface structure as a result of inter-fibre bonds. At its most simple, pressboard represents thick insulation paper made by a number of layers of fibre paper. In order for the pressboard to achieve an acceptable degree of mechanical and dielectric strength, the manufacturing process includes some stages which mainly involve a wet stage, compressing with high pressure and drying out at high temperature [18]. As a result, the whole process offers the production of structural strength of cellulose insulating material from loose cellulose fibre bundles.

In general, fibres may consist of approximately 50-90% of carbohydrate group, i.e. cellulose (40-80%) and hemicelluloses (10-40%) [20, 21]. Fibres may also consist of 5-25% of lignin [20, 21]. The majority of chemical properties of fibres are due to the insoluble celluloses that are derived from high-polymer carbohydrate consisting of glucose units [18, 20, 21]. This yields to the use of "cellulose-based" term for materials made of it such as transformer insulation pressboard and paper. Hemicellulose molecules are the second major components that facilitate the hydrogen bonding process, but the mechanical strength is reduced if their quantity exceeds about 10% [18]. Another disadvantage of hemicelluloses is their ability to 'hold on' to water which makes the paper/pressboard more difficult to dry out [18] and thus, this signifies its dominant role in the hydrophilic behaviour of the cellulose-based solid insulation. Meanwhile, lignin is a component of wood that binds to cellulose fibres to strengthen the cell walls of plants and add further to their matrix rigidity [20].

The structural strength of pressboard is determined by the stability of inter-fibre bonds that are established by sufficient bonding energy of hydrogen between OH-groups in the cellulose macromolecule [22]. Microscopic views (see Figure 2.2) have shown that pressboard insulation is a fibrous and porous structure with non-homogeneous surface [15, 22], although it can be categorised as having a homogeneous or a less homogeneous surface among its family [21]. The pore diameter within the fibre structures of pressboard varies from 10 nm to 7 μm [23]. These pores provide paths for fluid (i.e. oil and water) to penetrate by diffusion and swelling mechanisms [22]. This apparently shows that the pore structures cause impurities to reside within the cellulose

insulation and thus, imperfections of structural homogeneity create weak spots within the pressboard for space charges to trap. Mitchinson in [15], based on the microscopic view, suggested that the inhomogeneous and porous conditions of pressboard increases nearer to the bulk oil. The conditions may become maximised on the surface of impregnated pressboard and can be associated with the decreasing mass density of fibres from the centre of bulk pressboard towards the surface that eventually affects the swelling condition of the oil-impregnated cellulose fibres. Within the weak dielectric region of pressboard, the mean free path length of accumulated electrons will be such that activation energies are achieved that can lead to the tearing of hydrogen bonds from the chemical structure of cellulose and ionisation processes [22].

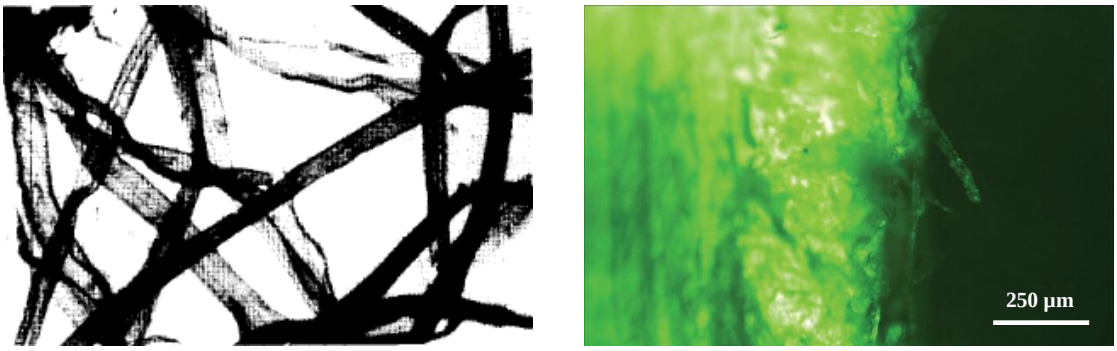

(a) Loose structure of cellulose fibres in pressboard [22]

(b) Non-homogeneous condition of pressboard edge [15]

Figure 2.2: Microscopic view of pressboard insulation

2.3 Moisture within Oil and Pressboard

Moisture is one kind of impurity besides oxygen, oil aging products (in particular acids) and charged particles (e.g. copper) which can exist within pressboard and oil transformer insulation. Moisture in oil is measured in parts per million (ppm) using weight of moisture in micro gram (µg) divided by the weight of oil in gram (g). Moisture concentration in pressboard/paper is typically expressed in percentage (%) in which the weight of moisture is divided by the weight of dry oil-free pressboard/paper. It is a common practice to measure the moisture content in oil by the Karl Fischer titration [24] and estimate the moisture in oil-impregnated cellulose insulation by different equilibrium curves [25]. However, the equilibrium curve method was not applied in this research for experimental purposes. The preparation of pressboard samples with different moisture levels will be explained in Section 3.3.1. The paper or

pressboard can contain much more moisture than oil. For instance [25], a 150 MVA, 400 kV transformer with about seven tons of paper can contain as much as 223 kg of water. A typical power transformer can contain about 80,000 litres of oil. If a 20 ppm moisture concentration in oil is assumed, this is equivalent to about 2 kg of water which is very much less than the water in the paper.

2.3.1 States of Water in Oil and Pressboard

The unique nature of moisture, formed from polar molecules, is that it acts as a medium in which some substances can dissolve. This gives water as a high capacity for dissolved ions and thus it readily becomes conductive. Its presence as a degradation agent can significantly reduce the dielectric strength of transformer insulation under thermal and electric stress. Lundgaard et al [26] has calculated that a humidity of 4% in the cellulose-based insulation can shorten a transformer's operational lifetime by 97.5%. Hence, moisture plays a critical role in transformer life. In addition, the various states of moisture existence, either physically or physicochemical states in the oil [25, 27, 28] and pressboard [25, 27] insulation, also convey the role of water in reduction of dielectric strength.

Basically, there are three possible states of water in transformer oil [25, 27, 28], i.e. either as dissolved water (no physical properties of liquid water - individual or small groups of water molecules), or as dispersed water (having physical properties of liquid water when moisture in oil exceeds the solubility saturation value - colloidal sizes or emulsion) or as bound water (e.g. adsorption of water to solid impurities or chemisorptions of water molecules with any chemical compound such as oil molecules). The first two states are the physical state of water existence, whilst the third state is a physicochemical state of water presence in oil.

On the other hand, the presence of water in pressboard can be in four possible states [25, 27], i.e. either as absorbed free water, or as free water in capillaries, or as vapour or may be adsorbed on surfaces and capillary walls as a monolayer or polymolecular layers. The first three states are associated with the physical state, whilst the last state of water follows the laws of adsorption [27], thus can also be considered as a physicochemical state.

2.3.2 Source of Water in Power Transformer Insulation System

Sokolov identified three main sources of water build up in transformer insulation [29]. The first source is the residual moisture after manufacturing process of new transformer. The moisture typically resides in the "thick structure" elements of insulating components particularly plastics that used for leads, OLTCs and etc which need much longer drying time in comparison with pressboard. The second source is the water that ingresses from the atmosphere which is also the main source of contamination in transformer. This can happen either directly (i.e. insulation exposure to air during installation or maintenance) or indirectly (i.e. nature of fluid flow due to difference in water concentration or gradient between atmospheric pressure and pressure in tank). The third source is the moisture presence due to aging decomposition of cellulose and oil. Many discussions related to this third source of moisture have been reported elsewhere, e.g. [26, 30, 31]. Experimental results by Lundgaard et al [26] found that moisture level increases approximately 0.5% for every time the depolymerisation (*DP*) value of the cellulose is halved by degradation, i.e. one chain scission number (*CSN*) in equivalent which is similar to what has been highlighted by Emsley [30]. Chain scission number represents the average number of chain scissions per cellulose chain unit to describe ageing and is often calculated using [26, 32, 33]:

$$CSN = \frac{DP_{new}}{DP_{aged}} - 1 \tag{2.1}$$

Where DP_{new} is *DP* value before aging period and DP_{aged} is *DP* value after aging period. The insulation system may also experience further increase of moisture under the endurance of thermal stress particularly with the presence of cellulose paper in the transformer oil [31].

2.3.3 Effect of Moisture at the Oil-pressboard Interface

The inhomogeneous surface and pores of pressboard which allow a diffusion process to take place in combination with the physicochemical properties of fibres as a strong adsorbent may facilitate two stages of moisture adsorption [27]. First, there is a formation of a strong monolayer on the surface and within pores of the pressboard. Table 2.1 shows the case of amount of moisture in the range of 3 to 4 % as a function of

temperature that can produce a monolayer as a result of the adsorption process. Then, as the amount of adsorbate increases, polymolecular layers will exist. It should be noted that as the thickness of water layer increases, the water may have more and more physical properties of free water. As a result, this will further increase the conductivity of the pressboard surface.

In addition, water content in the oil-impregnated paper/pressboard also causes the chemical ageing mechanisms of cellulose through hydrolysis and oxidation processes [22, 26, 34, 35]. Another aging mechanism is pyrolysis, i.e. an ageing mechanism when high temperature is also present which can lead to slow combustion [26, 35, 36]. These ageing mechanisms can lead to the formation of dissolved gases such as hydrogen and carbon monoxide [34] and acidic products such as furan derivatives and carboxylic acids [26, 35]. Acidic products are destructive to fibre structure [35]. Over time, the ageing processes with the presence of acidic products will lead to further water generation [26, 35] and further increases in the conductivity at the oil-pressboard interface.

Table 2.1: Water content of cellulose paper (forming a monolayer) versus temperature [27]

Temperature (^{o}C)	Moisture of a monolayer, (wt%)		
	Cable paper "K-120"	Pressboard "EMC"	Capacitor paper "KOH-2"
23	4.38	4.60	
26			4.22
29	4.25	4.44	
45	3.86	3.92	4.08
70	3.44	3.30	3.25

It is likely that the moisture adsorption processes at the interface may support the experimental results by Dai et al [37] that new and aged pressboard with moisture content of approximately 3% suffers a reduction in partial discharge inception voltage (PDIV) of between 25 to 40% in comparison with dry pressboard (new and service aged) and thus enhances the surface discharge phenomenon. Based on the earlier experimental work by Mitchinson [9], it is believed that the formation of white marks during surface discharge at the oil-pressboard interface is the result of a drying out process which was proposed earlier by Sokolov [2, 11]. DGA data by Dai et al [37]

have suggested that the white marks are caused by the creation of gaseous channels in the pressboard. Based on their DGA results, they explained partial discharge energy from the surface discharge activity is high enough to vaporise the moisture and break the oil molecules to generate gases in which, over time, gas expansion would push the oil out of the pores of the cellulose pressboard to form white marks. Their work has verified the drying out processes within the pressboard pores. A later work by other authors [38] with high moisture content in pressboard immersed in larger oil volume (15 litres) compared to 2 litres used in [37] has shown remarkable DGA data. This shows the effect of different moisture levels to the DGA data as a result of surface discharge at the oil-pressboard interface. However, the larger oil volume is still very small compared to a real transformer (180 MVA/220 kV may contain about 45000 litres of oil). Therefore, further work in terms of other PD measurements might be required to understand the surface discharge phenomena and its detection for condition monitoring purposes. This will be discussed in Chapter 3 of this thesis.

On the other hand, it is also worth noting the importance of moisture content in a power transformer in the study of static electrification phenomenon. Static electrification, also known as flow or streaming electrification, is a phenomenon where static charge is built up on the pressboard surface due to oil flowing across pressboard in the power transformer for cooling purposes [39]. It has been reported that for a composite system of oil and cellulose-based solid insulation, increasing the water content in pressboard [40] and oil [41, 42] which would increase the conductivity may reduce the electrostatic charge generation at the interface. In contrast, a dry pressboard surface may become insulating enough and lead to large charge accumulation as a result of oil convection [43], until it reaches values at which it is possible to cause discharge [43, 44]. This condition may become worse when it is away from any grounded metal [44]. Therefore, with the consideration of the extensive research on the degradation processes that are associated with the failure of a power transformer, it appears that the water content in pressboard must take into account that undamaged, dry and clean oil-impregnated pressboard usually exhibits 0.5-1.0% of water content [45]. In terms of moisture level in oil, for instance, a maximum relative humidity of new mineral oil of 40% RH maximum is comparable to dry oil [46]. It is worthwhile noting that 40% RH in mineral oil is equivalent to approximately 20 ppm moisture content based on typical water solubility of 55 ppm in mineral oil at 20°C [47].

2.4 Empirical Study of Creepage Discharge at the Oil-pressboard Interface

Empirical studies relating to discharge activities at the oil-pressboard interface have been conducted by several investigators over many years. Some suggest that the surface discharge phenomenon is due to static electrification [43, 44], while other investigators focus on the interactions of electric field with the insulation system, e.g. [9, 10, 37]. In the case of power transformers, static electrification has been blamed for failures in the early 1970's in the Japan and early 1980's in the US [39]. In the UK [48], the current view of National Grid is that static electrification is not thought to be the mechanism responsible for the reported electrical breakdown at the inter-phase pressboard of power transformer. However, it may be associated with the effect of moisture on the dielectric integrity of barriers within transformers that are subjected to large electrical stress from transformer winding. Hence, this section focuses on the literature review relating to experimental works concerned with surface discharges under the effect of electric field distribution at the interface.

2.4.1 Effect of Material Properties and Permittivity of Oil-impregnated Solid

Before the phenomena of creeping discharge at the oil-pressboard interface reported in the literature is discussed, it is worthwhile considering the comparative works by some authors on creeping discharge for different material properties and permittivity of solid materials immersed in transformer oil. Dielectric solid materials such as glasses and plastics are characterised as having a compact structure and not being porous. These factors make them different when compared to the pressboard that is light, fibrous and porous form of solid insulation [15, 22, 23]. This initial analogy of physical presentation of the material suggests that the type of materials and surface roughness may offer different results in creepage discharge phenomenon. In fact, investigations particularly conducted on plastic type materials, i.e. polypropylene ($\varepsilon_{pp} = 2.3$), polyethylene ($\varepsilon_{pe} = 2.2$), polycarbonate ($\varepsilon_{pc} = 2.9$) and Bakelite ($\varepsilon_b = 5$) under the influence of AC [49] and impulse [50] voltages have reported that discharge patterns among the plastic materials are significantly different in terms of the number of branches, final length of the discharges and luminosity. The total electrical charge

deposited on the surface of Bakelite is about twice as high as the polycarbonate [50]. These suggest that creeping discharge at the oil-solid interface depends on physiochemical properties of the solid insulation and its surface geometry. In addition, different discharge currents have also been observed. Hence, when considering the cellulose-based pressboard with a porous, fibrous and non-homogenous surface structure, one can also hypothesise different results compared to other materials.

An earlier work [51] has shown that flashover event under ramp voltage at the interface is enhanced by the permittivity mismatch between the transformer oil and the solid material. The permittivity mismatch can be recognised from the permittivity ratio:

$$\varepsilon_{ratio} = \frac{\varepsilon_{liquid}}{\varepsilon_{solid}} \tag{2.2}$$

The experimental work has compared the electric strength at the oil-solid interface for different types of solid materials of which one is pressboard. The permittivity of the pressboard has been estimated on the basis of mass density. The electric strength is improved when the permittivity of solid materials is closer to the oil permittivity, i.e. permittivity matching between the oil and solid material. Similar results have been obtained in [52] under AC and impulse stresses on pressboards with different permittivity as well as polyethylene and polypropylene.

However, it has been reported [51] that the results of percentage of damaged solid are not correlated with the result of electric strength. It is not a surprise when the percentage of damaged pressboard is relatively higher compared to other materials due to its high mismatch permittivity with the oil and porous and fibrous structure. But, the percentage of damaged polycarbonate (lower permittivity than pressboard) is smaller than the polyphenylene oxide that has lower permittivity ($\varepsilon_{po} = 2.6$) than both the polycarbonate and pressboard and that closer to the transformer oil. This suggests that the damage level is not dependent on the permittivity matching condition if comparison is made between different materials, but it shows the influence of material properties. Therefore, for the sake of old transformers that are still in operation, the study of potential degradation behaviour at the oil-pressboard interface that may lead to failure, requires attention from the research community.

2.4.2 Pre-breakdown Phenomena at the Oil-pressboard Interface

Pre-breakdown events have been generally accepted the key to breakdown mechanism in dielectric liquids. These include partial discharge activities (corona and surface discharges) and electrical streamers that develop into breakdown. In this section, the discussions focus on the case with the presence of oil-pressboard interface. Various waveforms of impulse voltage that are typically of positive polarity have been extensively used to understand the features of streamer propagation at the oil-pressboard interface [52, 53, 54, 55, 56], whilst very limited work using negative impulse voltage has been published [56]. This is probably due to the well-recognised severity of a positive impulse voltage compared to a negative one, i.e. the breakdown voltage for negative polarity is twice as high as for positive polarity [14, 55] and there is a higher streamer propagation velocity caused by the same voltage magnitude [57, 58]. The features of the streamer that have generally been studied include the breakdown voltage, streamer velocity, streamer structures and effect of level of applied voltage and gap distance. In terms of AC voltages, studies are more focussed on the measurement of PD inception and breakdown voltages and phase-resolved partial discharge (PRPD) patterns for condition monitoring purposes [12, 37, 52]. It should be noted that experimental work reported in the literature is based on two general orientations of the oil-pressboard interface with respect to the dominant direction of the electric field as shown in Figure 2.3.

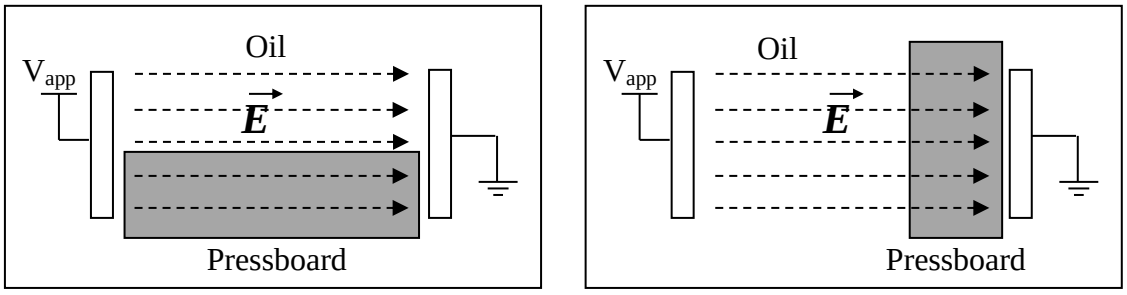

(a) Electric field direction is parallel with the oil-pressboard interface

(b) Electric field direction is perpendicular with the oil-pressboard interface

Figure 2.3: General orientations of oil-pressboard interface with respect to dominant direction of electric field (amended from [59])

For the case where the electric field is considered parallel with the oil-pressboard interface using point-plane electrode configuration, there is agreement between Massala

and Lesaint [54] and Lundgaard et al [55] that the presence of oil-pressboard interface does not change the 50 % breakdown voltage when impulse voltage was applied, i.e. similar with the results obtained for an open oil gap. However, experimental results by Dai et al [37] using AC voltage provides more information based on different levels of moisture within pressboard. The breakdown voltage with the presence of dry (less than 0.5 %) pressboard has also been reported relatively similar with the open oil gap, but, a slight reduction in the breakdown voltage level has been observed when wet pressboard up to about 3 % have been used as shown in Figure 2.4. In order to study the effect of moisture level in the pressboard [37], the needle tip touches the pressboard surface and the needle is placed so that its symmetry axis is at certain angle to the horizontal surface of the pressboard surface which was proposed earlier by Mitchinson et al [12] to study surface discharge at the oil-pressboard interface.

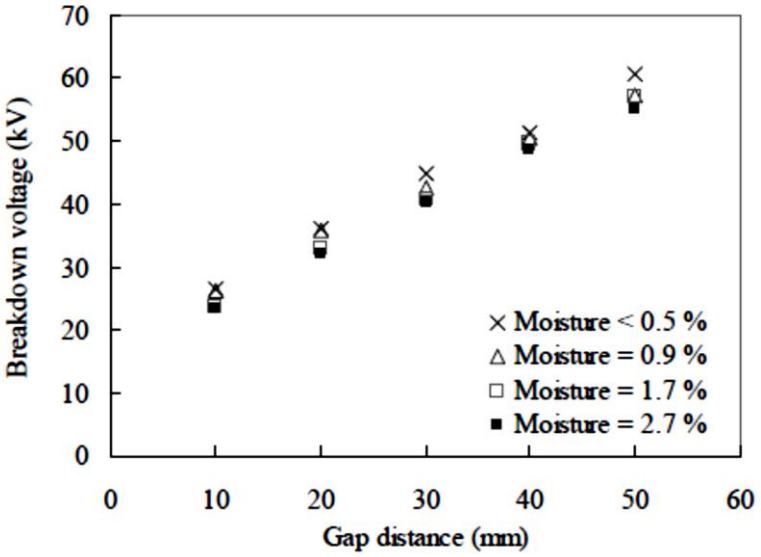

Figure 2.4: Breakdown voltage on wet pressboard compared to dry pressboard impregnated in dry oil [37]

In his experiment, Mitchinson [9, 12] has observed that the breakdown process at the oil-pressboard interface occur in four distinct stages as illustrated in Figure 2.5. The experiment was conducted by increasing the AC voltage gradually. As seen in Figure 2.5, the first event occurs at PDIV level. During this first stage, no visual activity has been observed but the occurrence of PD activity is known based on the monitoring data from the PD measurement system. As the voltage increases, the second stage occurs when a corona-like event is visible at the needle tip. This stage is observed to occur at a voltage level that is above the PDIV level and lower than the flashover

voltage, which is also called the sustained PD voltage range. Surface discharges can be sustained for long periods without surface flashover or breakdown as long as the voltage is within this range. Next, as the voltage is increased closer to the flashover voltage, the third stage occurs when streamers are observed from the earth bar and distinct crackling is heard (arcing event at the earth electrode). Finally, as the voltage is increased further (flashover voltage), a surface flashover occurs and causes electrical breakdown.

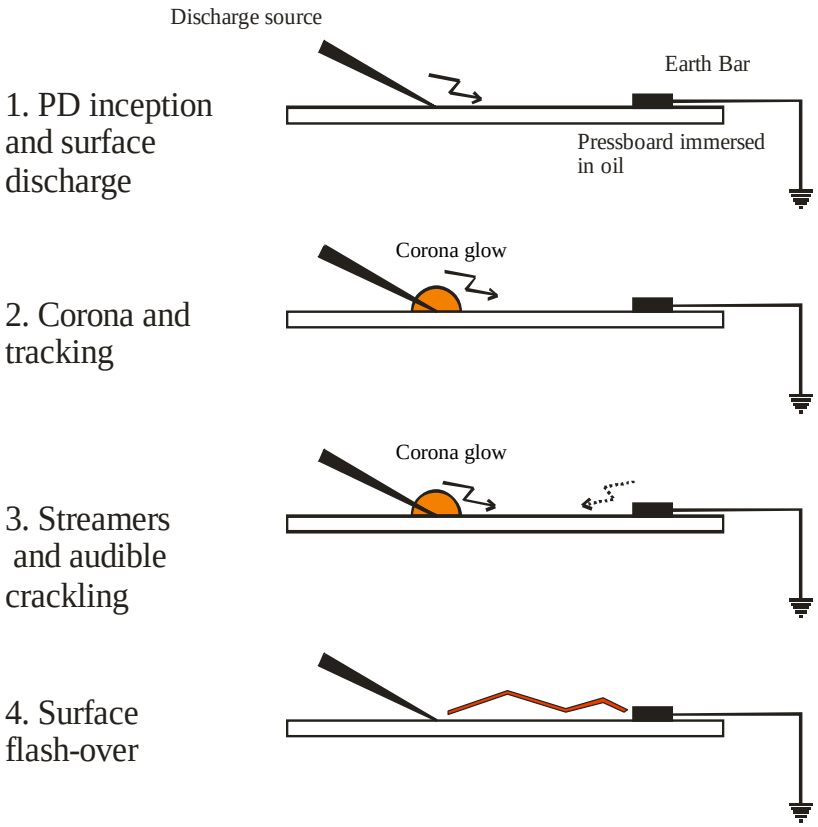

Figure 2.5: Representation of surface flashover stages [9, 12]

Mitchinson et al [9, 12, 15] have also experimentally studied the features of surface discharge under AC voltages and these have been discussed in Section 1.2.2. However, very limited data has been published for correlation with the explained features. The typical PRPD plot of PD activity indicating surface tracking activity at the oil-pressboard interface in compliance to IEC 60270 at a sustained PD voltage level (above an inception voltage and lower than the flashover voltage) is shown in Figure 2.6, from which the source of PD activity is hard to determine. However, it appears that the tracking activity may consist of both the surface discharge and corona-like events. This is based on the occurrence of PD activity at the first and third quadrants (surface

discharge) and at the peak area of the applied voltage (typical corona in air is recognised by relatively similar discharge magnitude at peak regions whereby peak of positive cycle indicates corona at earth point and peak of negative cycle signifies corona at HV point) [60, 61]. The formation of white marks as a gaseous channel during surface discharge at the oil-pressboard has been experimentally verified by Dai et al [37] based on their DGA data and their theoretical analysis on the formation of white marks has been discussed in Section 2.3.3.

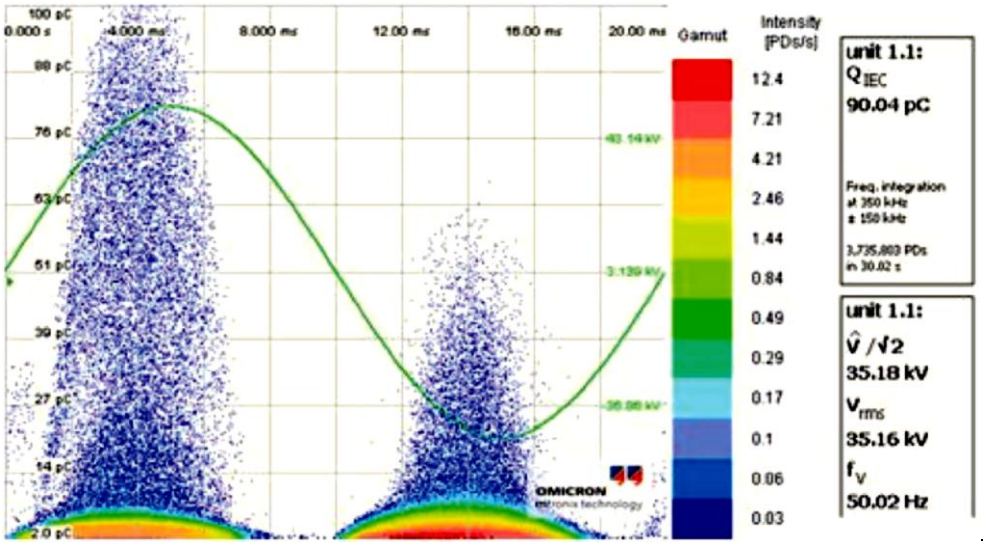

Figure 2.6: PRPD plot with needle-bar configuration at 35 kV and 35 mm gap [15]

In a power transformer, water level in pressboard is typically very much larger than in the oil [25] due to the ability of cellulose paper to hold water [25, 27]. Therefore, it appears that the study of surface discharge at the oil-pressboard interface based on different moisture content in pressboard is more significant [37, 62]. Table 2.2 shows the effect of different pressboard conditions on the breakdown and PD inception voltage levels for a gap distance of 30 mm. The table shows that moisture content leads to approximately 15 % reduction of surface breakdown voltage and 30 % reduction of PDIV among the same pressboard family, i.e. between dry and wet new pressboard and between dry and wet aged pressboard. On the other hand, the use of aged pressboard leads to 5-8 % reduction in surface breakdown voltage and 6-12 % reduction in PDIV when comparison is made between dry new and aged pressboard and between wet new and aged pressboard. Such a reduction may be due to the surface condition of aged pressboard as it smoother compared to the new pressboard [9]. In addition, an aged pressboard taken out from transformers that have been service for a certain period may

be contaminated by ageing by-products from the ageing mechanisms [22, 26, 34, 35] or particles trapped in the pressboard pores as a result of electro-hydrodynamic (EHD) forces from AC electric field [63]. Drying the aged pressboard will not remove the contamination and degradation agents completely from the pressboard pores. Based on the results shown in Table 2.2, it can be deduced that the moisture content in pressboard plays a more critical role in surface discharge at the oil-pressboard interface rather than the surface roughness of a pressboard and contamination trapped in the pressboard.

Table 2.2: Creepage discharge on different pressboard condition in 30mm gap distance [62]

	Dry virgin board	Wet virgin board (2.7-2.8 %)	Dry aged board	Wet aged board (2.8-2.9 %)
Surface breakdown voltage	46.9kV	40.2kV (14% reduction)	43.2kV (8% reduction)	38kV (19% reduction)
PDIV	38.8kV	27.4kV (29% reduction)	36.2kV (7% reduction)	24kV (38% reduction)

While moisture in pressboard has been said to play an important role in surface discharges at the oil-pressboard interface, experimental work in [37] has shown a general understanding on the effect of oil quality determined by moisture content in it. The experiment was conducted by comparing the surface discharge data when dry pressboard is immersed in dry and wet oil. It has been reported that both the breakdown and PD inception voltages decrease when wet oil with moisture content of 34 ppm is used. More importantly, the results of tests with and without the pressboard are very similar. These observations suggest that the surface discharge at the oil-pressboard interface is predominantly determined by the quality of the oil when the pressboard is dry and clean.

On the other hand, for the condition where the electric field is perpendicular to the oil-pressboard interface, Lesaint and Massala [53] conducted an experiment in which the distance between the needle tip and earth plane was fixed to 5 cm or 10 cm, whilst the position of pressboard was varied between both electrodes. The presence of pressboard

has increased the breakdown voltage level. This reflects the function of pressboard as an insulation barrier between phases in power transformers. However, as the gap between the needle tip and pressboard barrier increases, the breakdown event is dominated by the oil, i.e. the breakdown voltage level decreases until relatively similar to the breakdown voltage in oil gap without the barrier. Such results were observed due to the natural behaviour of streamer propagation that expands within a roughly conical outer volume and thus, oil-dominated breakdown occurs when at a certain gap, the area of solid surface is smaller than the roughly conical cross section. Liu et al [56, 64] in an experiment that covered the earth electrode with cellulose paper to function as a barrier also observed an increment in breakdown voltage level when the paper thickness was increased from 0.2 to 2 mm. At the same time, the needle-barrier gap was fixed at 2 mm in which this led the needle tip and earth electrode gap was 12.5 to 45 times shorter than the experimental work by Lesaint and Massala [53]. Liu et al [56, 64] have suggested that the ratio between the oil gap (needle to barrier gap) and barrier thickness plays an important role in such behaviour. In their experiment, the breakdown event always led to the barrier being punctured, thus an explanation based on conical cross section as already discussed is not applicable. Nevertheless, it appears that the effect of ratio between needle-barrier gap and barrier thickness seems also as valid as the earlier experimental results obtained by Lesaint and Massala [53].

In the case of electrode configurations that apply the electric field in the perpendicular direction with the pressboard barrier [53, 64], a streamer is initiated at the needle tip and propagates towards the pressboard surface. Then, once the streamer reaches the pressboard surface, there are two phenomena that occur, i.e. the streamer then changes its propagation (i.e. from perpendicular direction to that parallel with the pressboard surface) and creeps along the surface and at the same time, the streamer also leads to charge deposited and distributed in the barrier. The latter observation is supported by the result that electric field did not fall to zero after the occurrence of a breakdown event [53]. This can be associated with the accumulation ability of generated charges that are dependent on the space charge decay time in a system. In the case of oil-pressboard interface, it has been reported in a work using pulse electroacoustic (PEA) technique that 90% of the charges in oil-immersed paper with 120μm thickness take about 2 hours to disappear [65]. The latter phenomenon is also supported by the event of the pressboard being punctured, suggesting a competition between streamer

propagation along the surface and some charges that concentrate in a perpendicular direction to the pressboard surface [64].

In terms of the velocity of streamer propagation, the parallel orientation has been reported to play an important role in enhancing the velocity of streamer propagation along the pressboard surface compared to the perpendicular field orientation. It should be noted that the velocity at which breakdown occurs is typically an average value based on the HV-earth electrodes distance and time to breakdown [53, 54, 55, 56, 64]. Massala and Lesaint [54] and Lundgaard et al [55] have reported similar observation in which, as the voltage increases, fast mode streamer (3^{rd} mode: ≥ 10 km·s^{-1} or 4^{th} mode: ≥ 100 km·s^{-1} [66, 67]) can be observed at any voltage above the minimum breakdown level, whilst without the presence of oil-pressboard interface, such streamer modes can only occur at a voltage that is about twice the breakdown voltage. In other words, the acceleration voltage appears at a lower level. Acceleration voltage is a level at which the streamer changes from a slow mode: 1^{st} and 2^{nd} mode to a fast mode: 3^{rd} and 4^{th} mode. Their results also suggest that up to a minimum breakdown voltage, streamers propagate at an average velocity of approximately 2 km·s^{-1} (2^{nd} mode streamer [66, 67]). Figure 2.7 shows the transition of streamer average velocity with respect to the applied voltage in the transformer oil with and without pressboard. However, Lundgaard et al [55] has also reported that a slow velocity streamer propagation could change to a fast mode. The slow velocity streamer was found to cause weak darkening path on the pressboard surface, whilst the fast velocity has led to a burnt track on the pressboard surface, as shown in Figure 2.8.

In contrast, for the case of perpendicular orientation, Lesaint and Massala [53] have reported that the streamer average velocity increases slightly and remains low at approximately 2 km·s^{-1} as voltage increases up to approximately twice the 50% breakdown voltage as shown in Figure 2.9. A relatively similar average velocity has also been obtained by Liu et al [56] at the 50% breakdown voltage. Then, as seen in Figure 2.9, as the voltage level reaches the acceleration voltage, the effect of needle-barrier gap is seen to be significant. As the needle-barrier gap is large (5 cm), the tendency of streamers to speed up increases. However, in the case of short needle-barrier gap (1.2 cm), the tendency to speed up decreases whereby the average velocity is less than 4 km·s^{-1} after the acceleration voltage is largely exceeded. It has been highlighted that when large needle-barrier gap was used and above acceleration voltage,

the 3rd mode streamer has been observed propagating from the needle tip towards the pressboard surface. Then, as the streamer reaches the pressboard surface, it slows down to about 2 km·s^{-1} (2nd mode) until breakdown. Hence, it appears that the result of short needle-barrier gap shown in Figure 2.9 is caused by slower streamer propagation from the needle tip towards the pressboard surface.

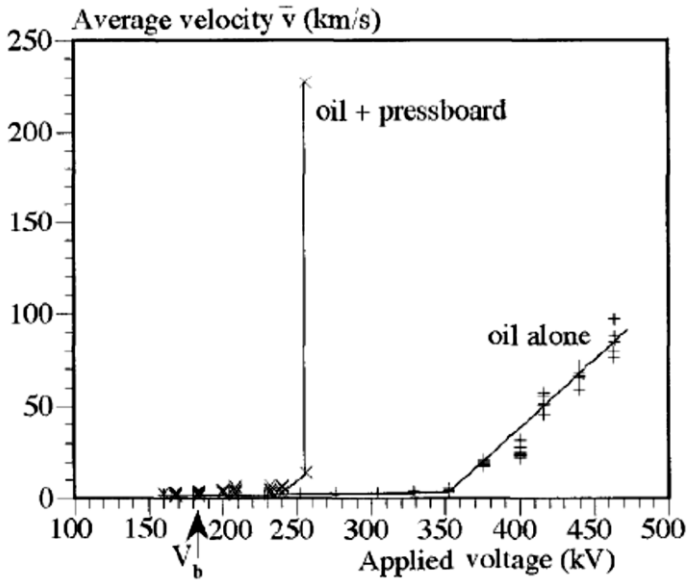

Figure 2.7: Average breakdown velocity recorded at overvoltages with and without pressboard surface (parallel configuration), needle-plane gap of 10 cm [54]

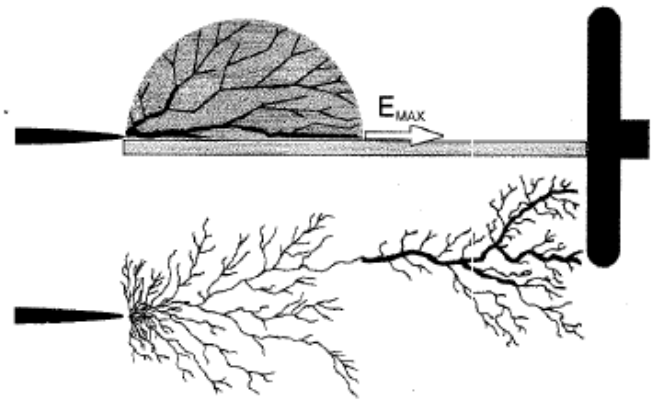

Figure 2.8: Positive streamer propagation along oil-pressboard interface. Upper: The positive streamer model. Lower: Actual tracks observed on pressboard surface [55]

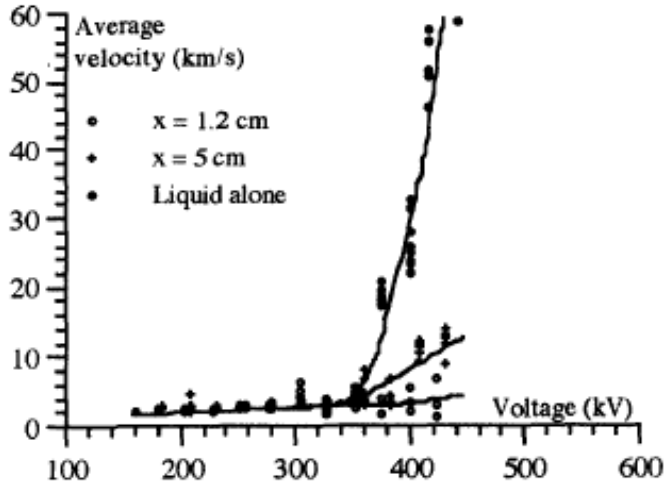

Figure 2.9: Average breakdown velocity recorded at overvoltages with and without pressboard surface (perpendicular configuration), needle-plane gap of 10 cm [53]

2.4.3 Effect of Electrode Configurations on the Damage of Oil-impregnated Pressboard in the study of Surface Discharge

As shown in Figure 2.3, the positions of solid insulation and electrodes in an experimental setup determine the electric field distributions at the oil-pressboard interface. Electric field distributions which can be expressed in terms of tangential and perpendicular components to the solid surface play important roles in surface discharge propagation on the pressboard surface [9, 10]. It has been reported in [10] that the use of cylinder-plate and sphere-plate electrode configurations so that perpendicular orientation is achieved (see Figure 2.3 (b)) was unable to promote surface discharge over a certain area of the centre of the pressboard where the electrodes were placed. No tracking damage has been observed within the respected area and this has been regarded as due to lack of a tangential component of electric field at the pressboard surface. The point-plane method as shown in Figure 2.10, on the other hand produces a more directional and intense electric field towards the solid surface from localised and inhomogeneous electric field at the edge of the needle compared to other methods that already mentioned. This method has been widely used to study surface discharge phenomena of various types of solid material, e.g. [50, 53, 57, 64]. The method may be suitable for more compact solid materials such as glasses and plastics, however, fibrous and porous pressboards may suffer from the disadvantages of this configuration. It has been recognised that the pressboard can get punctured during the experiment under AC

[9] and impulse [64] voltages. The method leads to uncertainty of the pressboard time to failure and thus shows the drawback of the point-plane method in gaining more information on the behaviour of surface discharge phenomenon at the oil-pressboard interface. It appears that the perpendicular component of electric field is responsible for most of the bulk damage and puncture event of the pressboard [10], which is due to electric field distribution in the porous pressboard, not at the needle tip [64]. In addition, the point-plane method does not follow the general principles for measurement of surface tracking where the voltage application and earth electrodes are on the same side as outlined in the Comparative Tracking Index (CTI) specification [68].

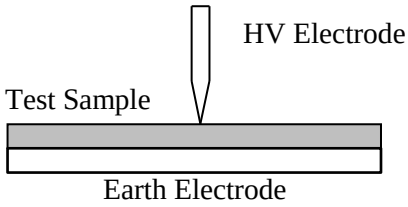

Figure 2.10: Point-plane electrode configuration (fulfilled the perpendicular orientation shown in Figure 2.3 (b))

The point-plane electrode configuration has also been used in a way so that the electric field is in parallel with the oil-pressboard interface as shown in Figure 2.11 (a) in the study of streamer propagation at the oil-pressboard interface under impulse voltages [53, 54, 55] as discussed earlier in Section 2.4.2. On the other hand, in the study of surface discharge under the influence of AC voltages [12, 37], the needle is placed so that the tip touches the pressboard surface and the symmetry axis of the needle is at certain angle that is nearly horizontal to the pressboard surface. In this thesis, the experimental works under AC voltages to study the behaviour of surface discharge at the oil-pressboard interface are based on the latter approach as shown in Figure 2.12. The method which has been earlier proposed in [12] and is called the needle-bar electrode configuration. It has been recognised that both configurations lead to similar observation in terms of breakdown events, i.e. the breakdown voltage with and without the presence of oil-pressboard interface is comparable [37, 54, 55]. However, as mentioned earlier in Section 2.4.2, the use of the latter configuration has shown some reduction in the breakdown voltage when wet pressboard is used [37]. This is obvious and is shown in the measurement of PDIV under different moisture contents for pressboard [37]. If configurations in Figure 2.11 and Figure 2.12 are used, it is likely

that the latter configuration that places the needle tip on the pressboard surface is being better suited to study the effect of moisture content in the pressboard compared to the former configuration. Therefore, this qualitative comparison suggests the advantage of the latter approach in the study of surface discharge at the oil-pressboard interface although no experimental comparison has yet been reported.

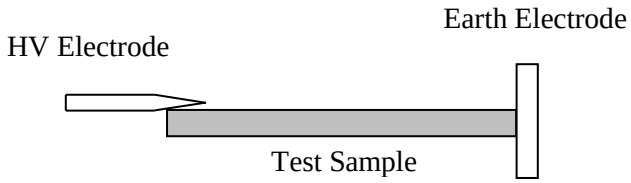

Figure 2.11: Point-plane electrode configuration (fulfilled the parallel orientation shown in Figure 2.3 (a))

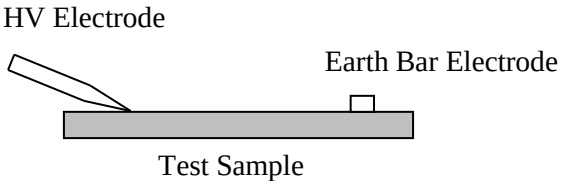

Figure 2.12: Needle-bar electrode configuration (fulfilled the parallel orientation shown in Figure 2.3 (a))

While the performance of configuration shown in Figure 2.11 is unknown regarding surface discharge at the oil-pressboard under AC voltages, the needle-bar electrode configuration has been reported useful to give a positive impact on the research of surface discharge at oil-pressboard interface under AC voltages [9, 15, 37]. Most importantly, this configuration has been reported to be useful in promoting surface discharge that can be sustained for a comparatively long time without surface flash-over or breakdown [9, 15]. Hence, this experimental arrangement provides an opportunity to gain more information regarding surface discharges at the oil-pressboard interface.

2.4.4 Measurement for Detecting Surface Discharge at the Oil-pressboard Interface

As previously mentioned in Section 1.2.2, surface discharge at the oil-pressboard interface can be classified as the most dangerous fault condition for composite insulation within power transformers because it can lead to catastrophic failure under normal operating conditions. Therefore, measuring such a phenomenon that precedes failure is very important to provide useful information for any condition monitoring programme of large power transformers. CIGRE [6] has recommended two methods for detecting the surface discharge problems in large power transformers, i.e. PD and DGA measurement techniques. However, both techniques are not classified as being good for detecting the surface discharge activity at the oil-pressboard interface. Instead, their sensitivity to detect surface discharge activity in power transformer is classified as 'fair' (level 4 out 6). For the DGA measurement, experimental results have shown that this is due to relatively small volume of pressboard barrier compared to the oil volume [38].

In terms of PD measurement techniques, as far as the literature is concerned, not much PD measurement data to characterise the surface discharge behaviour (i.e. white marks formation, full discharge and earth arcing) has been published. The data that are available only state the magnitude of apparent charge corresponding to the formation of white and carbonised marks [16, 37] in which not much interpretation can be made for condition monitoring purposes. Hence, this thesis focuses on the correlation between the surface discharge behaviour (i.e. white marks formation, full discharge and earth arcing) and PD measurement data (PRPD patterns) based on different moisture levels in the pressboard. The typical connections for PD measurement in compliance with the IEC 60270 [69] are shown in Figure 2.13. The connection shown in Figure 2.13 (a) which is used throughout this research is generally used in practice. The connection depicted in Figure 2.13 (b) can provide a better sensitivity, but a suitably designed protection system is required to protect the coupling device if the test object fails.

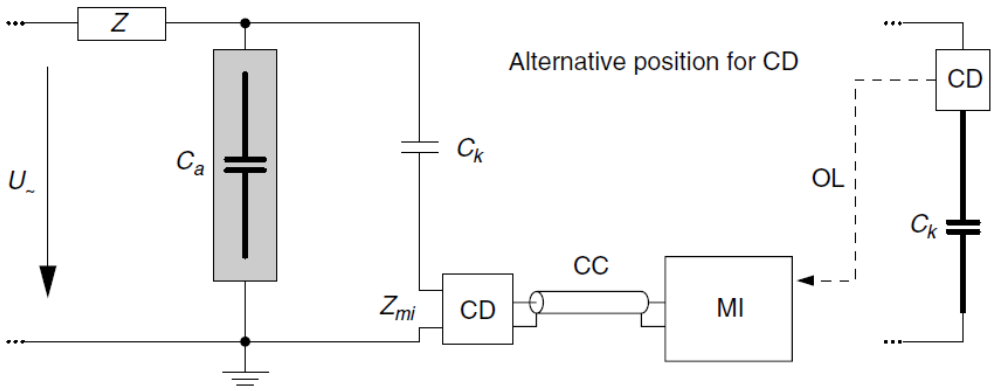

(a) Coupling device CD in series with the coupling capacitor

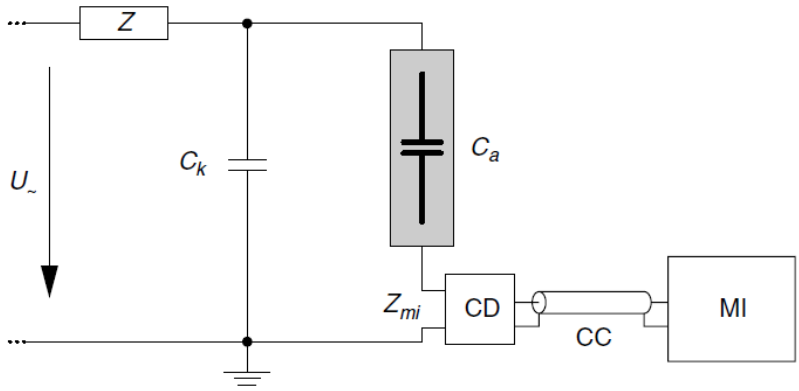

(b) Coupling device CD in series with the test object

$U_{\sim}$	high-voltage supply	C_k	coupling capacitor
Z_{mi}	input impedance of measuring system	CD	coupling device
CC	connecting cable	MI	measuring instrument
OL	optical link	Z	filter
C_a	test object		

Figure 2.13: Typical PD measurement connections [69]

2.5 Surface Discharge Modelling Approach

2.5.1 Physical Model of Oil-pressboard Interface

The microscopic view of a pressboard edge shown in Figure 2.2 (b) suggests that the oil-pressboard interface is not a clean edge with the presence of dimples and individual fibres. Surface discharge experiments by Mitchinson et al [15] have shown that discharges at the oil-pressboard interface may occur in two paths due to dual

colouration during the full discharge phenomenon as shown in Figure 2.14. The condition of pressboard edge and dual colouration nature suggest that the oil-pressboard interface is complex. Based on these observations, Mitchinson et al [15] have proposed a physical model of the oil-pressboard interface as shown in Figure 2.15. This thesis will model the surface discharge phenomenon at the oil-pressboard interface by adopting this physical model.

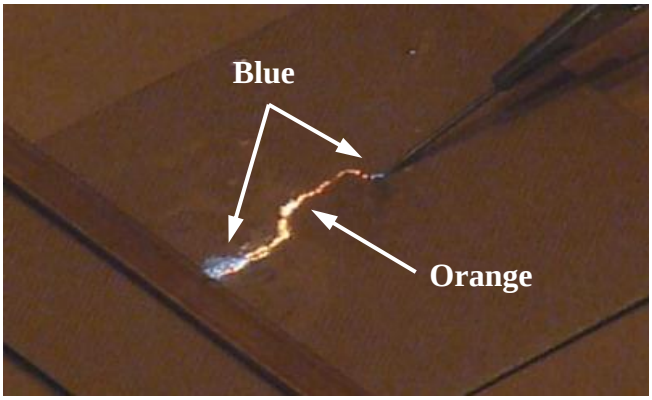

Figure 2.14: Full discharge with dual colouration during surface discharge experiment [15]

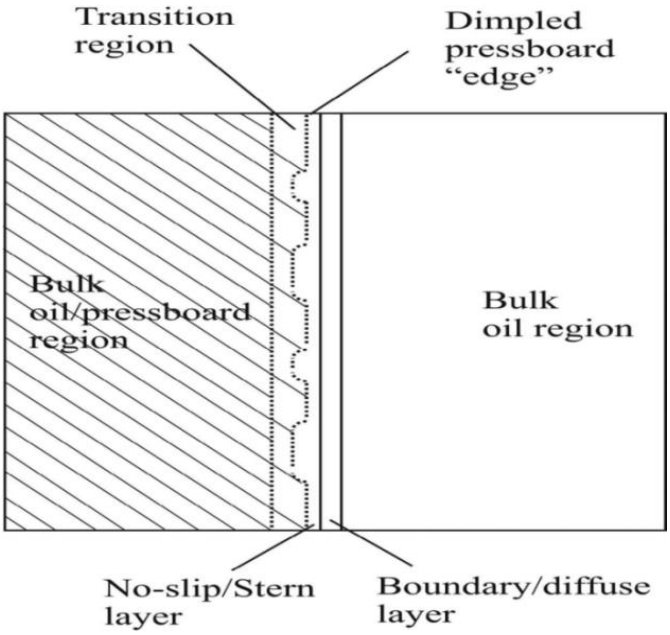

Figure 2.15: Physical model of the oil-pressboard interface [15]

The physical model shown in Figure 2.15 proposes that in the bulk of oil-pressboard region, there exists a thin region called a transition region which is very near to the boundary of the pressboard surface. This is the region where dimples and individual

fibres are present. Meanwhile, in the bulk oil region, two important regions can exist, i.e. (1) no-slip region which is equivalent to the compact layer of electric double layer (EDL) – this is very close to the pressboard surface, (2) boundary layer that can be linked to the diffusion layer in the EDL model. In general, the EDL is a fundamental electrical phenomenon that describes the space charge profile at the interface in the liquid region when solid surfaces are brought into contact with a liquid [70, 71].

It has been suggested that the transition region and no-slip region are places where the mingling of oil molecules, pressboard, and other species (such as water) occurs. Hence, this provides a region for space charge to accumulate and drift toward the region of lower field intensity [15]. With respect to Figure 2.14, both the transition region and no-slip region have been suggested as the first path (orange colour) for the discharges, whilst the second path (blue colour) of discharges occurs in the boundary layer. This second path is also a path where breakdown discharge may occur in oil at higher energy levels.

Based on the literature, in order to model the discharge related phenomena at the oil-pressboard interface in power transformers, i.e. static electrification and pre-breakdown streamer, researchers have emphasised three key parts in the model. These are (1) the governing equations in the oil region, (2) an assumption for the insulation status of the pressboard, i.e. perfectly or non-perfectly solid insulator and (3) the boundary condition at the oil-pressboard interface. Hence, the following sections will discuss these aspects.

2.5.2 Governing Equations in Oil

The charge transport continuity equation has been widely used to model the behaviour of charge carriers, i.e. positive and negative ions and electrons in dielectric system. In the case of dielectric liquid in power transformers, the equation has been used to study the static electrification problem at the oil-pressboard interface [72, 73, 74] and streamer propagation for breakdown mechanism under step or impulse voltages without [59, 75, 76, 77, 78, 79] and with [59, 80] pressboard. In general, the charge transport continuity equation can be expressed as:

$$\frac{\partial N_i}{\partial t} + \nabla \cdot \vec{F_i} = G_i - R_i \tag{2.3}$$

Where N_i is the density of each charge carrier (mol·m^{-3}), i.e. positive or negative ion or electron and $\vec{F_i}$ is the total flux density vector (mol·m^{-2}·s^{-1}) due to the movement of each charge carrier. The right hand side of the charge continuity equation depicted in Equation (2.3) is the source term which depends on the generation, G_i and recombination, R_i of the ionic species. The total flux density vector for each charge carrier can be expressed as:

$$\vec{F_i} = -D_i \nabla N_i \pm N_i \mu_i \vec{E} + N_i \vec{u} \tag{2.4}$$

Where D_i is the diffusion coefficient (m^2·s^{-1}) for each charge carrier, $\vec{E}$ is the electric field vector (V·m^{-1}), μ_i is the mobility (m^2·s^{-1}·V^{-1}) for each charge carrier and $\vec{u}$ is the fluid velocity (m·s^{-1}). The first term on the right hand side of Equation (2.4) represents the movement of the charges due to the diffusion process and the second term accounts for the electro-migration of each charge carrier due to the influence of the electric field distribution of the system. The third term represents the movement of the charge carrier due to fluid convection (typically applied in the study of static electrification and neglected in the study of pre-breakdown streamer). It should be noted that the first term (diffusion term) is also usually neglected in the pre-breakdown streamer model due to the dominant role played by the migration current contributed by each charge carrier. The '$\pm$' sign for the migration term in Equation (2.4) accounts for the direction of charge migration, whereby, the '$+$' sign is used for positive ion and the '$-$' sign is used for negative polarity charge carriers (negative ion and electron).

In order to determine the electric field distribution, the charge transport equations for each charge carrier are coupled with Poisson's equation:

$$\nabla \cdot (-\varepsilon_0 \varepsilon_r \vec{E}\,) = \left(N_p - N_n - N_e\right) q N_A \tag{2.5}$$

Where ε_0 and ε_r are the permittivity of free space (8.854×10^{-12} F·m^{-1}) and relative permittivity of the material respectively, N_p, N_n and N_e are the density of positive ions, negative ions and electrons (mol·m^{-3}) respectively determined from the charge transport

equation (Equation (2.3)). Also, q is the elementary charge (1.6022×10^{-19} C) and N_A is the Avogadro's number (6.023×10^{23} mol^{-1}).

Charge generation plays an important role in the conduction mechanism in a dielectric liquid such as transformer oil. For modelling purposes, this is described by the generation term G_i in Equation (2.3). Electric field dependent ionic dissociation theory has been used by Gafvert et al [81, 82] to predict electric field distribution as a result of high voltage application in mineral oil with and without pressboard using a plane-plane electrode. In their work, the simulated electric field distributions agree with the electro-optic Kerr measurements. In addition, Gafvert et al [82] showed that, by using the charge transport model, the simulation result can predict the experimental data better than the ohmic model. The electric field dependent ionic dissociation theory, developed by Onsager [83] explains the effects of external electric field on the conductivity of dielectric liquid in general. Based on this theory, a dielectric liquid contains a certain density of neutral ion pairs, N_0 (mol·m^{-3}) and an equal density (mol·m^{-3}) of free positive ions, N_{p0} and negative ions, N_{n0}. Without an external electric field, the dissociation of neutral ion pairs and recombination of positive and negative ions depend on two kinetic rate constants, i.e. dissociation rate constant, K_d (s^{-1}) and recombination rate constant, K_r (m^3·mol^{-1}·s^{-1}). The charge generation approach without external voltage application is typically used in the study of static electrification [72, 73, 74]. With the presence of external electric field, the dissociation rate constant K_d is a function of electric field:

$$K_d = K_d^0 f(|\vec{E}|) \tag{2.6}$$

Where K_d^0 is the zero field dissociation constant (s^{-1}) and $f(|\vec{E}|)$ is the electric field dependent function, which relates the increase in the dissociation rate to the electric field level. The electric field dependent function is defined as:

$$f(|\vec{E}|) = \frac{I_1(4b)}{2b} \tag{2.7}$$

Where,

$$b = \sqrt{\frac{q^3|\vec{E}|}{16\pi\varepsilon_0\varepsilon_r k^2 T^2}} \tag{2.8}$$

I_1 is the modified Bessel function of the first kind, k is the Boltzmann's constant (1.38×10^{-23} J·K^{-1}) and T is the absolute temperature (K).

In thermal equilibrium without any external electric field stress, the relation between dissociation and recombination can be described as:

$$N_0 K_d^0 = N_{p0} N_{n0} K_r \tag{2.9}$$

Therefore, when considering Equation (2.6) and Equation (2.8), the charge generation rate $G_D(|\vec{E}|)$ (mol·m^{-3}·s^{-1}) based on the Onsager theory can be formulated as:

$$G_D(|\vec{E}|) = N_{p0} N_{n0} K_r f(|\vec{E}|) \tag{2.10}$$

On the other hand, in an attempt to model streamer propagation in mineral oil using COMSOL Multiphysics, a finite element analysis software package, O'Sullivan et al [75, 84] showed electric field dependent ionic dissociation is unlikely to be the crucial mechanism to streamer development in transformer mineral oil because the dissociation of ions only occurs in the region close to the needle tip (HV electrode). It should be noted that discharges during the initiation and propagation of streamers are associated with PD events in the dielectric liquid [85]. Therefore, since this thesis deals with modelling of surface discharge at the oil-pressboard interface that involve creeping streamer along the pressboard surface, the charge generation mechanism due to electric field enhanced ionic dissociation has not been considered in the model.

Recently, research in the modelling of pre-breakdown streamers in dielectric liquids has shown progress through the use of an electric field dependent molecular ionisation theory based on Zener theory of electron tunnelling in solids [86] as the charge generation mechanism. The mechanism of field dependent molecular ionisation explains the generation of electrons and positive ions under the influence of an electric field, thus making it very different compared to the mechanism of field dependent ionic

dissociation already discussed. By using point-rod electrode configuration and applying a step voltage, O'Sullivan et al [75, 76] have shown that the electric field dependent molecular ionisation is the key mechanism for streamer development in transformer oil. Then, with similar electrode geometry and voltage type, Hwang et al [59, 78] extended the work on various types of mineral oil and also explained the physics of fast mode streamers as well as considering an oil-pressboard interface in the model [59]. A further extension by Jadidian et al [79, 80] has studied streamer propagation under lightning impulse voltage in mineral oil with and without pressboard. In general, for streamer development in an open oil gap, their simulation results using COMSOL Multiphysics agree with experimental data reported by others [55, 67] in terms of the velocity of streamer propagation. In an earlier work, Devins et al [87] also applied the Zener model to qualitatively explain the propagation of positive streamer in dielectric liquid from their experimental results. Experimentally, they successfully showed the field ionisation rate is proportional to the density of ionisable molecules and inversely proportional to the ionisation potential of the ionisable species. Eventually, the streamer velocity also increases. Based on the Zener model [86], the charge generation rate $G_F(|\vec{E}|)$ (mol·m^{-3}·s^{-1}) can be expressed as:

$$G_F(|\vec{E}|) = \frac{N_0 q a |\vec{E}|}{h} exp\left(-\frac{\pi^2 m^* a \Delta^2}{q h^2 |\vec{E}|}\right) \tag{2.11}$$

Where N_0 is the density of ionisable species (mol·m^{-3}), a is the molecular separation distance (m), h is the Planck's constant (6.626×10^{-34} J·s), m^* is the effective electron mass (kg) and Δ is the molecular ionisation energy (J).

For a composite insulation system, Hwang et al [59] and Jadidian et al [80] have shown the importance of permittivity mismatch for surface flashover phenomenon along an oil-immersed dielectric. If the permittivity of the oil-immersed dielectric is higher than the oil, the streamer in oil tends to divert its direction towards the interface due to the charge transfer towards the interface. On the other hand, by matching the permittivity, the tendency of diversion towards the interface reduces. If the permittivity of the oil-immersed dielectric is lower than the oil, the streamer is forced to remain propagating in the oil rather than at the interface. This is due to the repulsive image charge in the oil-immersed dielectric [88]. In their work [59, 80], with the presence of oil-impregnated

pressboard that is in parallel orientation with the electric field (due to 2-D axial symmetry applied in the model, the pressboard was assumed as a tube), the simulation results have shown that the pressboard surface aids streamer development and increases the probability of breakdown. Under a perpendicular field orientation, the modelling results qualitatively agree with experimental work reported in [53, 64], i.e. the streamer propagates in oil from the needle towards the pressboard and as it touches the pressboard surface, it creeps along the surface. Also, the breakdown time increases (reduction in streamer velocity) once the streamer reaches the pressboard surface.

Based on models developed using COMSOL Multiphysics software, the field dependent molecular ionisation theory is considered for this thesis. It should also be noted that the modelling work in this thesis (Chapter 5), only considers positive streamers. This is due to the fact that for a negative streamer, the use of field dependent molecular ionisation model requires a higher voltage to initiate a streamer [77]. Since the experimental work applied a very much lower voltage to measure surface discharge at the oil-pressboard interface, the experiments are for lower electric fields compared to those required for negative streamer propagation to breakdown as reported in the literature. To model PD events due to a negative streamer requires another model preceding the field dependent molecular ionisation and is considered as one area for further development.

In addition to the generation mechanism, the generated charge carriers are also subject to recombination processes. The possible recombination processes that may occur include recombination between positive and negative ions, recombination between positive ions and electrons and electron attachment to neutral molecules (thus reducing the number of electrons and increasing the number of negative ions in the liquid dielectric). The coefficient rate of positive and negative ions recombination K_{rpn} ($m^3 \cdot s^{-1} \cdot mol^{-1}$) is determined using Langevin's equation [88]:

$$K_{rpn} = \frac{q}{\varepsilon_0 \varepsilon_r}(\mu_p + \mu_n)N_A \tag{2.12}$$

Where μ_p and μ_n are the mobility ($m^2 \cdot s^{-1} \cdot V^{-1}$) for positive and negative ions. The mobility of positive and negative ions has been measured to be 1×10^{-9} $m^2 \cdot s^{-1} \cdot V^{-1}$ [81]

and this value is used by many researchers in the study of static electrification [72, 73, 74] and pre-breakdown streamers [59, 75, 76, 77, 78, 79, 80].

Researchers from all over the world have measured hundreds of values for electron mobility in liquid hydrocarbons [89]. At room temperature (296 ± 2 K) the electron mobility for several liquid hydrocarbons can range from 0.01×10^{-4} to 100×10^{-4} $m^2\cdot s^{-1}\cdot V^{-1}$, which is very high ($1\times10^3$ to 10×10^6 times larger) compared to the mobility of positive and negative ions. The value of 1×10^{-4} $m^2\cdot s^{-1}\cdot V^{-1}$ has been typically used to model the pre-breakdown streamer in transformer oil. It should be noted that the Langevin's recombination theory is based on the concept of recombination cross-section [88]. If this theory is applied for the recombination between positive ions and electrons, the energetic electrons that move at higher mobility would lead to overestimation in the recombination coefficient value [75, 88]. Due to the overestimation problem, the models of streamer propagation in oil (discussed earlier in this section) have used the value of coefficient rate for positive and negative ions recombination K_{rpn} as the coefficient value for recombination between positive ions and electrons K_{rpe}. A similar approach has also been used in modelling pre-breakdown streamers in water [90]. Considering the recombination processes that have already been discussed, the recombination rate ($mol\cdot m^{-3}\cdot s^{-1}$) can be expressed as:

$$R_{pn} = N_p N_n K_{rpn} \tag{2.13}$$

$$R_{pe} = N_p N_e K_{rpe} \tag{2.14}$$

Where R_{pn} is the recombination rate between positive ions and negative ions and R_{pe} is the recombination rate between positive ions and electrons.

Electron attachment with neutral molecules may also occur in a dielectric liquid to form negative ions and reduce the number of electrons. Electron attachment is modelled via an attachment time constant, τ_a (s) to describe the lifespan of an electron in a dielectric liquid. This recombination model has been used in the modelling of pre-breakdown streamers in oil [59, 75, 76, 77, 78, 79, 80] and water [90] with the time constant of 2×10^{-7} s. The impact of electron attachment on the overall streamer propagation process is reasonably small due to the longer time scale for negative ions to be generated compared to the generation of positive ions and electrons due to field

dependent molecular ionisation [75]. The electron attachment rate, EA (mol·m^{-3}·s^{-1}) can be described as:

$$EA = \frac{N_e}{\tau_a} \tag{2.15}$$

2.5.3 Governing Equations in Pressboard

In the computational modelling of the oil-pressboard interface, the porous condition of pressboard has been considered by some authors [72, 73, 74, 82] and not by others [51, 59, 80, 91]. In 1977, Taylor [51] detailed the importance of surface geometry of a solid on the electric field stress enhancement at the interface region. No details on the model have been mentioned, but based on the computational power available at that time, it is believed that the model did not consider any charge carriers modelled using the charge transport equations as were used in more recent works [59, 72, 73, 74, 80, 82, 92]. The exclusion of surface roughness by recent authors is to simplify the computational run time and memory usage.

It has been recognised that most reported research that considers the porous structure of pressboard is related to static electrification problems in power transformers [72, 73, 74]. No validation work has been reported except by Cabaleiro et al [74]. Their model shows a qualitative agreement with experimental results. In general, the consideration of pressboard as a porous material leads to the pressboard being modelled as an imperfect insulator, i.e. ($\sigma \neq 0$). For example, the bulk conductivity of a pressboard at the temperature of about 20 °C is in the order of 1×10^{-14} to 1×10^{-12} S·m^{-1} depending on its moisture content [74, 93]. To consider the pressboard as a porous material, in the study of static electrification [72, 73, 74], the authors assume similar generation and recombination processes in the liquid region also occur in the pressboard region but with different parameter values. Cabaleiro et al [74], on the other hand, has also included the adsorption and desorption processes between the ionic species and free active cellulose radicals in the pressboard model. Since the study of static electrification involves oil convection, the pressboard is represented as a static fluid, thus the convective term in Equation (2.5) is neglected.

Gafvert et al [82] also consider the pressboard as a porous material in their reported model of an electric field distribution with validation using electro-optic Kerr measurement. To model the pressboard as porous material, they assumed similar processes in the oil region also occur in the pressboard but with different parameter values. With the assumption of low volume fraction of oil inside the oil-impregnated pressboard, charge generation due the electric field enhanced ionic dissociation is then neglected.

While all studies that consider the pressboard as a porous material are not related to pre-breakdown streamer, works by Hwang et al [59] and Jadidian et al [80] using COMSOL Multiphysics, a finite element analysis (FEA) software package, have particularly modelled pre-breakdown streamers at the oil-pressboard interface without taking account of the pressboard as a porous material. The pressboard has been assumed to function as a perfect insulator, i.e. the pressboard medium is set to have zero conductivity ($\sigma = 0$). Hence, the charge transport equations are only applied in the oil region and the current that flows through the pressboard is purely displacement current. These models have considered some crucial points for boundary setting that are discussed in the next section.

2.5.3 Boundary Conditions

Boundary conditions at the interface play an important role in the charge and electric field behaviour at the interfacial region. With the assumption that pressboard is a porous material [72, 73, 74, 82], the boundary condition for the charge transport equation at the interface is set to be continuous and consequently the difference in flux on either side of the boundary is zero, i.e.:

$$\hat{n} \cdot \left(\overrightarrow{F_{oil}} - \overrightarrow{F_{pb}}\right) = 0 \tag{2.16}$$

Where $\hat{n}$ is the unit vector normal to the boundary and $\overrightarrow{F_{oil}}$ and $\overrightarrow{F_{pb}}$ are the total flux density vectors ($mol \cdot m^{-2} \cdot s^{-1}$) in oil and pressboard respectively. This formulation allows charge transfer between the two media.

On the other hand, by considering the pressboard as a perfect insulator, the boundary condition at the interface is such that two main cases can occur [59]:

Case 1: All volume charges (positive and negative ions and electrons) in the liquid travelling to the interface are impeded by the solid and remain as volume charges in the dielectric liquid, very near to the surface.

Case 2: All volume charges in the liquid travel to the interface and become surface charge.

The first case is a condition when the boundary condition for the charge transport equation at the oil-pressboard interface is set to zero normal flux, i.e.:

$$\hat{n} \cdot \vec{F_i} = 0 \tag{2.17}$$

If the model is dominated by migration current from each charge carrier (i.e. the second term on the right hand side of Equation (2.4), the boundary condition in Equation (2.17) leads to no conduction current flow at the interface, i.e. the oil's normal conduction current is zero at the interface. This boundary condition has been used by authors who study surface discharge at the air/gas-solid interface [94, 95, 96].

On the other hand, case 2 is a condition when the difference between fluxes on either side lead to a net flux density on the surface, i.e.:

$$\frac{\partial N_s}{\partial t} = \hat{n} \cdot \left(\overrightarrow{F_{oil}} - \overrightarrow{F_{pb}}\right) \tag{2.18}$$

Where $\frac{\partial N_s}{\partial t}$ is the time derivative of the surface charge density (mol·m^{-2}·s^{-1}). If the model is dominated by the migration current from each charge carrier, Equation (2.18) represents the flow of conduction current into the surface. Eventually, this current causes surface charge N_s (mol·m^{-2}) to be built up at the interface. This approach has been used by Hwang et al [59] and Jadidian et al [80] in the modelling of surface flashover at the oil-pressboard interface. It is worth noting that simulation work in [59] has also highlighted that the boundary condition for charge transport equations must be a conditional boundary condition to avoid an inherent error in COMSOL Multiphysics.

Since the model only accounts for the conduction current due to positive and negative ions and electrons, the normal component of the total positive ion flux density vector is:

$$\hat{n} \cdot \overrightarrow{F_p} = \begin{cases} 0 & if \quad \hat{n} \cdot \vec{E} < 0 \\ \hat{n} \cdot \overrightarrow{J_{c\_p}} & if \quad \hat{n} \cdot \vec{E} \geq 0 \end{cases} \tag{2.19}$$

The normal component of the total negative ion flux density vector is:

$$\hat{n} \cdot \overrightarrow{F_n} = \begin{cases} \hat{n} \cdot \overrightarrow{J_{c\_n}} & if \quad \hat{n} \cdot \vec{E} \leq 0 \\ 0 & if \quad \hat{n} \cdot \vec{E} > 0 \end{cases} \tag{2.20}$$

The normal component of the total electron flux density vector is:

$$\hat{n} \cdot \overrightarrow{F_e} = \begin{cases} \hat{n} \cdot \overrightarrow{J_{c\_e}} & if \quad \hat{n} \cdot \vec{E} \leq 0 \\ 0 & if \quad \hat{n} \cdot \vec{E} > 0 \end{cases} \tag{2.21}$$

Where, $\overrightarrow{J_{c\_p}}$, $\overrightarrow{J_{c\_n}}$ and $\overrightarrow{J_{c\_e}}$ are the conduction current density vectors ($mol \cdot m^{-2} \cdot s^{-1}$) due to the migration of positive ions, negative ions and electrons respectively.

The inherent error is caused by the boundary condition called zero diffusive flux:

$$\hat{n} \cdot (-D_i \nabla N_i) = 0 \tag{2.22}$$

that often used as an outlet for any particles to transport out by convection flow only. In order to uphold the zero diffusive flux condition, the COMSOL Multiphysics places numerical 'ghost' particles so that no diffusion across the boundary [59]. In the case of charged particles (for instance the electrons), if the normal electric field to the interface is positive (i.e. the electric field direction is outward of the surface), in order to sustain the zero diffusive flux boundary condition, the interface becomes an inlet for the electrons from the pressboard into the oil [59]. As a result, these electrons becoming the real charge and contributing to the total charge density in the oil region. This condition is illustrated in Figure 2.16.

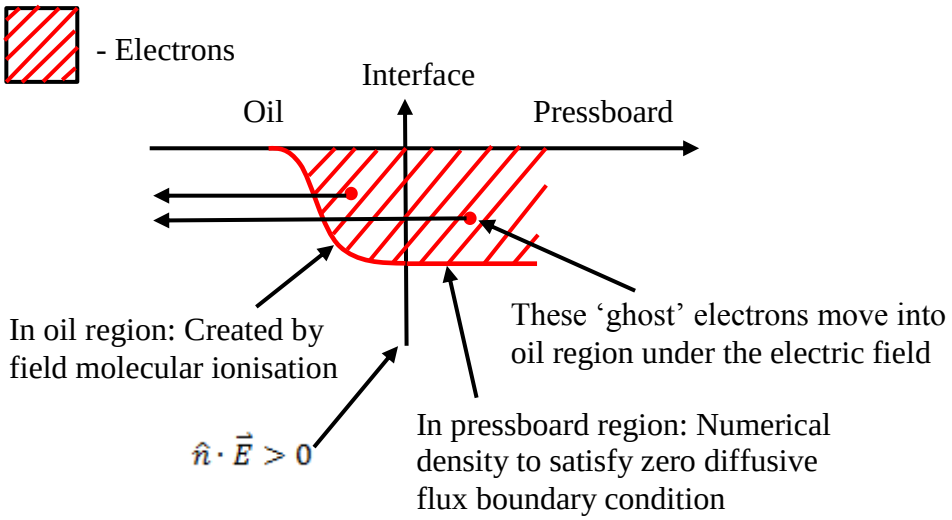

Figure 2.16: A pictorial example of an inherent error condition that might occur to enforce a zero diffusive boundary condition when the normal electric field to the interface is positive (amended from [59])

2.6 Summary

This chapter has summarised the research relevant to surface discharge at the oil-pressboard interface. The chemical properties of transformer oil and cellulose-based pressboard in general have been analysed. Each hydrocarbon group in the mineral oil contributes to the physical characteristics of the oil as a dielectric liquid for large transformers. Inter-fibre bonds determine the structural strength and geometry of pressboard that is porous with non-homogeneous surface structure. These features promote the usefulness of pressboard as an oil-impregnated solid barrier in a power transformer. However, such a composite insulation system has various issues at the oil-pressboard interface. These include degradation mechanisms as a result of chemical reaction particularly with the presence of contamination and degradation agents at the interface and the likelihood of failure mechanisms such as static electrification as a result of oil convection for cooling purposes as well as a reduction in surface flashover voltage due to creep stress along the oil-pressboard interface. Moisture at the interface is generally regarded as the key catalyst for the degradation and failure mechanisms.

Permittivity mismatch between oil and solid pressboard has been shown to cause a reduction in the surface flashover breakdown voltage level. Experimental data shows that the presence of an oil-pressboard interface in a perpendicular configuration with

respect to the dominant electric field direction will increase the level of 50% breakdown voltage compared to that of an open oil gap. In addition, it reduces the tendency of the streamer to speed up the moment the streamer reaches the pressboard surface. On the other hand, when the oil-pressboard interface is in parallel orientation with the electric field, the streamer propagation is enhanced by lowering the level of acceleration voltage (voltage level at which streamer changes from slow mode to fast mode), although the 50% breakdown voltage is similar to that in an open oil gap. Nevertheless, it appears that when moisture is present in the pressboard, the surface flashover voltage decreases slightly and there is significant reduction in the PDIV level. This shows the critical role of moisture in pressboard in enhancing creeping discharge phenomenon at the oil-pressboard interface.

Surface discharge at the oil-pressboard interface has been regarded as the most dangerous failure mode in a power transformer because it can cause a catastrophic failure under normal operating conditions. However, CIGRE has classified the probability of detecting this problem using two recommended methods, i.e. DGA and PD measurements, at a 'fair' level. This is quite worrying because there are many old power transformers with oil and pressboard as insulating material in operation. While experimental DGA data are in agreement with the 'fair' status classified by the CIGRE, it appears that not much PD data relating to surface discharge behaviour has been published, thus leading to a lack of information for condition monitoring purposes. Therefore, this thesis focusses on correlating PRPD data with the respective PD events during surface discharge at the oil-pressboard interface.

The porous structures within pressboard suggest that the oil-pressboard interface is very complex than one can expect. A physical model based on the microscopic view at the pressboard edge and dual colouration during a full discharge event has been proposed in a previous work at the University of Southampton. This thesis considers the physical model required to numerically study surface discharge behaviour at the oil-pressboard interface using COMSOL Multyphysics, a finite element software package. Electric field dependent molecular ionisation theory based on Zener model has been reported to be the important charge generation mechanism for streamer propagation in oil with or without pressboard. With some appropriate assumptions, the porosity of pressboard can be modelled by introducing similar governing equations in the oil into the pressboard. In addition, boundary conditions also play an important role with model performance.

Chapter 3

Surface Discharge Characteristics at the Oil-pressboard Interface under AC Voltage

3.1 Introduction

This chapter focuses on surface discharges at the oil pressboard interface by investigation of the characteristics of significant PD activity based on laboratory work. The development of surface tracking is accompanied by corona-like activity around the needle tip upon increasing the voltage level into the sustained PD discharge region [9] as well as the formation of white marks on the pressboard surface. The corona-like glow is a sign that ionisation and secondary avalanches are taking place [13, 14]. Surface discharges can be sustained for a long period without surface flashover or breakdown as long as the surface breakdown voltage is not exceeded [9, 15]. After long periods of surface discharge, full discharges may occur across the pressboard surface, bridging the high voltage electrode and the earth without resulting in a complete electrical breakdown [15]. The occurrence of this full discharge leads to a relatively small leakage current flowing to earth that is unlikely to trip protection systems such as leakage current relays. However, the occurrence and characteristics of the full discharge is still not fully understood. Thus, identifying their presence and relating them to PD activity at the oil-pressboard interface may provide a mechanism for early detection of inter-phase barrier board creep stress failure. The degradation behaviour of surface discharge at the oil-pressboard interface before the occurrence of a full discharge is studied based on different moisture levels in pressboard.

3.2 Experimental Setup

The surface discharge experiments were conducted in an oil bath with dimensions of 600 mm × 300 mm × 150 mm filled with 25 litres of transformer mineral oil containing approximately 18-22 ppm moisture. The moisture content in the mineral oil was measured using a coulometric Karl Fischer titration equipment. Figure 3.1 is a schematic diagram of the experimental setup. The experimental apparatus was placed in a faraday cage to reduce unwanted noise during PD measurement.

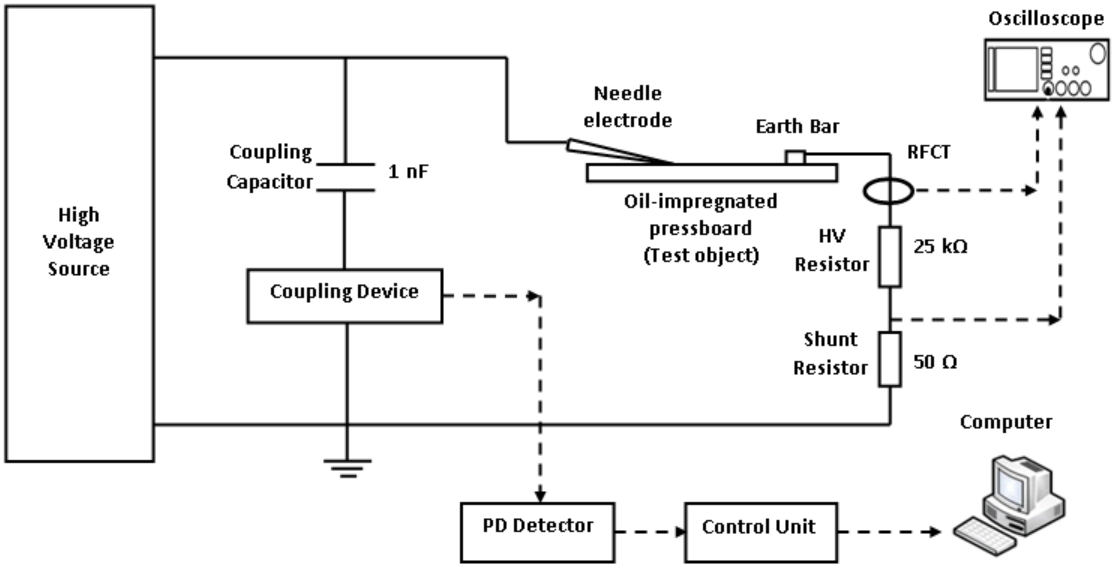

Figure 3.1: The Surface Discharge Experiment

3.2.1 Needle-bar Electrode Configuration

A needle-bar electrode configuration [12] has been used to promote surface discharges at the oil-pressboard interface. The needle discharge source is placed at an angle close to horizontal on the pressboard and at some distance from an earthed conductor bar which is also placed on the pressboard surface as shown in Figure 3.1. This configuration ensures a strong component of the field along the pressboard surface and minimises the vertical component of the field through the pressboard. A comparison study using 3-D geometry (70 μm of needle tip radius and 30 mm distance between needle tip and earth bar) in COMSOL software without the contribution of space charge has been conducted to investigate the effect of needle position in terms of its angle with respect to the pressboard surface. The simulation results of the electric field distribution

are shown in Figure 3.2. The results depict that decreasing the angle of needle electrode from perpendicular to the pressboard surface to 30° has caused the maximum value of electric field component that parallel with the pressboard surface to increase by 20% (from about 1.5×10^{8} V·m^{-1} to 1.8×10^{8} V·m^{-1}). The results also demonstrate that the maximum value of electric field component that perpendicular with the pressboard surface is reduced by 15% (from approximately 2×10^{8} V·m^{-1} to 1.7×10^{8} V·m^{-1}). Thus, it is reasonable to assume that the electrode configuration used in the experiment enhances surface discharges at the oil-pressboard interface. Moreover, this configuration also significantly reduces the possibility of the pressboard being punctured compared to a more traditional point-plane electrode configuration shown in Figure 2.10.

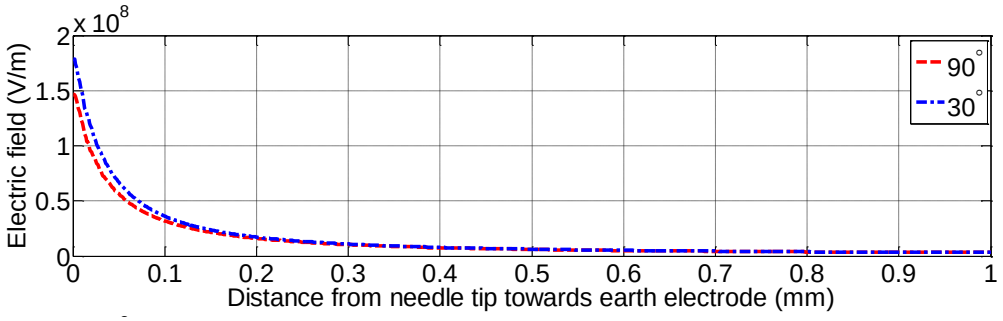

(a) Electric field component parallel with the pressboard surface

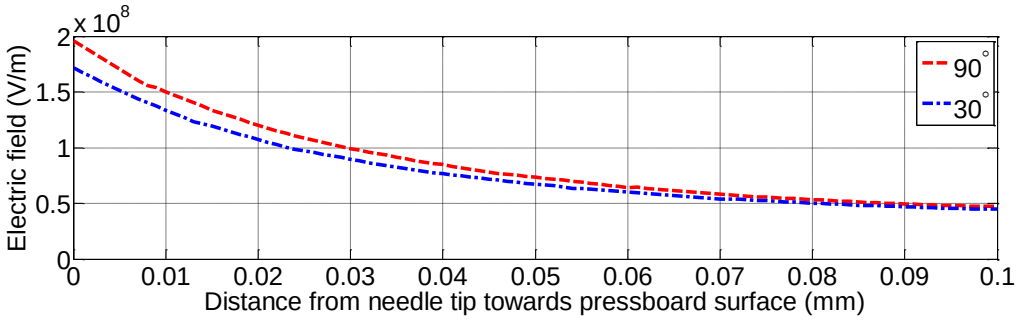

(b) Electric field component perpendicular with the pressboard surface

Figure 3.2: Distribution of electric field components based on different angles of needle electrode to the pressboard surface

3.2.2 Partial Discharge Measurement

An OMICRON Mtronix PD measurement system (MPD 600) [97] was used to monitor and record the PD measurement data of important events during the surface discharge experiment which includes corona-like discharges, formation of white marks and full discharges. The standard connection approach, to protect the coupling device if the test object fails [69] had been used whereas the coupling device is connected in series with the coupling capacitor as shown in Figure 3.1 instead of in series with the test object. As previously mentioned in the literature review, surface discharges can be sustained for a long period without surface flashover or breakdown if the applied voltage at the needle tip is above the surface PDIV but less than the surface flashover voltage. Therefore, the PD measurement system is also used to determine the PDIV of the pressboard surface. This approach allows the useful range of applied voltage to be determined.

3.2.3 Leakage Current Measurement

Two types of current transducer were used in the surface discharge experiment to measure the leakage current due to full discharge event (see Figure 3.1). The current transducers are a shunt resistor of 50 Ω and a radio frequency current transformer (RFCT). The RFCT works at a bandwidth of 10 kHz to 250 MHz. The leakage current was measured using a digital oscilloscope (DPO7254, 2.5 GHz, 40 GSample·s^{-1}).

For protection purposes, the power supply is equipped with a built-in overcurrent relay that is set to trigger if the secondary (HV side) current exceeds 20 mA. In addition, a HV resistor of 25 kΩ was used along with the shunt resistor to provide a voltage divider for current measurement. As depicted in Figure 3.1, the HV resistor is connected on the earth side rather than on the HV side of the experimental setup as normally used [37]. This is because the experiment was conducted to investigate the behaviour of surface discharges by stressing the oil-pressboard interface under constant root mean square (RMS) voltage at the needle tip. It should be noted that the previously reported full discharge event in [15] did not cause complete breakdown and was observed without the use of a HV resistor. Therefore, a reduction in the leakage current magnitude is expected with the use of a HV resistor. Coaxial line surge protectors were also used to protect the input stage of the oscilloscope via the shunt resistor and RFCT.

3.3 Experimental Procedure

3.3.1 Pressboard Sample Preparation

Clean pressboard of 1.5 mm thickness was cut into pieces of size approximately 100 mm × 100 mm. These pressboard pieces were then dried in accordance with BS EN 60641-2:2004 [98], i.e. drying in a ventilated oven at 105 °C for a minimum period of 24 hours. The samples were considered "dry" when the board mass was almost constant, i.e. a variation of ± 0.5% between two successive drying and weighing instants separated by one hour. To achieve a target percentage of moisture content, the dried pressboard samples were left under laboratory atmospheric conditions (i.e. air temperature of 17-18 °C and relative humidity (RH) of 85-95 %) to absorb moisture until the required mass increment were obtained from the dried condition. The conditioned pressboard samples were then placed in the test chamber as shown in Figure 3.3. The test chamber is equipped with vacuum functions for oil-pressboard impregnation processes. In the impregnation processes, a vacuum was drawn and stopped when the level of 20 mbar was reached. Then, the chamber was filled with the degassed clean mineral oil. The performance of the test chamber in oil-pressboard impregnation has been detailed in [9]. For the purpose of this research, four conditioned oil-impregnated pressboard samples were prepared, i.e. dry pressboard (less than 0.5 %) and pressboard conditioned to 3 %, 6 % and 9 % moisture content.

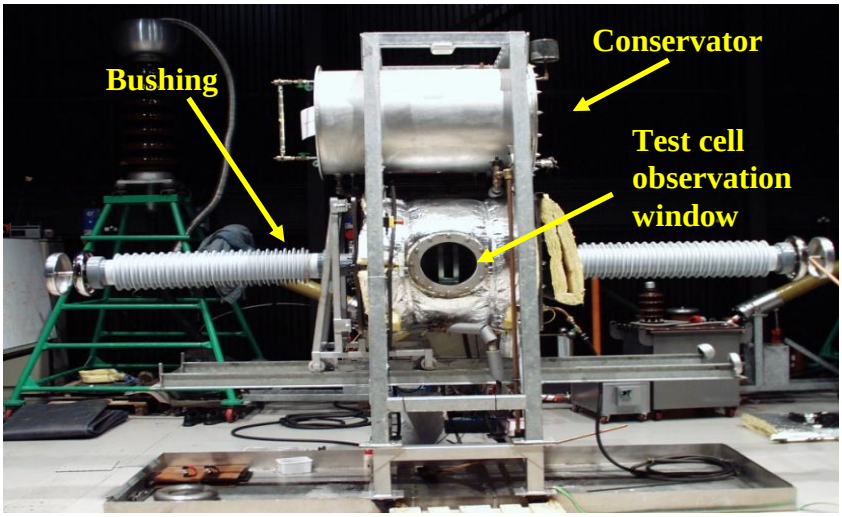

Figure 3.3: Side elevation of test cell showing observation window, conservator and bushings [9]

3.3.2 Level of Applied Voltage

The needle electrode and earth bar were placed 30 mm apart to limit the effects of flashover or breakdown on the measurement equipment. The appropriate voltage level for the experiment can be determined from the range between the PDIV and surface flashover voltage levels [9]. Therefore, prior to the surface discharge experiment, both the PDIV and surface flashover voltage levels were measured to establish the voltage range over which there is no immediate flashover or breakdown during the experiment at the specified distance and sufficient to facilitate surface discharging. Results presented in this chapter and Chapter 4 are based on surface discharge experiments under 30 kV of AC voltage for a period of 7 hours for each test unless stated otherwise. The value of 30 kV was selected based on the experience of using a lower voltage, i.e. 25 kV, where it took an extremely long period to see the first full discharge with pressboard having 6 % and 9 % (by weight) moisture content.

3.3.3 Data Collection

In general, two types of experiment were undertaken on the oil-impregnated pressboard samples. Firstly, a simple experiment was undertaken to examine the PD inception and flashover voltages for a predefined gap setting, (i.e. 30 mm) so that a suitable range of voltage for a second experiment, (i.e. the surface discharge experiment) could be established. Here, PD inception was defined as the voltage under which PD are initiated above the threshold of 20 pC which is four times higher than the usual background noise level for the experiment. The threshold value of 20 pC was chosen to ensure that it would be a consistent starting point to record PD data irregardless of oil/pressboard condition and level of background noise.

Subsequently, a series of surface discharge experiments were conducted on conditioned oil-impregnated pressboard to monitor and record any significant changes in the surface discharge behaviour based on the evolution of the PRPD pattern obtained from the PD measurement system. The bandwidth for the PD measurement system was set to 15 MHz ± 750 kHz, a non-standard bandwidth compared to the bandwidth proposed in IEC 60270 [69]. The selection of this bandwidth was based on the frequency domain that can be supported by the PD measurement system that is a best match with the frequency component of PD pulses during surface discharges at the oil-pressboard interface. This

will be discussed further in Section 4.4. A digital camera with ability to capture 24 frames per second (fps) was used to monitor and record any visual activity during the surface discharge experiment such as arcing at the needle tip and earth bar as well as capturing full discharge events. Hence, it is possible for imaged events to be correlated with the PD data obtained.

The full discharge event that leads to leakage current flow at the oil-pressboard interface is captured using an appropriate triggering method that is discussed in Section 4.2. Through this method, the characteristics of full discharge event can be analysed by means of leakage current measurement. Details on the full discharge event are discussed in detail in Chapter 4.

3.4 Results and Discussion

3.4.1 Partial Discharge Inception and Flashover Voltages

The PD inception voltage and surface flashover voltage for 30 mm gap between needle tip and earth bar as a function of pressboard moisture content are shown in Figure 3.4. The error bars for the PDIV and flashover voltage represent the standard deviation calculated using 20 and 3 statistical data respectively. The figure shows a voltage range between PD inception level and surface flashover level over which sustained PD exists without breakdown for different moisture levels within the pressboard. The establishment of this range provides an opportunity to conduct a surface discharge experiment with sustained PD without breakdown and consequently, the behaviour of surface discharge at the oil-pressboard interface can be investigated. Therefore, for the purpose of this research, an AC voltage level of 30 kV has been used in the surface discharge experiment, however, the observations from a preliminary experiment that used 25 kV AC voltage will also be discussed to aid understanding on the behaviour of surface discharges at the oil-pressboard interface.

With reference to Figure 3.4, for the dry pressboard, the ratio of flashover voltage to inception voltage is 1.72, whilst for pressboards containing moisture, the ratio is between 1.85 to 1.95. An initial hypothesis is that the presence of moisture in the pressboard has greater impact on PD inception than on breakdown voltage. It is also worth noting that

the flashover voltage for 3 % moisture is lower compared to the dry boards as noticed in Figure 3.4, which conforms the results reported in [37]. However, as the moisture level increases to more than 3 %, there is almost no change in the flashover voltage level. The latter supports the view in [15] that the occurrence of surface flashover at the oil-pressboard interface is in the free-oil boundary layer rather than along the transition zone/EDL/no-slip region where there is mixing of oil molecules, cellulose fibre and other species such as water. In terms of the PDIV level, significant reduction in the level is noticed for 3 % moisture in comparison with the dry ones. As the moisture level increases to greater than 3 %, there is slight reduction in the PDIV level. This indicates the importance of moisture in pressboard to initiate PD locally close to the needle tip.

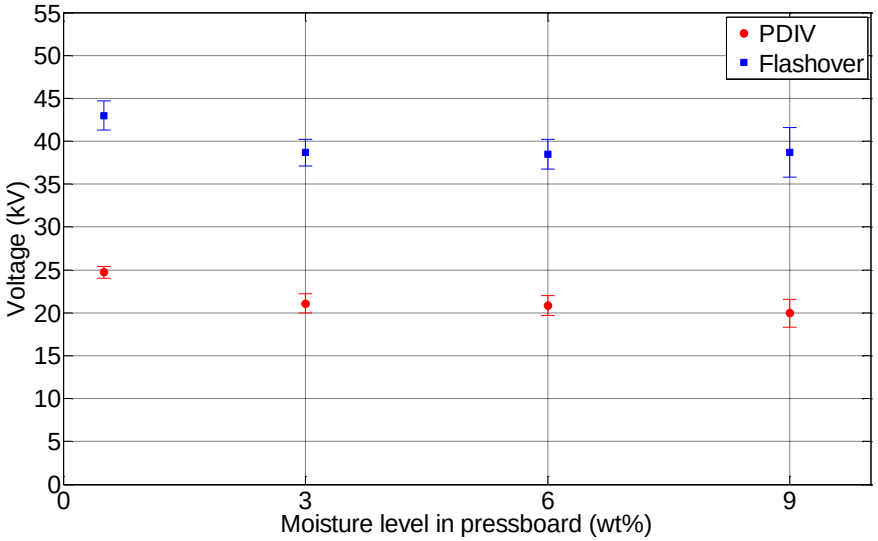

Figure 3.4: Partial discharge inception voltage and flashover voltage as a function of pressboard moisture content for 30 mm gap between needle tip and earth bar

3.4.2 Features of Surface Discharge Observed

The surface discharge activity at the oil-pressboard interface was observed from a series of surface discharge experiments that has been described earlier on different pressboard samples. In general, the surface discharge activity through this experiment was observed to be similar to that previously reported [15].

At the beginning of the experiment, intermittent discharge activity at the needle tip in the form of arc or glow discharges is normally observed as shown in Figure 3.5. This

discharge keeps on occurring throughout the experimental period. After a certain period of time, white marks on the pressboard surface start to develop and then grow from the discharge source towards the earth bar (see Figure 3.6). The formation of white marks indicates the drying and vaporisation processes [2, 11] associated with different states of water that exist in the pressboard [25, 27] due to localised heating. This hypothesis can be supported by the reduction in PDIV level for wet pressboard compared to the dry pressboard reported in [37], which is also observed in this work, as shown in Figure 3.4. In the case of wet pressboard, a low ionisation energy is required to initiate the PD due to the presence of water in the transition region of pressboard. Meanwhile, for dry pressboard, the high PDIV may be determined by water presence in the oil region [37] or a very small amount of water present adsorbed to the cellulose.

Typically, when the white marks nearly reach the earth bar, repetitive bluish arcing occurs at the earth bar to bridge between the earth and the white marks as shown in Figure 3.7. This suggests that the points where the white marks end have the highest point of electric field with respect to the closest earth point due to charge accumulation and that this is sufficient to cause earth arcing discharges. Charge accumulation is due to charge movement during the development and propagation of white tracking marks, hence, suggesting that the white marks are providing a conducting path for surface currents to flow. The earth arcing discharges lead to some of the accumulated charges to flow to earth, while the ionisation processes at the oil-pressboard interface are still on-going during the surface discharges. This might explain why the bluish arcing at the earth bar is repetitive with a dead-time between each arc from a few micro seconds to a few minutes. The bluish colour of these arcs suggests their occurrence at the free-oil boundary layer of oil-pressboard interface [15]. Thus, this might be the reason why the white marks in Figure 3.8 never reach the earth bar although several full discharges have occurred.

Then, there is a full discharge that is usually visible in the form of arcs that temporarily bridge the needle tip and the earth bar (see Figure 3.9) without tripping the protection system installed in the power supply used for the experiment. This kind of full discharge is regarded as the first full discharge before the occurrence of subsequent full discharges with similar characteristics. Full discharges are believed to occur in the transition/EDL/no-slip region following the path of the white marks and then in the free-oil boundary layer of the oil-pressboard interface [15] at the area close to the earth

bar. This is based on the dual-colouration of full discharges and observations after the experiment that the white marks are near but never touch the earth bar although several full discharges have occurred. As shown in Figure 3.9, even though the streamers have bridged the gap, full discharges are typically characterised by weakly luminous streamers and partial illumination along the streamer path which contradict with the breakdown event that has continuous and high illumination intensity of streamer between electrode gap [14, 15, 67]. These characteristics are similar to those reported in [55, 67, 99, 100] for the case of positive streamers bridged long gap in bulk oil that did not lead to breakdown recorded using a streak camera. Such characteristics have been believed to correspond to low conductivity of streamer channels [99] which might also be the case of full discharges at the oil-pressboard interface. However, since full discharges at the oil-pressboard interface only appear following the conductive path of white marks, it can be hypothesised that the illumination level might be dependent on the amount of accumulated charges at the oil-pressboard interface. Therefore, it is logical to think of the path of white marks containing non-uniform density of space charge as a result of swept and trap mechanisms during surface discharges.

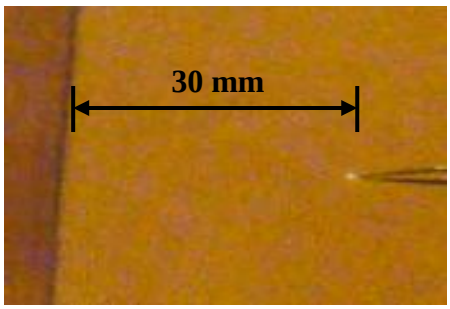

Figure 3.5: Arc discharges or glow at the needle tip

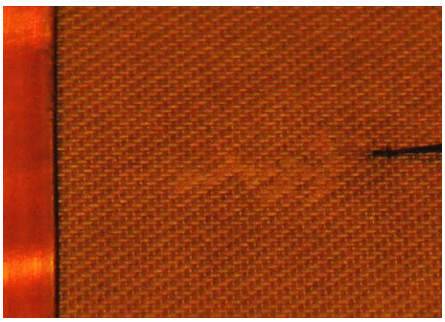

Figure 3.6: Initial growth of white marks

Figure 3.7: Arc discharges at the earth bar to connect the white marks

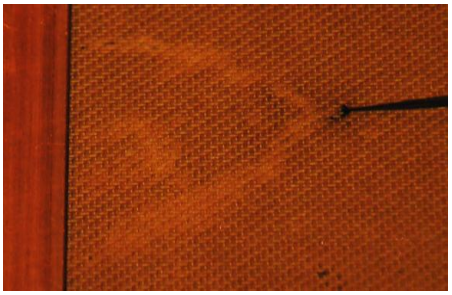

Figure 3.8: Pressboard surface conditions at the end of an experiment (after power off)

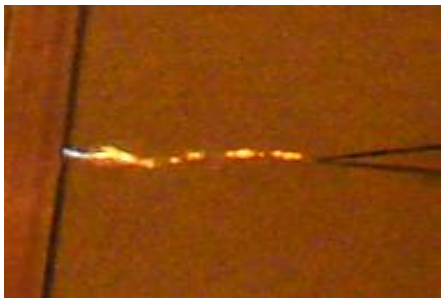

Figure 3.9: Full discharge without tripping the protection system

In order to aid understanding of the surface discharge behaviour, the processes in surface discharge are summarised in Figure 3.10. This figure represents the processes illustrated in Figures 3.5-3.9. The summarised processes suggest that the formation of white marks and their propagation from the needle tip toward the earth bar play an important role in surface discharge at the oil-pressboard interface until the occurrence of a first full discharge. Typically, immediately after the occurrence of full discharge, gas bubbles may arise from anywhere along the white tracking marks, suggesting that the full discharges are occurring in a gaseous phase. The appearance of these gas bubbles can be linked with the expansion of gases in the pressboard pores that are being pushed out due to charge movement during a full discharge event. The full discharge can re-occur with or without repetitive arcing at the earth bar and follows the same white

tracking marks or the continuous surface discharge creates new branch of white marks as a path for subsequent full discharges. The re-occurrences of full discharges will further degrade the condition of the pressboard surface. There are also black marks indicating carbonisation at the oil-pressboard interface which have also been reported in [15]. The carbonised surface follows the tracks of the white marks from the needle tip but does not necessarily extend along the whole distance. Another feature is random production of tiny gas bubbles and smoke that are observed near to the discharge tip and at the earth bar during arcing events. These phenomena are most likely caused by a rise in temperature of the needle tip that is large enough to cause local evaporation of the more volatile element of the mineral oil.

(a)	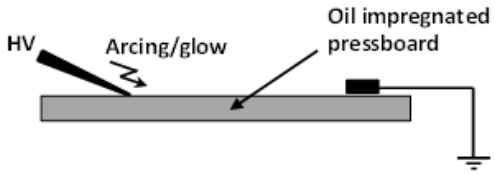	• Early stage • Arcing discharge or glow at the needle tip (Figure 3.5)
(b)	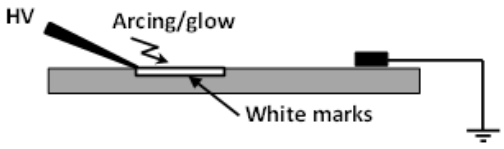	• White marks develop and propagate towards the earth electrode (Figure 3.6) • Rare occurrence and very low light intensity of arcing discharge or glow at the needle tip
(c)	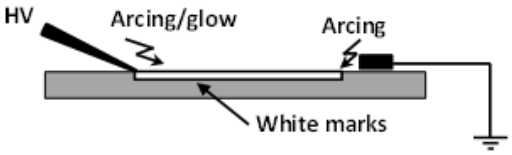	• White marks almost reach the earth electrode (Figure 3.8) • Repetitive bluish arcing discharge at the earth electrode to bridge between the earth and the white marks which can continue for a few seconds or minutes (Figure 3.7)
(c)	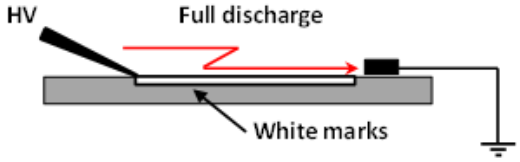	• Full discharge event (Figure 3.9) • Can re-occur with or without repetitive earth arcs

Figure 3.10: Processes in surface discharge at the oil-pressboard interface until the occurrence of first full discharge

3.4.3 Surface Discharge Behaviour in Correlation with Measured Data on Different Moisture Level in Oil-impregnated Pressboard

The importance of characterising the partial discharge condition in a large power transformer has been discussed earlier in Section 1.2.3. Throughout the research, correlation between PD activity and measured data for different moisture levels in pressboard have been undertaken and classified against the processes depicted in Figure 3.10. In reality, these processes may be expected to continue within HV oil-pressboard insulation systems found in HV plant from minutes to months or even years until the occurrence of a first full discharge which may be detected by the protection system. This depends on the severity of the full discharge event and is governed by many parameters such as the tip of discharge source, voltage level (higher in practical application), electric field distribution (lower in practical application) and contamination condition of the oil and pressboard. Therefore, analysing the measured data relating to observed processes for pressboards having different moisture levels is important to develop diagnosis and to characterise the defects in a HV power transformer for the purpose of condition monitoring and ultimately to facilitate the development of a prognostic programme.

The PRPD patterns for the early stage (Figure 3.10 (a)) of the surface discharge experiment for different moisture levels in the pressboard are shown in Figures 3.11-3.14. The data were obtained after 5-10 minutes of the experiment and very similar data can be observed for several minutes to hours dependent on the pressboard moisture level and random localised PD activity. For all data, the PD events occur in the first and third quadrants of the AC voltage cycle as well as at the peak of positive and negative half cycles indicating there are both surface discharge and corona-like activities. The discharge magnitudes are greater at the negative peak.

By comparing the results at the early stage for different moisture levels, it is clear that as the moisture level increases, the number of discharge events increase and there are PD events initiate earlier in phase, i.e. at lower voltages for each half cycle. This could be due to the influence of the constructive superposition effect [101] between the electric field from space charge accumulation at the oil-pressboard interface and the external electric field at the needle tip. Therefore, lower PD inception levels were recorded on the PRPD pattern compared to the PDIV level shown in Figure 3.4 that was

determined before the surface discharge experiments were started. The results for the early stage of the surface discharge experiment depict the increment in severity level of defects at the oil-pressboard interface as moisture level in the pressboard increases.

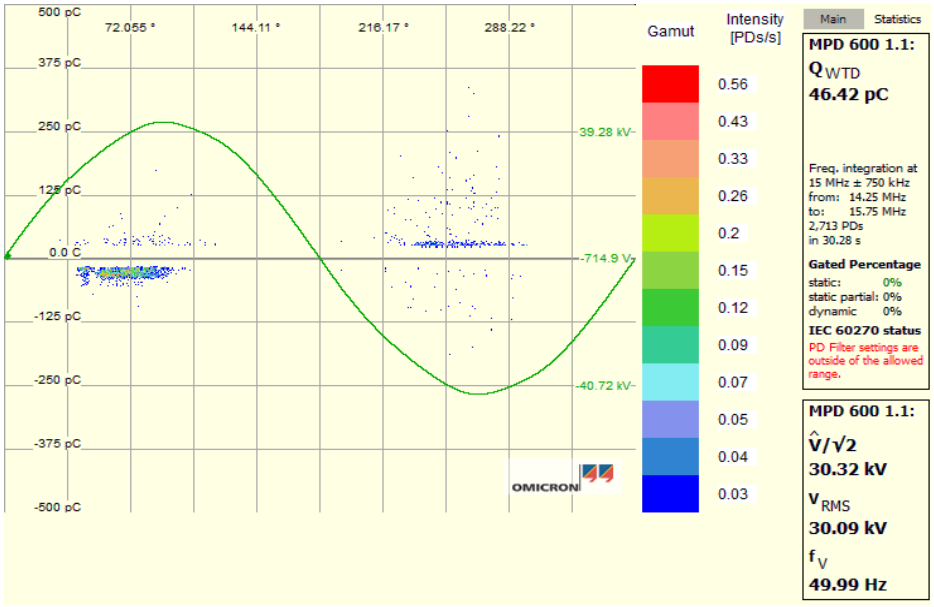

Figure 3.11: PRPD for the early stage on dry pressboard for a period of 30 s

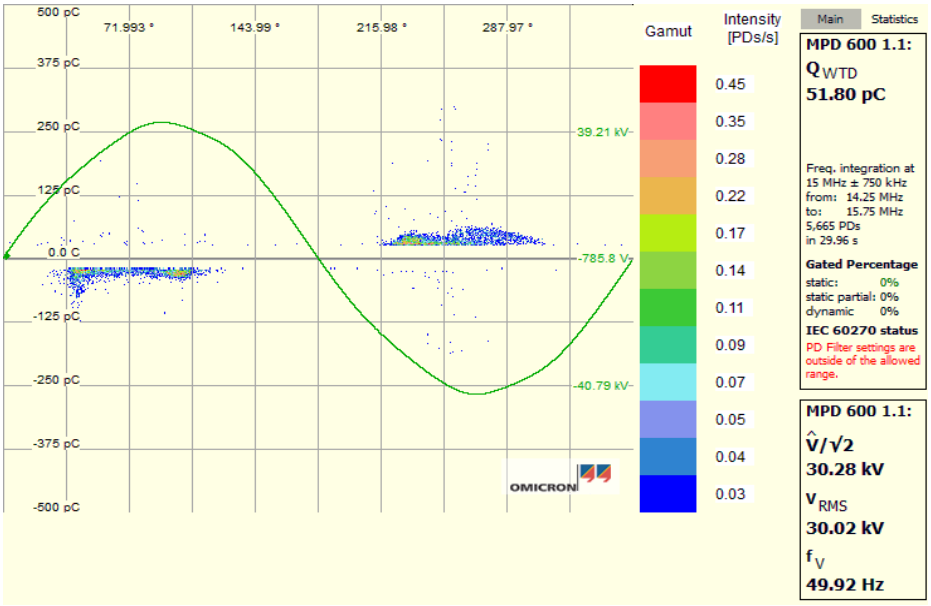

Figure 3.12: PRPD for the early stage on 3 % moisture pressboard for a period of 30 s

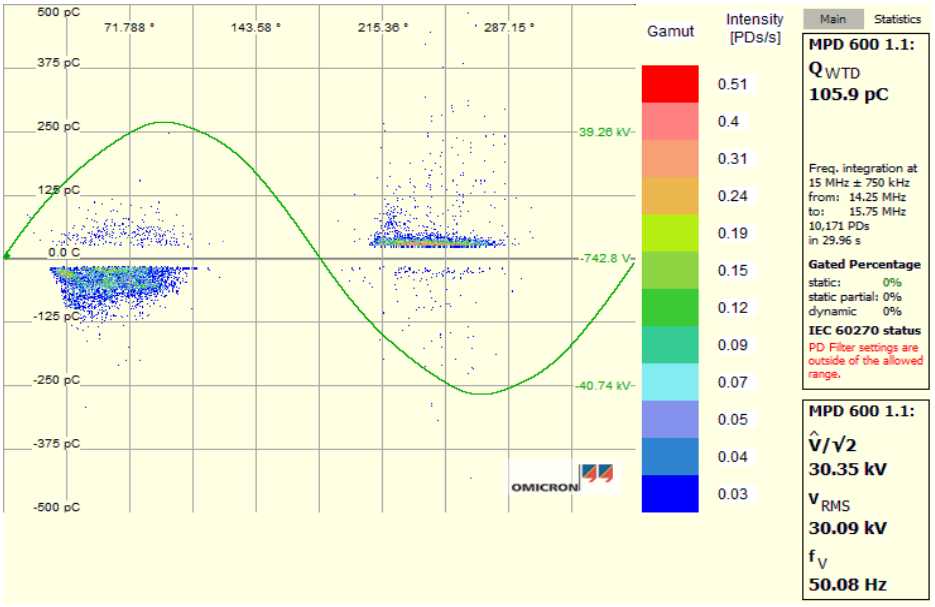

Figure 3.13: PRPD for the early stage on 6 % moisture pressboard for a period of 30 s

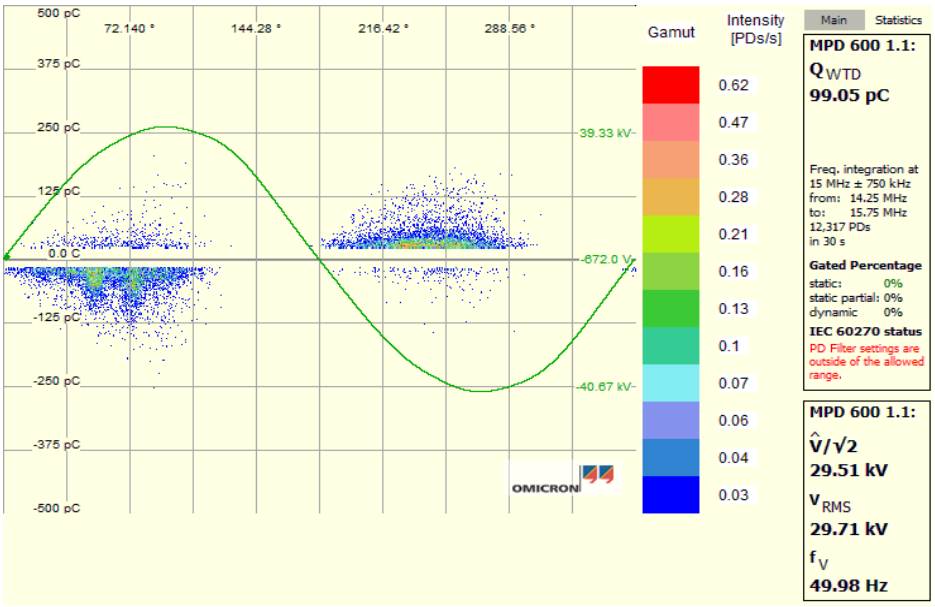

Figure 3.14: PRPD for the early stage on 9 % moisture pressboard for a period of 30 s

After a certain period which is normally once the white marks have developed over half of the gap distance or more (Figure 3.10 (b)), there are changes in the PRPD results. Typically, the discharge magnitudes reduce as depicted in Figures 3.15-3.18. For every moisture level, the PRPD pattern indicates the PD events consist of surface discharge and corona-like activities at lower discharge magnitudes compared to those noticed during the early stages of the surface discharge experiment (see Figures 3.11-3.14). It is also noted that the inception voltages for every half cycle increase whereby most of the

PD events occur later in phase compared to those obtained during the early stage of the experiment. Moreover, the discharge number also decreases when compared to the early stage data for the respective moisture level. There are no significant differences among the wet pressboards (comparison between Figures 3.16, 3.17 and 3.18) when the white marks have propagated over half of the gap distance. However, the discharge number for dry pressboard is very much lower than the number of PD events recorded for the wet pressboard.

It is important to highlight that the changes in PRPD data from Figures 3.11-3.14 to Figures 3.15-3.18 are comparable to the problem reported previously [8] that there was a falling trend from the monitoring data history of a large power transformer, but, eventually it suffered from an unexpected fault. These findings also support the suggestion to revise the usual practice in condition monitoring to associate a decreasing trend or the absence of an increasing trend as a healthy condition [6]. Figure 3.19 shows an example of a decreasing trend of average discharge data history obtained from the surface discharge experiment from the initial stage of the experiment until the white marks have propagated about halfway of the gap distance. After approximately 30 minutes of electrical stress, the mean discharge value decreased dramatically to approximately 37 pC (typically less than 50 pC) as clearly shown in Figure 3.20. Sometimes, this value can be as low as 15 pC which is less than the defined PD threshold setting, i.e. 20 pC.

The changes in PD activity (comparing Figures 3.11-3.14 and Figures 3.15-3.18) might be due to increases in the destructive superposition between the high electric field from space charge accumulation at the interface and the external electric field at the needle tip. This is probably due to the fact that the formation of white marks increases the surface conductivity and leads to changes in the distribution of external electric field among the needle tip and the white mark branches. Therefore, the field distribution leads to a reduction in external electric field due to surface current flow along the white marks and ultimately increases the effect of destructive superposition in electric field. However, since the external field is still higher than the space charge field, the propagation of the white marks will continue towards the earth bar.

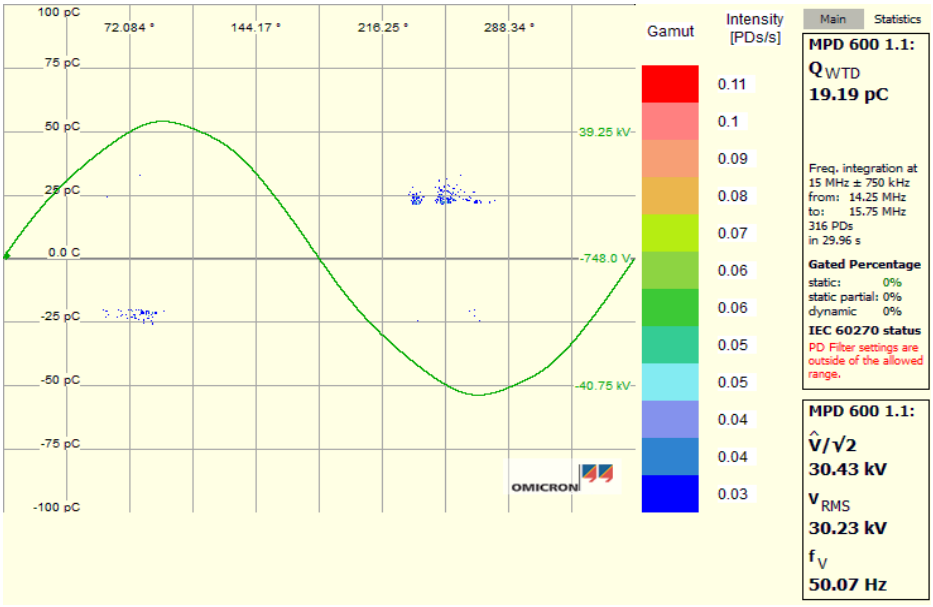

Figure 3.15: PRPD when the white marks have developed about halfway across the 30 mm gap on dry pressboard for a period of 30 s

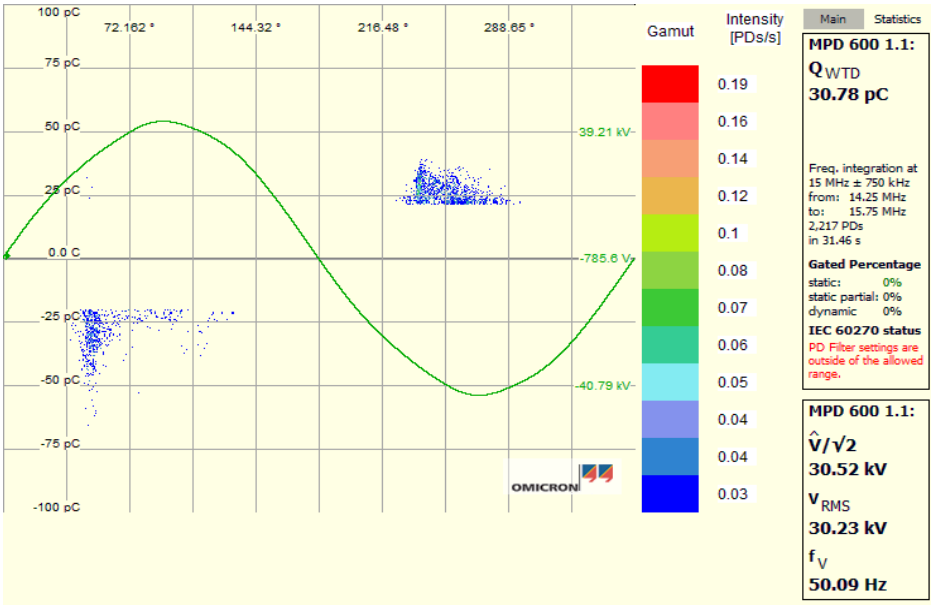

Figure 3.16: PRPD when the white marks have developed about halfway across the 30 mm gap on 3 % moisture pressboard for a period of 30 s

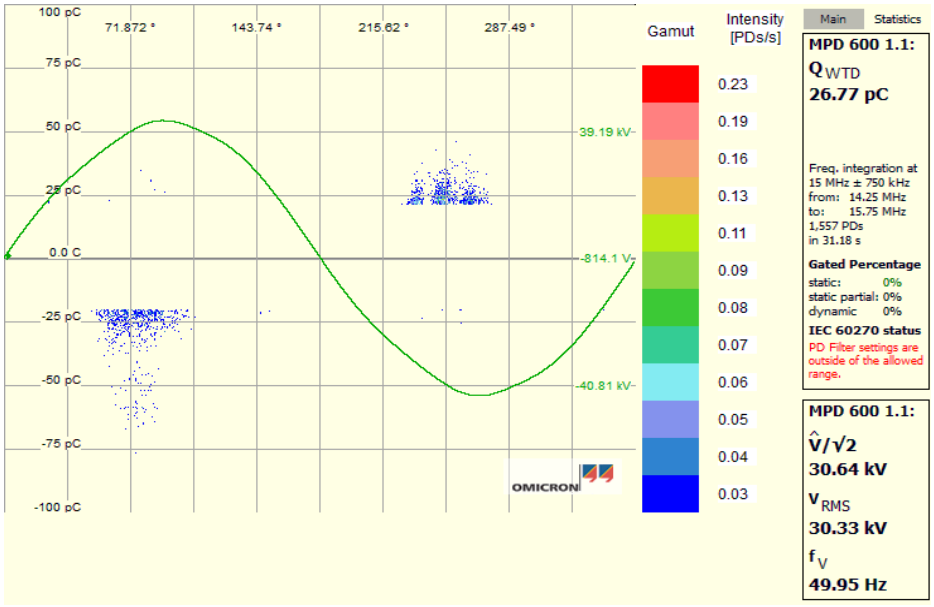

Figure 3.17: PRPD when the white marks have developed about halfway across the 30 mm gap on 6 % moisture pressboard for a period of 30 s

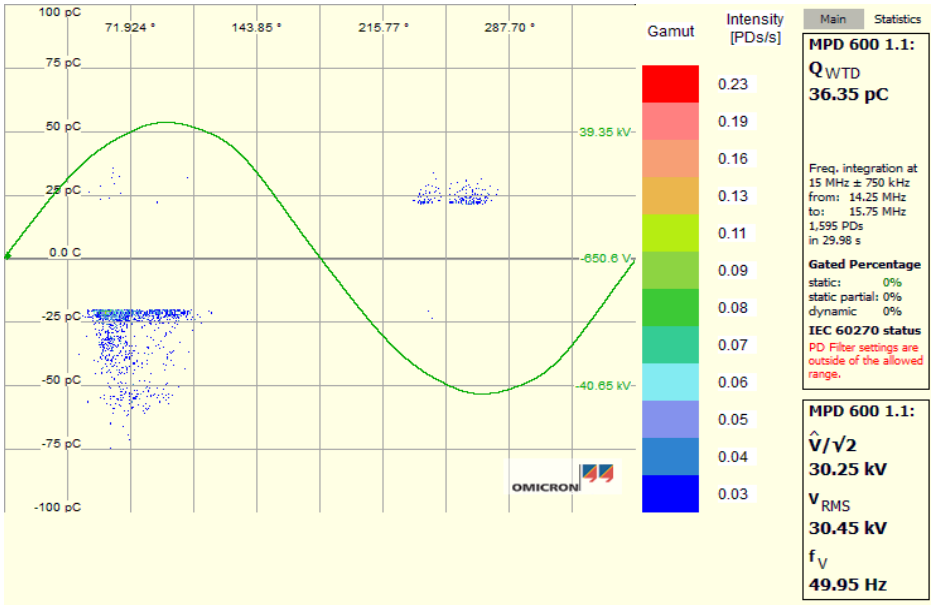

Figure 3.18: PRPD when the white marks have developed about halfway across the 30 mm gap on 9 % moisture pressboard for a period of 30 s

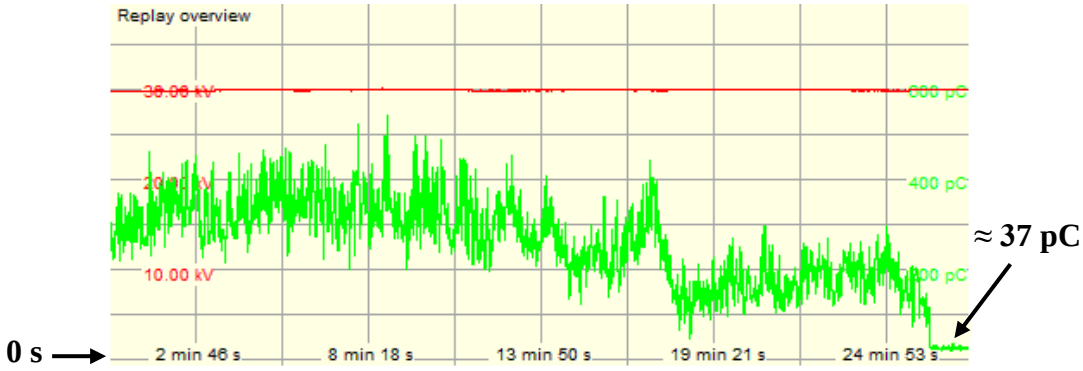

Figure 3.19: History of mean discharge data from the initial stage of the surface discharge experiment until the white marks have developed about halfway of across the 30 mm gap

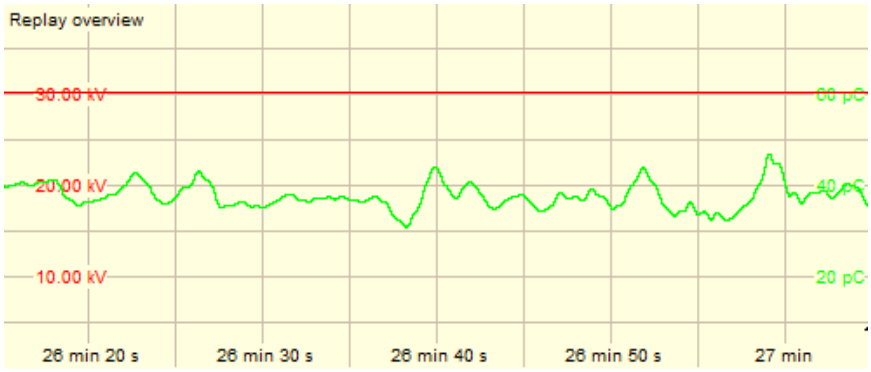

Figure 3.20: History of mean discharge data after the white marks have developed about halfway across the 30 mm gap (zoomed-in of the last part in Figure 3.19)

Correlation between the arcing events (Figure 3.10 (c)) and the respective PRPD data have also been undertaken. There is no significant difference in the PRPD data between the different moisture levels of pressboard. Figure 3.21 shows two different PRPD results obtained during which there are repetitive arcs at the earth bar. The figure shows that the PD events occur in the first and third quadrants of the AC voltage cycle signifying there are surface discharges. However, in Figure 3.21 (a) there are high magnitudes of PD events at the peak of positive and negative half cycles, whilst in Figure 3.21 (b), only at the positive peak as arcing event at the earth bar were observed. This indicates that the arcing events at the earth bar are high magnitude corona-like events with positive streamer phenomenon or both positive and negative streamers in nature.

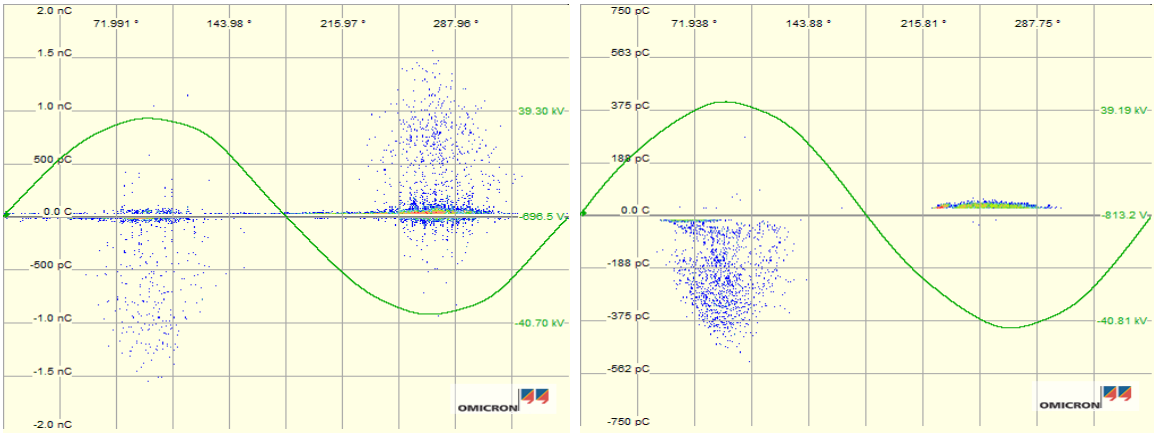

(a) High PD magnitude at the peak of both half cycles (PRPD data for 15 s)

(b) High PD magnitude only at the peak of positive half cycle (PRPD data for 21 s)

Figure 3.21: Different PRPD data during which several repetitions of arcing events at the earth bar occurred

It should also be noted that there are PD activities before the zero crossing of the AC cycle, i.e. at both second and fourth quadrants which is believed due to degradation at the oil-pressboard interface. This can be explained by excessive space charge accumulation at the interface that increases the interface conductivity until the occurrence of an arcing event at the earth bar that causes a conduction at the oil-pressboard interface between the needle tip and the earth bar for a very short time interval (period of one or more PD pulses due to arcing events, i.e. a few microseconds). As a result, there is a constructive electric field between the external field and space charge field before the zero crossing points [101]. Throughout the experiment, PD activities at the second and fourth quadrants only appear once there are earth arcing events to connect the first white mark channel to approach the earth bar. For all tested pressboards, starting from this time, the occurrence of PD activities before zero crossing points can occur and disappear alternately until the end of the experiment due to the movement of space charge over the gap distance.

The arcing event at the earth bar can continue for a few seconds to minutes. Consequently, there is a first full discharge that bridges the gap between the needle tip and the earth bar (see Figure 3.10 (d)). There is no significant difference that can be deduced from the PRPD data for different moisture levels in the pressboard. An example of the PRPD data during which there is a full discharge event is shown in Figure 3.22. The figure shows that there is high density of apparent charge at both

peaks of the AC cycle signifying the full discharge is a corona-like event. The high density of apparent charge is seen at less than 500 pC. It is also noticeable that a high density of apparent charge appears at lower voltages compared to those recorded during the early stage of the experiment and arcing at the earth electrode. Details on the full discharge event will be discussed in Chapter 4 by means of analysis of the leakage current waveforms.

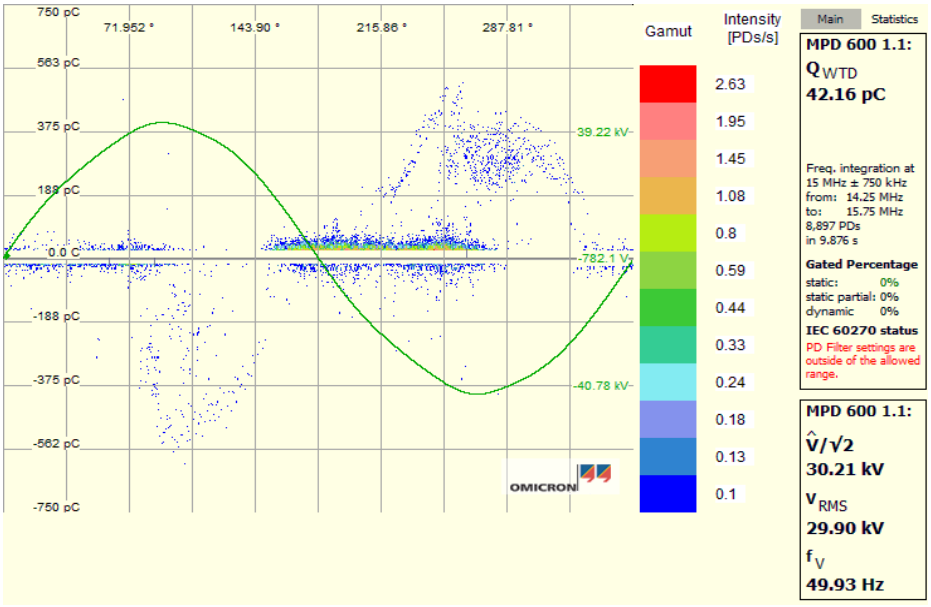

Figure 3.22: PRPD during which a full discharge event is occurred

3.4.4 Effect of Moisture Level on White Marks Formation

It is worth noting that different moisture contents in the pressboard will result in different periods of time for the white marks to grow until the occurrence of a first full discharge. This finding signifies the importance of knowing the moisture level in pressboard and its role in estimating the life time of the in-service transformers. Table 3.1 shows the period of time for the white marks to develop until there is a first full discharge occurrence. The results show that, for the case of wet pressboard, the period of time for the white marks to reach the earth bar increases as the moisture level increases. Since white marks formation is an indication of moisture evaporation, therefore, excessive presence of moisture at the interface requires more heat energy from PD activities to evaporate the moisture during the process of white mark growth. However, apparently, the dry pressboard is in its own league whereby it requires a significantly longer period compared to the wet pressboard.

Table 3.1: Period of time for white marks to grow until first appearance of full discharge event as a function of moisture level in pressboard

Voltage applied	Approximate period based on different moisture levels within pressboard			
	< 0.5 %	3 %	6 %	9 %
25 kV	Never tested	4 hours	7 hours	More than 8 hours
30 kV	5 hours	0.8 hours	1.2 hours	1.8 hours

3.5 Summary

An experiment has been developed to study surface discharges at the oil-pressboard interface. The processes in the surface discharge at the oil-pressboard interface have been discussed and correlated with respective PD data. The results suggest that different moisture levels in pressboard lead to different PRPD characteristics at the early stage of surface discharge and require different periods of time for the white marks to bridge the needle tip and earth electrode. This information may assist in the development of condition monitoring strategies for large power transformers and ultimately allow prognostic analysis of their lifespan. The decreasing trend in PD data observed in this work is an important finding to show that such characteristics are not a reliable condition monitoring measure of health and it can be regarded as a key indicator of white mark propagation and surface discharge at the oil-pressboard interface. In reality, white marks propagation may take up to several years to reach an earth point, but damage created during its formation can be dangerous when there is sudden over-voltage event due to remote energisation or a lightning strike.

Chapter 4

Full Discharge Characteristics during Surface Discharge at the Oil-pressboard Interface

4.1 Introduction

This chapter focuses on the full discharge characteristics obtained during surface discharges at the oil-pressboard interface under AC voltages. As discussed in Chapter 3, a full discharge event can only occur once the white marks on the pressboard surface are close to the earth bar. The visible white marks indicate drying out processes of the pressboard through moisture evaporation and breaking of bonds of oil molecules to form more volatile compounds that can generate gases in the pressboard pores. Throughout an experiment, full discharges can re-occur many times due to the state of pressboard surface without flashover causing the protection system to trip. Full discharge is defined as a rare discharge event (usually visible in the form of arcs) that temporarily bridges the HV electrode and the earth at the oil-pressboard without resulting in a complete electrical breakdown. Typically, this event leads to a relatively small continuous leakage current flowing to earth at a level that is insufficient to trigger the protection system. This infers the importance of studying the characteristics of full discharges for condition monitoring purposes. In this thesis, the characteristics of full discharges are analysed by means of leakage current measurement. Correlation between leakage current measurements and PD monitoring data are discussed to provide useful information for development of condition monitoring methods to detect

surface discharging in a large transformer. In addition, by developing understanding of the full discharge characteristics, improvement in pressboard barrier design for power transformers may result.

4.2 Triggering Method for Leakage Current Measurement

It should be highlighted that results discussed in this Chapter are part of surface discharge experiment discussed in Chapter 3. In general, the experimental apparatus and connections are detailed in Section 3.2, whilst the experimental procedures are described in Section 3.3. However, in order to study the characteristics of full discharge event that appear to randomly occur, an appropriate triggering method is required to capture the leakage current waveforms. The selection of trigger mode was based on the typical time domain characteristic of the leakage current waveform as shown in Figure 4.1. The figure depicts a zoomed-in leakage current waveform measured via the shunt resistor as a result of full discharge event. The waveform consists of multiple current pulses that are superimposed with small continuous currents. Typically, full discharges lead to continuous currents of less than 10 mA as shown in Figure 4.1, i.e. half the overcurrent limit of the protection relay in the power supply. The continuous current is insufficient to trip the protection relay from the waveform and this provides an opportunity to trigger the oscilloscope using the timeout trigger mode through the advanced trigger function. Timeout is a trigger mode that will trigger on an event which remains high, low or either for a specified time period [102]. Figure 4.2 illustrates the characteristics of the timeout trigger mode for which the oscilloscope is triggered when the signal remains high after the time $T = T_2 - T_1$ has elapsed.

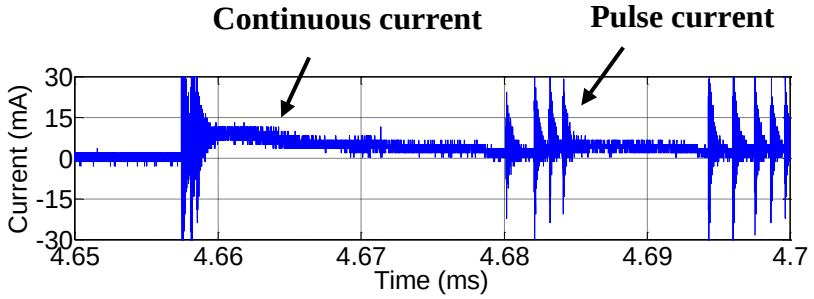

Figure 4.1: Part of leakage current waveform (zoomed-in view) due to full discharge event measured via shunt resistor that contains continuous and pulse currents

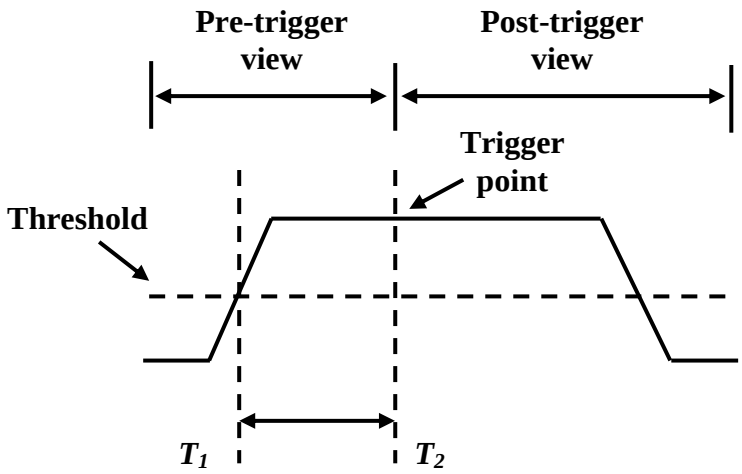

Figure 4.2: Timeout trigger characteristic

4.3 Measurement based on Frequency Bandwidth in IEC 60270

Before discussing the characteristics of full discharge based on the experimental setup that has been discussed in Chapter 3, it is worth highlighting the performance of a standard PD measurement system using IEC 60270 standard frequency bandwidth for detecting the multiple pulses shown in Figure 4.1 due to full discharges during surface discharge at the oil-pressboard interface. The random occurrence of full discharges infers that the PD measurement system must be able to detect and identify the full discharges for condition monitoring purposes. For this purpose, a conventional PD measurement system has been used to study the full discharge event by means of PD pulse waveforms. The experimental connections as shown in Figure 4.3 were used where the conventional PD measurement system (Robinson) offers synchronous measurement of PD pulses waveforms with leakage current waveforms via the shunt resistor and RFCT on the digital oscilloscope. This allows capture of raw measurement data, unlike the Mtronix PD measurement system (see Figure 3.1) that has its own PD measurement software installed on the computer. The conventional PD measurement system was set at the frequency bandwidth from 10 kHz to 300 kHz. The working bandwidth of the RFCT that was used in this research is from 10 kHz to 250 MHz. Hence, in order to facilitate the highest frequency signal that can be measured via the RFCT, i.e. 250 MHz, a sampling rate of 500 $MS \cdot s^{-1}$ was used for the digital oscilloscope throughout the experiment.

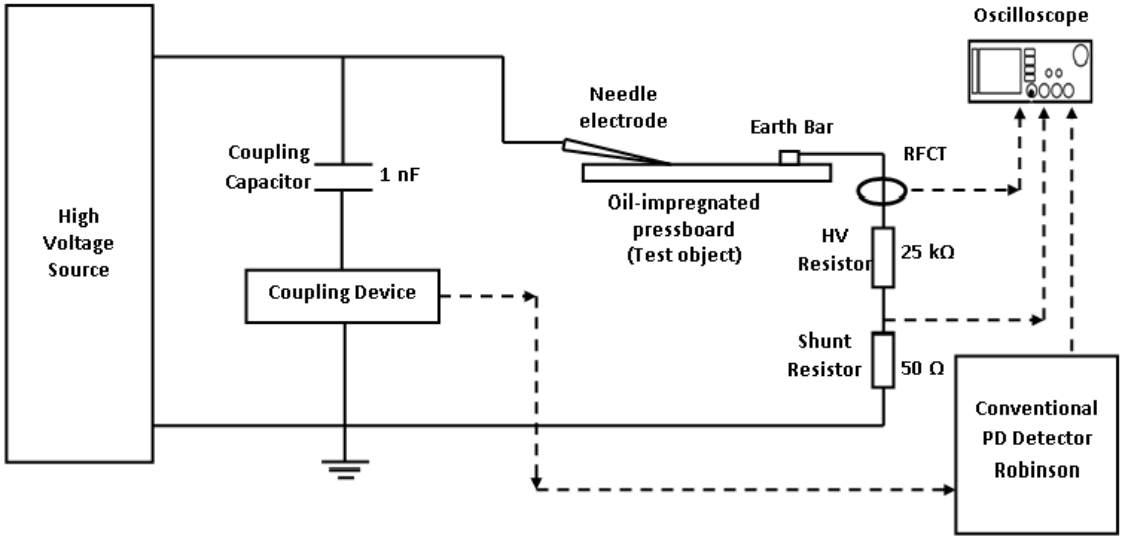

Figure 4.3: Experimental setup using conventional PD measuring equipment (Robinson) to study the full discharge event

Figure 4.4 shows the leakage current waveforms measured concurrently via the shunt resistor, RFCT and IEC 60270 PD measurement system (Robinson) due to a particular full discharge event. Figure 4.4 (a) shows the comparison between different transducers of a complete leakage current waveform in one half cycle of the AC voltage. A brief comparison from Figure 4.4 (a) suggests that the shunt resistor and RFCT produce very similar shapes of leakage current waveform. In contrast, the IEC 60270 PD measurement system produces a completely different waveform. The zoomed-in results shown in Figures 4.4 (b), (c) and (d) depict that the IEC 60270 frequency range has poor frequency integration for full discharge events that consist of multiple pulses that are very close to each other. The use of IEC 60270 leads to lost information about the complete current pulse waveform as well as attenuation and aliasing of important frequency components due to the limited bandwidth integration and its inability to resolve subsequent pulses. Therefore, further analysis on the characteristics of full discharges is impossible. On the other hand, results from the shunt resistor and RFCT suggest that both transducers can detect multiple pulse events as a result of full discharges by measuring complete leakage current waveforms. The RFCT gain is relatively low (i.e. the voltage magnitude measured via the RFCT is about half the voltage magnitude measured via the 50 Ω resistor) and hence it can miss some pulses of very low magnitude. Results from the shunt resistor and RFCT offer opportunities to further investigate the characteristics of full discharges during surface discharge at the

oil-pressboard interface for condition monitoring purposes. Both transducers also correspond to each other in terms of detecting individual current pulses.

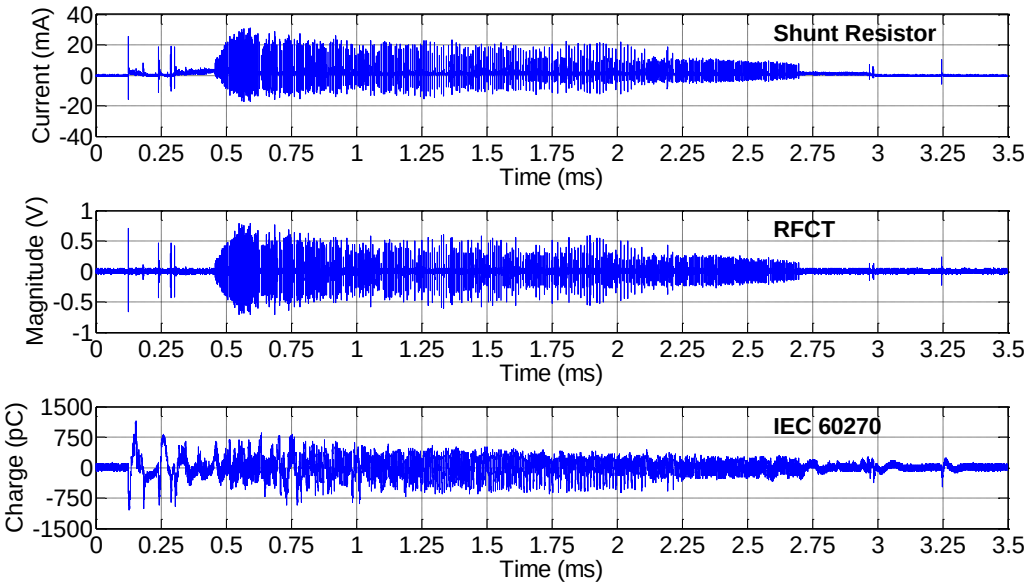

(a) A complete leakage current waveform in a positive cycle of applied voltage

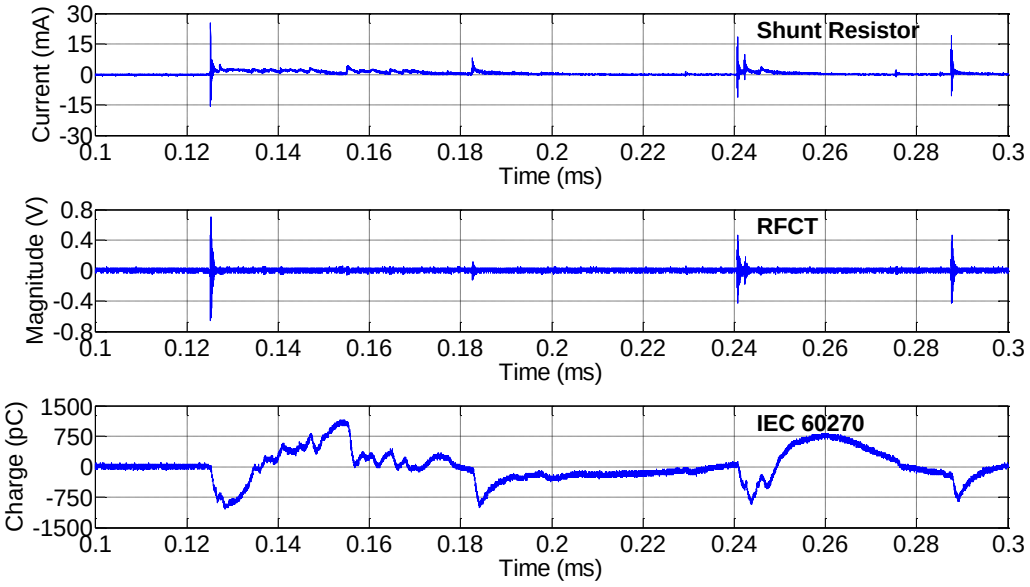

(b) Current pulses that are unevenly distributed at the early stage of leakage current waveform in (a)

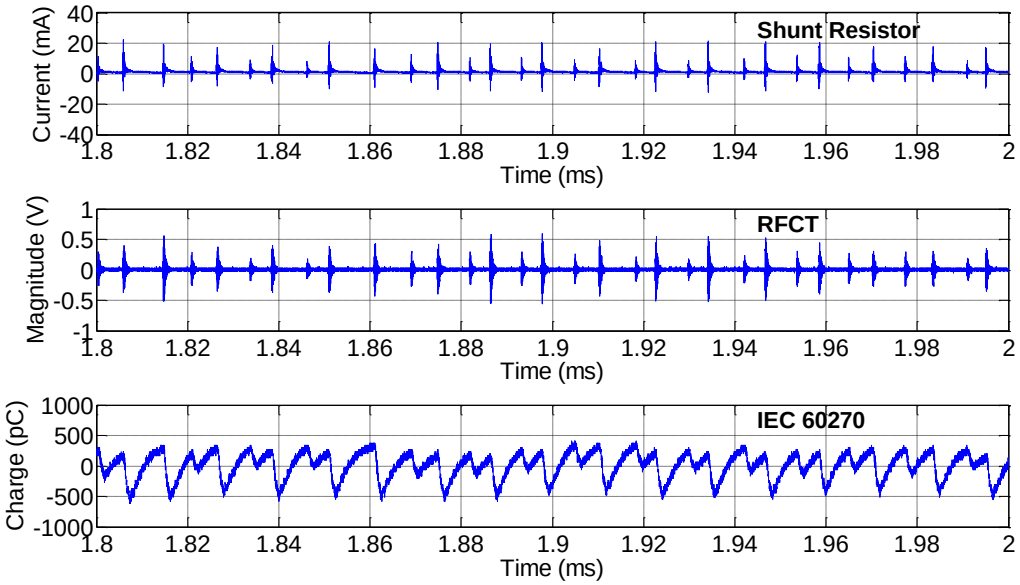

(c) Current pulses that are fairly evenly distributed at the middle stage of leakage current waveform in (a)

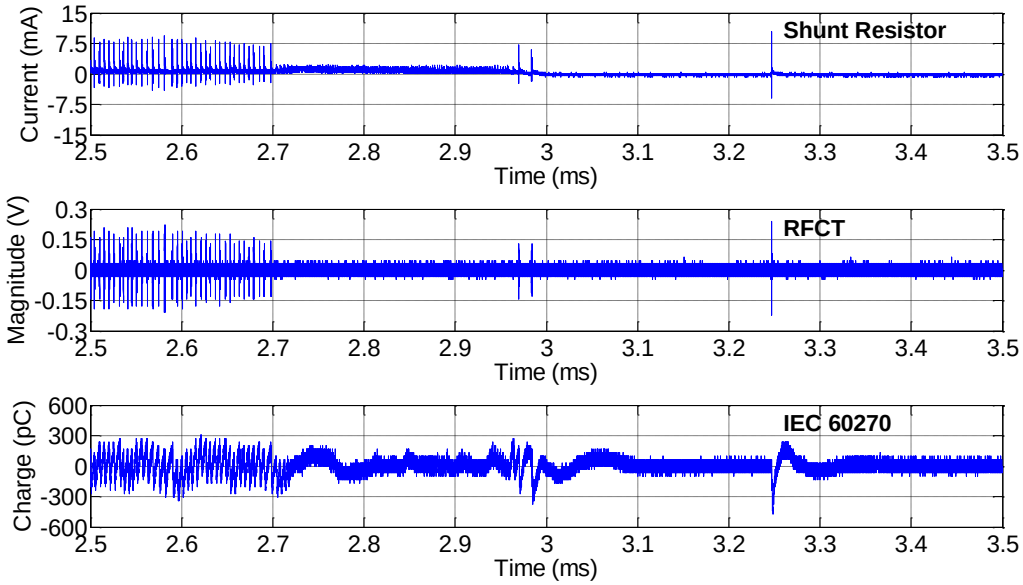

(d) Current pulses that are unevenly distributed at the final stage of leakage current waveform in (a)

Figure 4.4: Comparison between leakage current waveforms measured via shunt resistor, RFCT and IEC 60270 PD measurement system

4.4 Determination of Appropriate Range of Frequency Domain Integration for PD Measurement

The use of the RFCT as a current transducer for PD detection has become more widely applied in PD research and measurement technology due to its advantages in terms of wideband working frequency and coupling method, i.e. inductive coupling to the system being measured [103, 104, 105]. In this research, the RFCT used, has wider bandwidth (10 kHz to 250 MHz) compared to the IEC 60270 standard and as such ensures more frequency components from current waveforms due to full discharges can be captured for further analysis. The bandwidth of the RFCT also offers better frequency integration over the shunt resistor for frequency spectral analysis. The RFCT which works as an inductive coupling measurement device also makes it more practical than the shunt resistor if this approach was to be used for on-site measurement.

As mentioned in Section 4.2, the measurement of leakage current due to full discharge events is part of the surface discharge experiment discussed in Chapter 3 which used the MTronix PD measurement system for monitoring and recording purposes. The ranges of frequency domain integration of the Mtronix PD measurement system are freely selectable based on its maximum centre frequency of 32 MHz and maximum bandwidth of 1.5 MHz [97]. Therefore, after considering the limitation of the IEC 60270 standard frequency setting, it is important to perform frequency spectrum analysis on different PD sources during surface discharges at the oil-pressboard interface so that a proper frequency integration range can be set on the Mtronix PD measurement system.

Figure 4.5 shows the typical frequency characteristics of four different PD activities at the oil-pressboard interface during the surface discharge experiment. The frequency spectra were determined using a Fast Fourier Transform (FFT) by considering cumulative results of individual current pulses from RFCT measurement over a half cycle of applied voltage. In general, the frequency spectra shows that the current pulses generated during full discharges (see Figure 4.5 (a)) have similar frequency components with arcs/glow at the needle tip and arc discharges at the earth bar shown in Figure 4.5 (b) and (c) respectively which are associated with corona-like events. Those three events are significantly characterised by peaks in the two frequency ranges of 10 MHz to 60 MHz and 95 MHz to 105 MHz. In contrast, the genuine surface discharge

(without any arc or glow discharges) depicted in Figure 4.5 (d) lacks energy over the frequency range of 95 MHz to 105 MHz. It should also be highlighted that for all discharge types, there are two main frequency components, i.e. around 15 MHz and 50 MHz. Hence, based on the specifications of the Mtronix PD measurement system, the frequency integration range for PD measurement was set to 15 MHz ± 750 kHz for the purpose of this research.

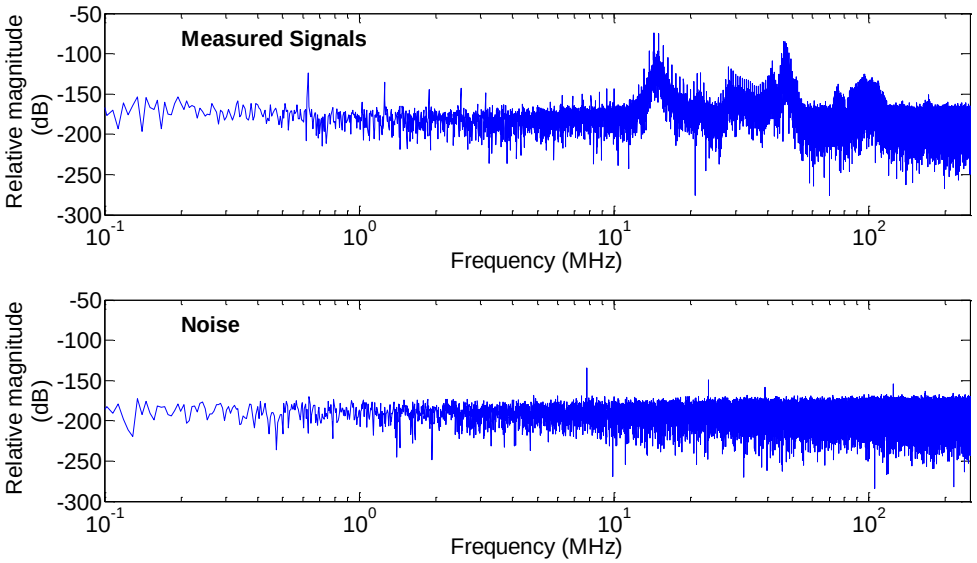

(a) Full discharge with 116 pulses

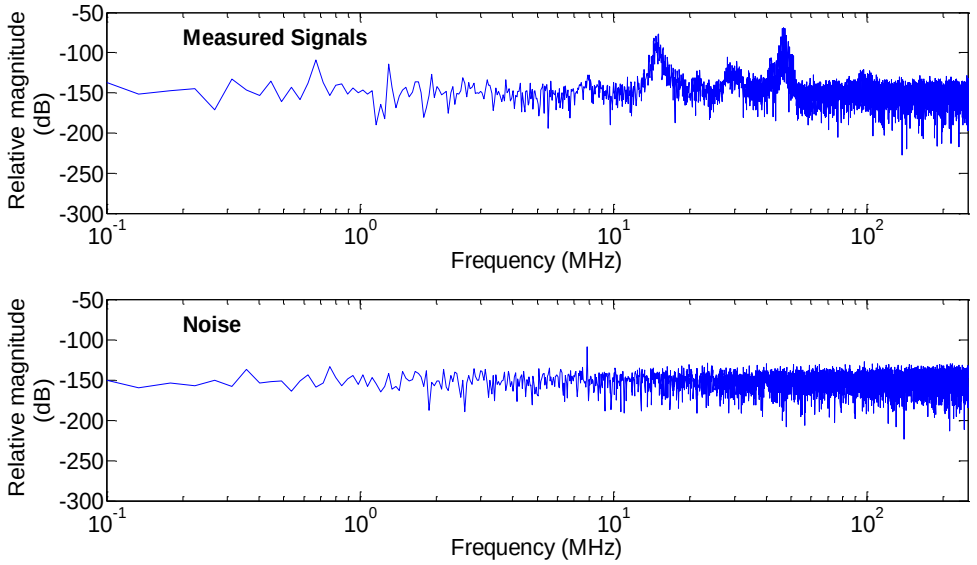

(b) Arcs/glow at needle tip with 14 pulses

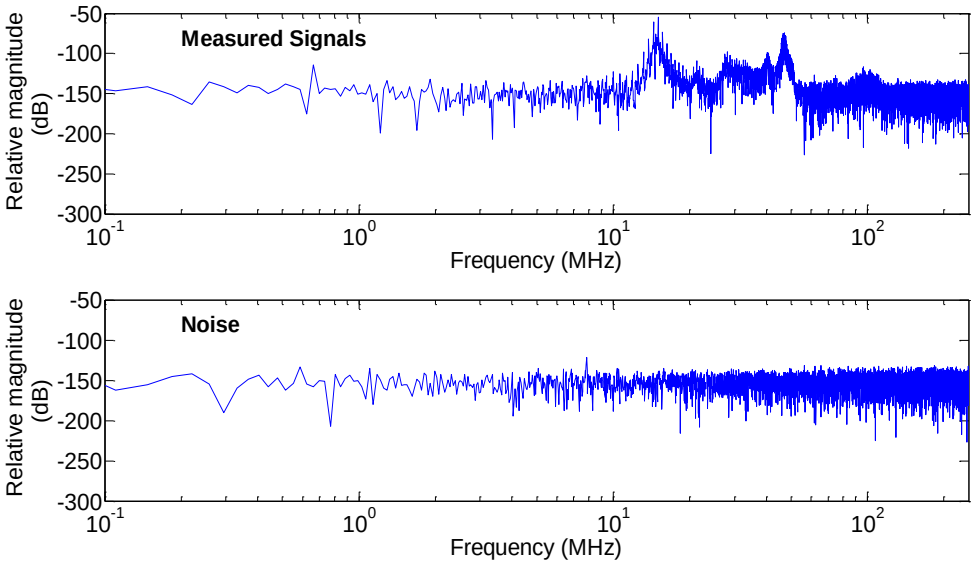

(c) Arcs at earth with 17 pulses

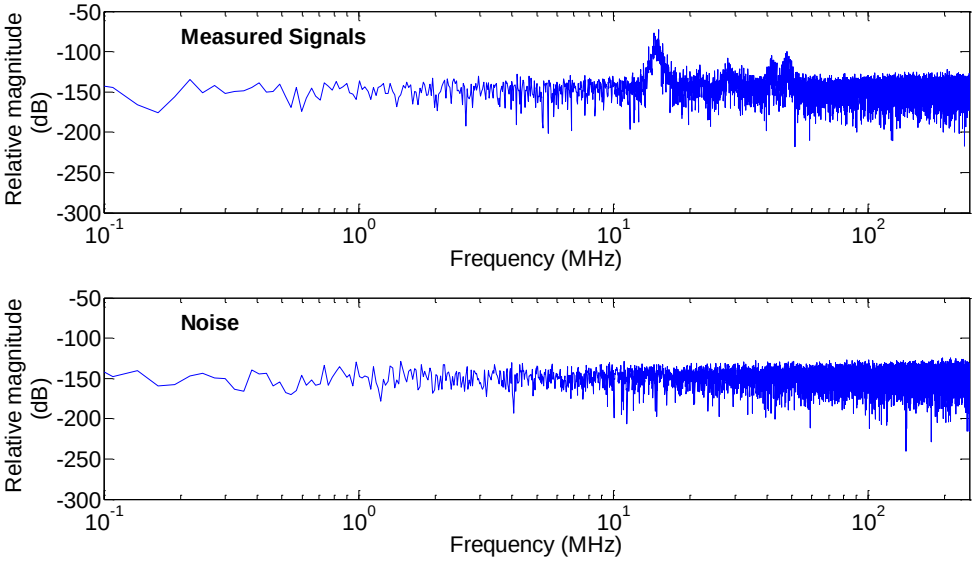

(d) Surface discharge with 23 pulses

Figure 4.5: Typical frequency spectra for different discharge sources measured via the RFCT during the surface discharge experiment

4.5 Analysis of Leakage Current Waveforms

4.5.1 Streamer Initiation and Propagation in Full Discharges

This section discusses the full discharge events by means of analysis of leakage current waveforms. By using this method, it is possible to further investigate the phenomenon of full discharge events in terms of initiation and propagation based on the measured discharge pulses. In general, the full discharges lead to the flow of relatively small continuous current of less than 10 mA in this experiment (see Figure 4.1) that is insufficient to trigger the protective relay. The recorded video shows that the full discharges are typically characterised by weakly luminous streamers and partial illumination along the streamer path such as shown in Figure 3.9. These characteristics are similar to the non-breakdown event when a positive streamer bridges an open oil gap as reported in [55, 67, 99, 100]. Such rare streamers in bulk oil correspond to voltage levels having low breakdown probability, such as 1 to 10 % [67] and 30 % [55]. This kind of streamer also leads to a relatively small continuous current, e.g. previous reported values of 20 mA at 92 kV applied voltage with a 50 mm point-plane gap arrangement [67].

The continuous current recorded in this research of typically less than 10 mA could be caused by a large number of weakly luminous branches propagating simultaneously from the needle tip as reported in [99]. It should be noted that the part of leakage current waveform shown in Figure 4.1 shows repetitions of continuous current and this is even more in the leakage current waveform shown in Figure 4.4 (a). This infers the ability of a large number of weakly luminous branches to reoccur during the full discharge event. The reoccurrences might be induced by space charge that resides along or near to the white mark channels on the pressboard surface. Therefore, this reinforces assumptions that luminous branches can reoccur anywhere between the needle tip and the earth bar during the streamer propagation.

Current pulses have been generally accepted to correspond with the light pulses measured via a photomultiplier tube (PMT) in the investigation of streamer propagation [14, 55, 67]. Each pulse would be associated with re-illumination of single main streamer channel including some or all branches within the streamer [14] that propagate until it stops at a certain distance or reaches the opposite electrode. The occurrences of

pulses in the leakage current waveforms can typically be divided into two types. The first one is current pulses that are unevenly distributed as illustrated in Figure 4.4 (b) and (d), whilst the second type is pulses that are fairly evenly distributed as clearly shown in Figure 4.4 (c).

The first type of pulse distribution (unevenly distributed) typically occurs at the early stage of leakage current waveform as can be seen in Figures 4.4 (a), 4.6 (b) and 4.7 (b). For instance, Figure 4.4 (a) shows that the pulses are separated by a few hundred nanoseconds to 525 µs. Pulse occurrences at the early stage might represent the initiation and initial propagation of a large number of weakly luminous branches of the streamer. This is based on the characteristic of continuous current that is superimposed with the current pulses over this stage. It appears that similar pulse distribution characteristics as in the earlier stage can repeat in the same half cycle of applied voltage as can be seen in the Figure 4.6 (b). This repetition suggests that full discharges may consist of reoccurrences of streamers that are sustainable until they are extinguished as a result of voltage reduction or polarity change.

The unevenly distributed pulses may also occur at the final stage of the detected leakage current waveforms as clearly shown in Figures 4.4 (d) and 4.7 (b). For example, Figure 4.4 (d) shows that the intervals between pulses are between 9 µs and 245 µs. During the final stage, the pulses are typically accompanied by significantly low or almost no continuous current component as demonstrated in Figure 4.4 (d) compared to those that occur at the early stage of leakage current conduction. This result is comparable to results obtained for bulk oil reported previously [55, 67], i.e. that no continuous currents were recorded once the streamer reaches the plane electrode. Moreover, the number of pulse occurrences is usually less than the number observed during the early stage of leakage current waveforms. The occurrences of these pulses could probably represent streamers that propagate and touch the earth bar with an observed bluish colour (see Figure 3.9) or initiation of a streamer that is weakly luminous and unable to propagate.

It is worthwhile noting that different polarity in the applied voltage has no effect on the pulse distributions within the leakage current waveforms. For instance, due to random discharge activity during streamer initiation and propagation in full discharges, pulse distributions are different between two results obtained during positive cycle (Figure 4.4

(a) and Figure 4.6 (b)). However, there are similarities between current waveforms obtained from different AC voltage polarity (compare Figure 4.4 (a) with Figure 4.7 (b)).

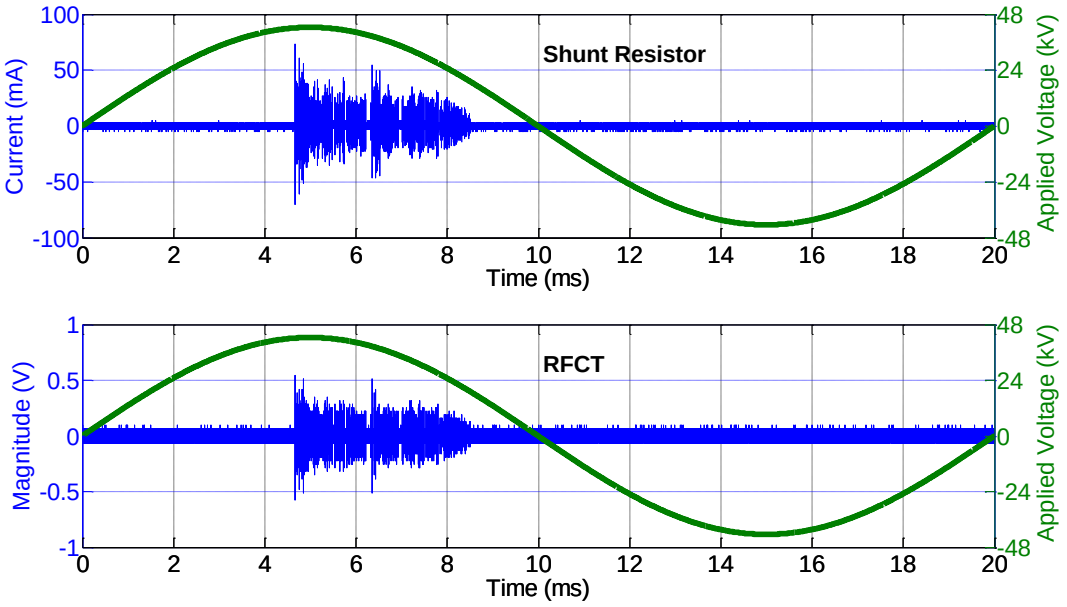

(a) Leakage current waveform with respect to a complete cycle of applied voltage

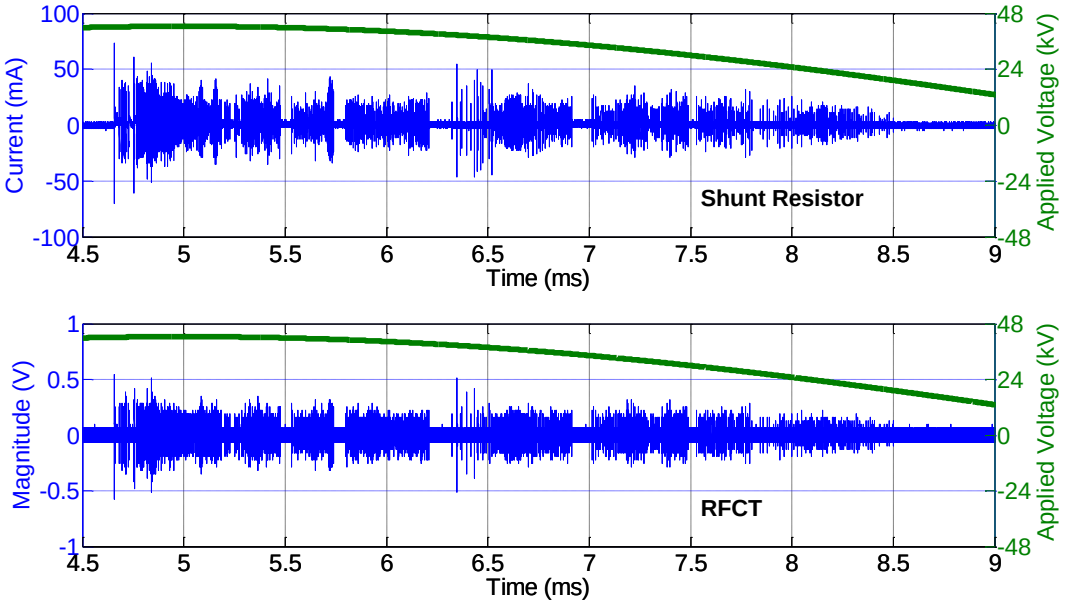

(b) Zoomed-in plot of leakage current waveform in (a)

Figure 4.6: Leakage current waveform of full discharge that only occurs in a positive cycle of applied voltage

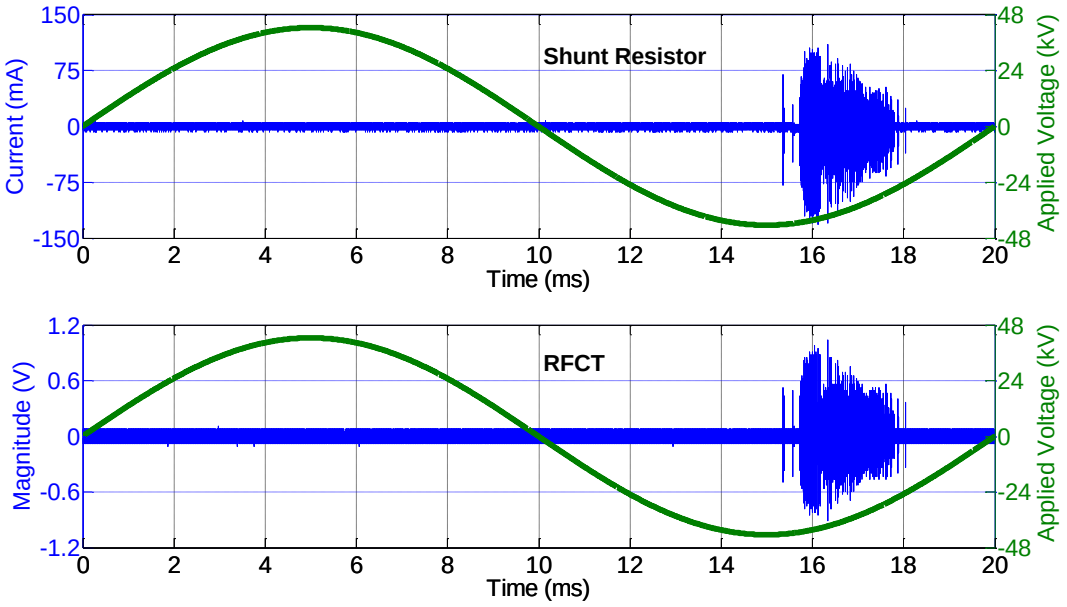

(a) Leakage current waveform with respect to a complete cycle of applied voltage

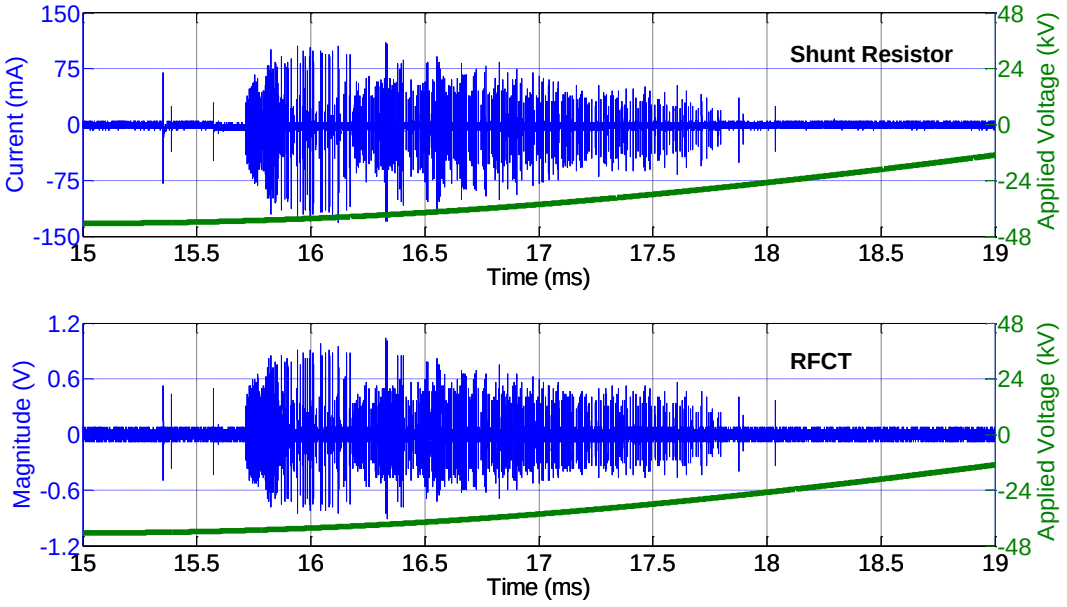

(b) Zoomed-in plot of leakage current waveform in (a)

Figure 4.7: Leakage current waveform of full discharge that only occurs in a negative cycle of applied voltage

In contrast, the fairly evenly distributed current pulses (second type) are typically observed during the middle stage as shown in Figure 4.4 (c). As seen in the figure, the pulses are distributed with short interval of approximately 3-6 μs. The occurrences of these fairly evenly distributed pulses exist over a long period (i.e. from a few hundred microseconds to a few milliseconds) and produce a train of pulses in the detected leakage current waveforms. This pulse train might represent the re-illumination and ionisation processes during the streamer propagation along the white mark surface. The white mark surface is the electrically weakest part at the oil-pressboard interface and may have trapped charges associated with it. Therefore, streamer propagation along this conductive surface promotes more ionisation processes and branches within the streamer and causes a significant increase in the number of pulses.

It is also important to note that the leakage current waveforms may consist of a few groups of pulse trains whereby pulses within each group are comparable or almost similar in magnitude for a certain period before there is an increment or reduction in magnitude of the subsequent pulse train occurs within the same half cycle. This has been seen in all leakage current waveforms recorded during this research. The first group of pulses that occurs approximately at the peak of the applied voltage suggests that the pulses represent corona-like events during the initiation and initial propagation of the full discharge streamer. The subsequent groups that have about similar magnitude within a particular group indicate that the streamer propagation during the full discharge event is a corona-like event although they do not occur at the peak voltage phases.

4.5.2 Correlation between Full Discharge Occurrences and Simultaneous Voltage

Throughout this experiment, full discharges can occur over a minimum of half cycle of the AC supply voltage. Figures 4.6 (a) and 4.7 (a) show two different leakage current waveforms during which the full discharges occurred only in a positive or negative cycle of the applied voltage. Figure 4.6 (a) represents a full discharge that occurs at the positive cycle, whilst Figure 4.7 (a) shows one that occurs in the negative cycle. Both figures show that full discharges are initiated at phases that are close to the peak of the supply voltage. Therefore, a certain threshold close to the peak of the supply voltage

must be exceeded to allow current conduction until the resistivity of the conducting path is high enough along with a reduction of constructive superposition in electric field to stop the conduction process. Similar conditions must also be satisfied for the cyclic full discharge events shown in Figures 4.8 and 4.9. However, over the subsequent cycles, the leakage currents are seen to increase in duration and occur at an earlier phase of the applied voltage. The cyclic full discharge might be explained by additional ionisation processes as well as the leakage current flowing. These additional processes cause charges to be trapped and then accumulate at the pressboard surface. The accumulated charges can be high enough for the opposite polarity voltage to cause a streamer for a full discharge event.

It would appear that at some point, the onset of leakage current waveforms earlier in phase leads to a significant reduction in the magnitude of current pulses once the applied voltage is close to its peak value as shown in the second and third AC cycles of Figures 4.8 and 4.9 correspondingly. This is probably due to a majority of the surface charges being swept to the earth electrode during current conduction over the earlier phase of the applied voltage, and thus reducing the total number of charges trapped at the oil-pressboard interface. As a result, the resistivity of the white marks channel increases and leads to low discharge activity which is probably localised activity of surface discharges rather than the continuation of current conduction to the earth bar. This argument of abnormal surface discharge that occurs during the second and fourth quadrants (contradicts the usual case that typically occurs at the first and third quadrants) is supported by the train of high current pulses in the following cycle of opposite polarity representing streamer propagation. The ability to continue to generate full discharges in the next half cycle could be due to accumulated charges on the surface of the pressboard from the discharge activity at the second or fourth quadrants that already mentioned. A high enough accumulated charge can cause another streamer to initiate and propagate bridging the gap. These cyclic full discharge events are usually followed by corona-like discharges that could be arcs at the needle tip and/or earth bar such as in the third cycle and last half cycle illustrated in Figures 4.8 and 4.9 respectively. This phenomenon reinforces the understanding that the full discharge has ended and such streamer arcs are unable to produce full discharges due to an insufficient number of local space charges.

It should be highlighted that all reported breakdown events in transformer oil with pressboard using needle-bar electrodes [9] and without pressboard using point-plane electrodes [106] occur in the positive cycle of an AC applied voltage. In addition, the non-breakdown events when a streamer bridged the oil gap under AC voltage also only occurred in the positive cycle [100]. These support other findings that the breakdown voltage under positive impulse is about 50 % lower than that for negative voltages [55, 56]. However, in this research, full discharges which involve streamer propagation bridging the gaps are not necessarily initiated and occur in the positive half cycle if results in Figures 4.6-4.9 are considered. This could be due to the effect of polarity changes under long periods of highly non-uniform AC electric field on the oil-pressboard interface. The non-uniform AC field would cause gradual movement of charge accumulation at the deteriorating oil-pressboard interface from needle tip to the earth bar electrode. This mechanism describes the reduction in dielectric strength around the area of white mark channels and hence, results in a more random initiation of positive or negative streamers than reported elsewhere.

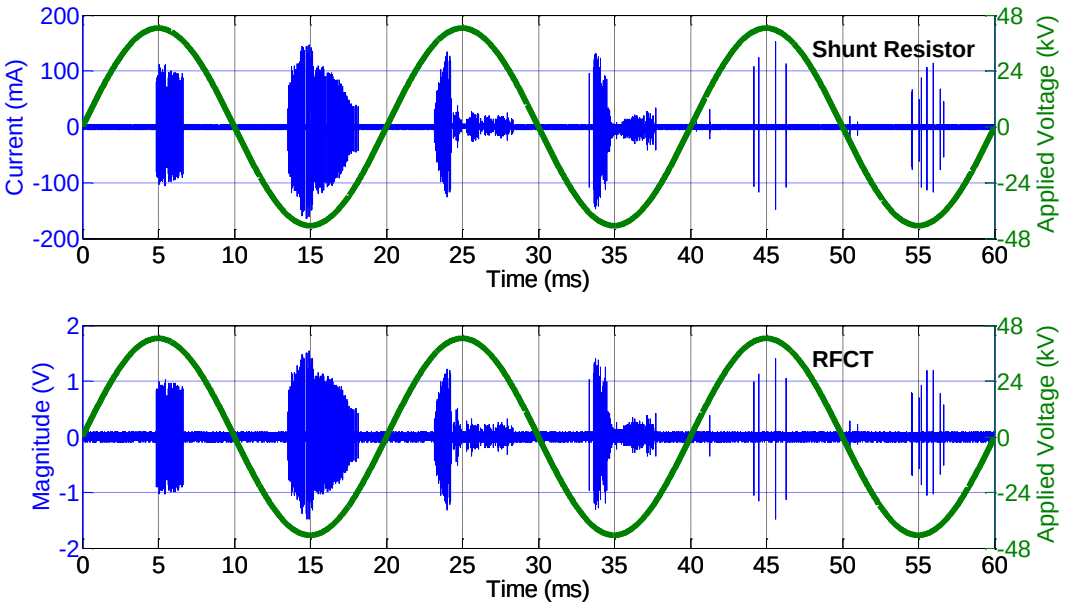

Figure 4.8: Cyclic leakage current waveform of full discharge initiated by positive streamer

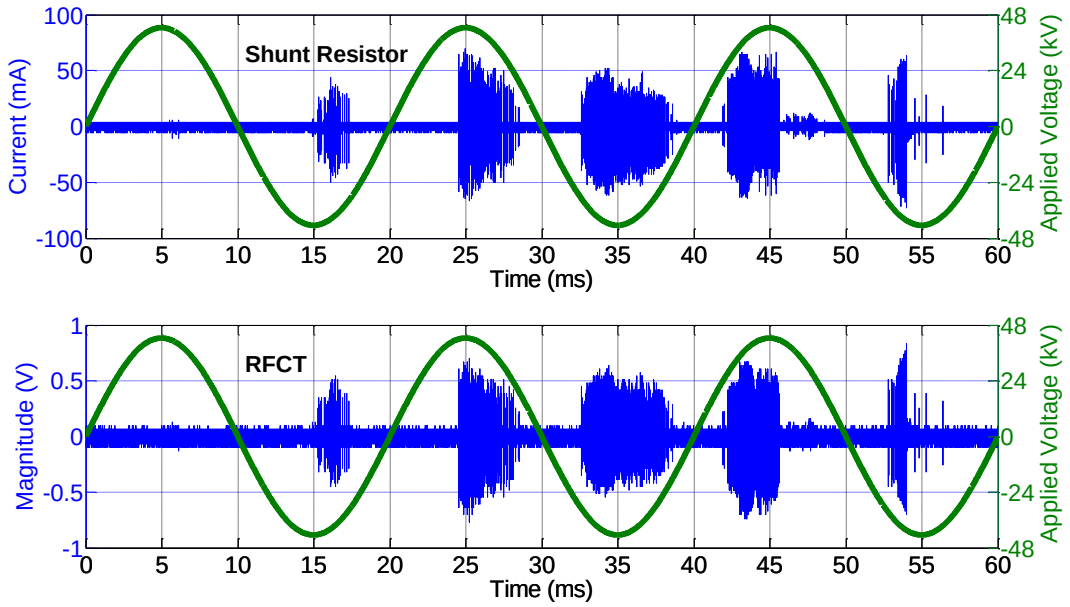

Figure 4.9: Cyclic leakage current waveform of full discharge initiated by negative streamer

4.5.3 Correlation between Leakage Current Waveforms and PRPD Data

For the benefit of developing a condition monitoring tool for detecting and identifying full discharges during surface discharge in large power transformers, it is necessary to correlate the leakage current waveform with the PRPD results obtained using the commercial PD detection system. This was achieved by determining the PRPD results for a respective full discharge event from the leakage current waveform measured via the RFCT. For instance, Figures 4.10-4.12 show the comparison between the PRPD results plotted using current pulses measured via the RFCT and the respective results obtained using the commercial PD detection system. Figures 4.10 (a), 4.11 (a) and 4.12 (a) represent the PRPD patterns based on the RFCT results shown in Figures 4.6, 4.8 and 4.9 respectively. Thus, it is referred to as the genuine PRPD results of a particular full discharge event with a certain period based on the bandwidth of the RFCT. On the other hand, Figures 4.10 (b), 4.11 (b) and 4.12 (b) represent short period of PRPD results for surface discharge at the oil-pressboard interface during which similar full discharge has been recorded using the Mtronix PD equipment. The latter PRPD results are based on the frequency integration setting for the Mtronix equipment as detailed in Section 4.4.

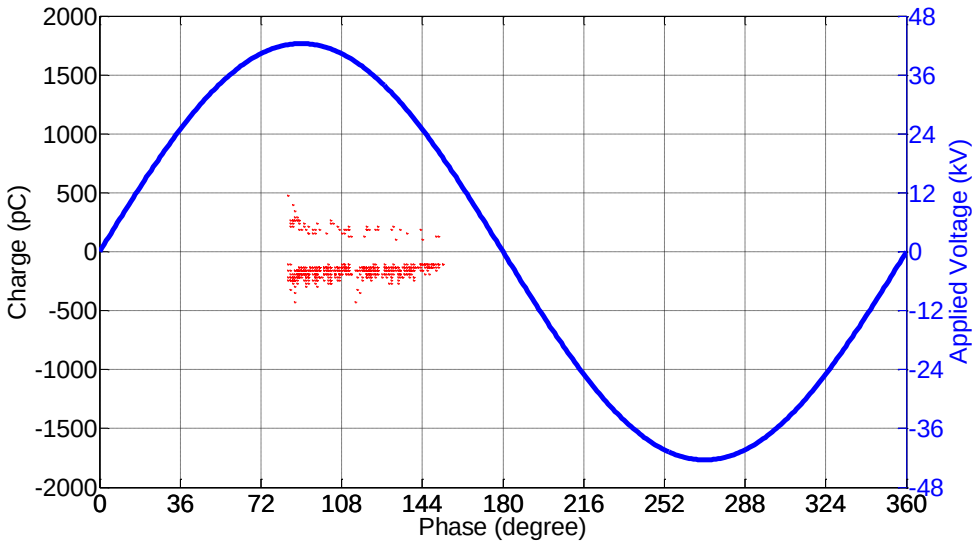

(a) PRPD for the leakage current measured via the RFCT that contains a total of 651 pulses

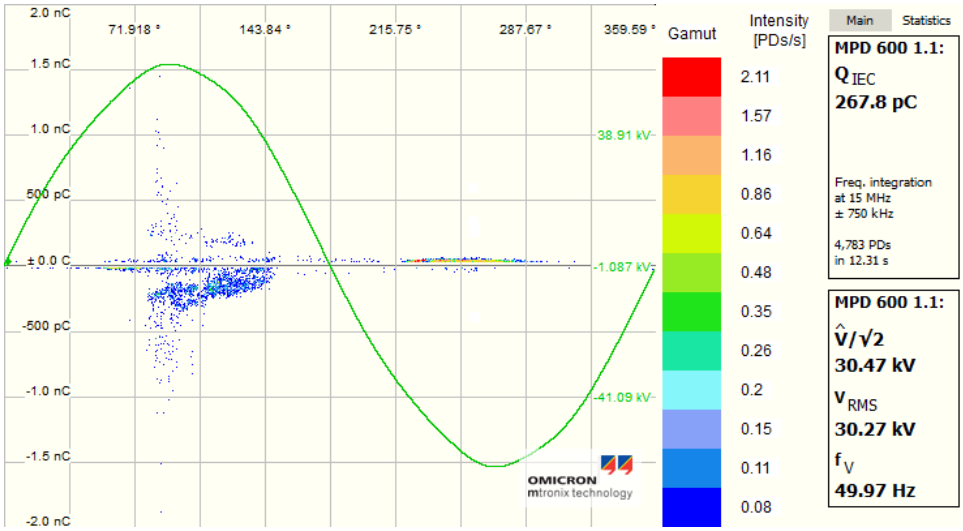

(b) PRPD during which a full discharge occurred

Figure 4.10: Comparison between the PRPD of a full discharge event plotted using the current pulses measured via the RFCT in Figure 4.6 and the commercial PD detection system

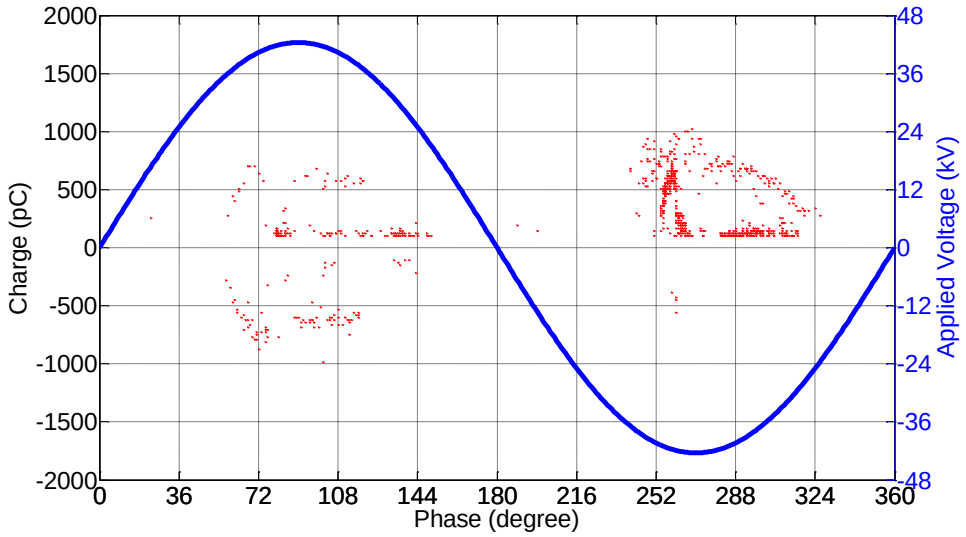

(a) PRPD for the leakage current measured via the RFCT that contains a total of 823 pulses

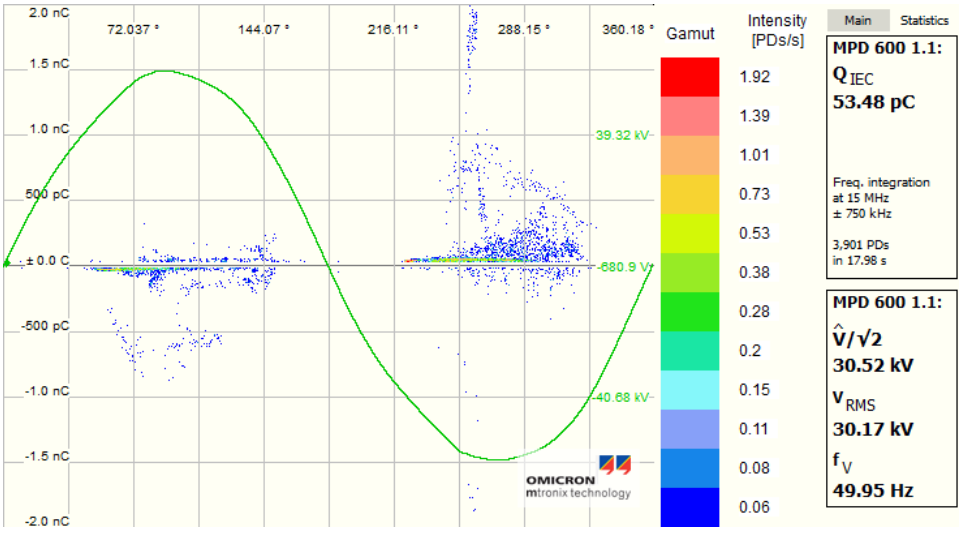

(b) PRPD during which a full discharge occurred

Figure 4.11: Comparison between the PRPD of a full discharge event plotted using the current pulses measured via the RFCT in Figure 4.8 and the commercial PD detection system

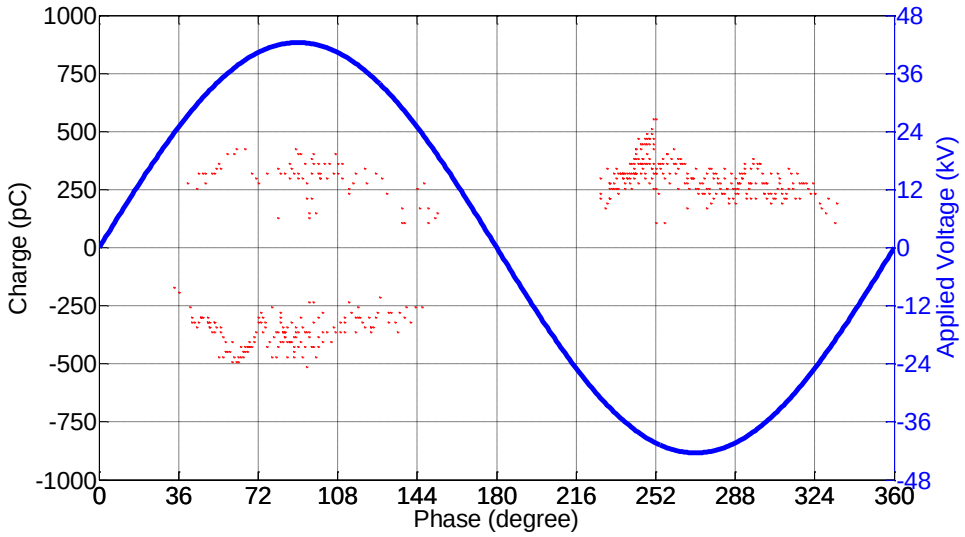

(a) PRPD for the leakage current measured via the RFCT that contains a total of 494 pulses

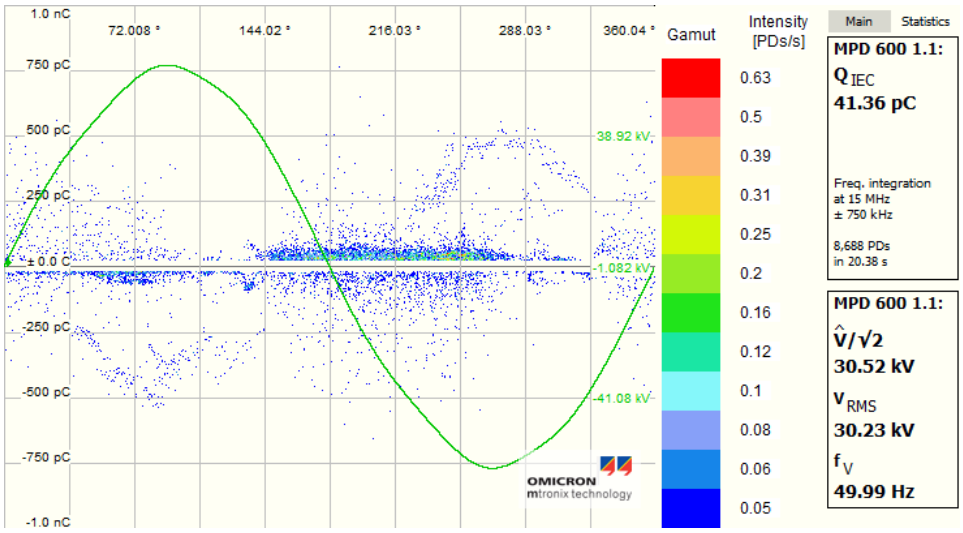

(b) PRPD during which a full discharge occurred

Figure 4.12: Comparison between the PRPD of a full discharge event plotted using the current pulses measured via the RFCT in Figure 4.9 and the commercial PD detection system

It has been observed that the moisture content within the pressboard (i.e. dry, 3 %, 6 % or 9 %), streamer polarity and number of leakage current cycles have no effect on the PRPD pattern and the magnitude of apparent charge as a result of full discharges. If results from the PD measurement equipment are considered, full discharge events

normally lead to a high density of apparent charge of less than 500 pC as depicted in Figures 4.10 (b) and 4.12 (b) as well as Figure 3.22, whilst in some rare cases the magnitude can be higher than that as shown in Figure 4.11 (b). Such apparent charge characteristics in terms of their pattern (apparent charge distributions) and magnitudes can also be observed in the genuine PRPD results of full discharges based on the current pulses measured via the RFCT as presented in Figures 4.10 (a), 4.11 (a) and 4.12 (a), although there are some discrepancies to be observed. Both measurement methods lead to similar PRPD patterns with corona-like shape based on the groups of PD events that occur with almost similar magnitudes around the peak of the applied voltage although there are also charges at the lower voltages. Hence, a brief comparison between both PRPD plots from different measurement methods would suggests that there is qualitative correlation between the non-conventional PRPD results and the PRPD obtained using the Mtronix PD equipment.

Any discrepancy between both PRPD results could be due to the differences in frequency bandwidth between both measurement methods as mentioned previously in Section 4.4 and issues of equipment sensitivity. The sensitivity of the Mtronix PD equipment is subjective to the performance of its coupling device that connected in series with the coupling capacitor and the auto gain function implemented in the software depends on the number and magnitude of any measured apparent charges. In contrast, the leakage current measurement is based on inductive coupling of the RFCT that measures current pulses directly onto the earth. All these also infer that the transfer function into the operational bandwidths between both measuring equipment will be different and could lead to some of the observed PRPD differences. Some obvious discrepancies that could be due to these technical factors can be seen in Figures 4.11 and 4.12, whereby there is no high positive apparent charge in the positive cycle of the Mtronix result (Figure 4.11 (b) and 4.12 (b)) compared to the ones obtained from the RFCT (Figures 4.11 (a) and 4.12 (a)). Moreover, it can be seen that a group of apparent charges in the negative cycle (at around 255º phase angle) at the range of 1.5-2 nC in Figure 4.11 (b) only appear with a magnitude of less than 1 nC in the RFCT plot (Figure 4.11 (a)). It is also noticeable that the apparent charge distributions in the negative cycle of the RFCT measured result (Figure 4.12 (a)) is different in shape compared to the PRPD data measured using the MTronix equipment shown in Figure 4.12 (b).

Besides the factors already discussed, random phenomena during surface discharge will also lead to some differences between the PRPD results. For instance, the Mtronix result shown in Figure 4.10 (b) consists of some PD events at the peak voltage with magnitude higher than 500 pC which is not seen at all in Figure 4.10 (a). This has been observed due to repetitive arcing at the earth bar before sudden occurrence of a full discharge.

4.6 Comparison between Dry Band Arcing and Full Discharge

In order to aid understanding of the mechanism that leads to full discharges, it is worthwhile to undertake a comparison study between the full discharges that occur during surface discharge at the oil-pressboard interface and the dry band arcing that occurs on the outdoor insulation. This section discusses on these aspects.

.

Dry band arcing has been well recognised as a phenomenon that can cause tracking damage on the outdoor insulation systems such as silicone rubber [107, 108, 109] and all-dielectric self-supporting (ADSS) cable [110]. Figure 4.13 shows a typical chronological process for the occurrence of dry band arcing [111, 112]. Clean outdoor insulation (Figure 4.13 (a)) is normally exposed to pollution (particularly rain water) that creates a wet surface condition and increases the surface conductivity (Figure 4.13 (b)) and eventually, promotes surface discharges. A long period of surface discharges would lead to the formation of dry-band conditions on the insulation surface as a result of water evaporation from drying out process as shown in Figure 4.13 (c). The evaporation of water due to localised heating during the surface discharges will cause the affected surfaces to have gradual loss of their hydrophobic properties, thus becoming hydrophilic and then creating a dry-band condition [113].

The change from wet surface condition to dry surface leads to a significant rise of surface resistance compared to the rest of the wet surface. This causes the majority of the applied voltage to be distributed across the dry band and yields a large non-uniform electric field at the edge of wet surface. It appears that the dry band region can be represented by a non-linear resistive component with [114] or without [115] a capacitive element (in parallel) which could be due to accumulated charges from ionisation and polarisation processes during the surface discharges. During the dry

band condition and considering the concentration of large non-uniform field, discharges may occur if the instantaneous local electric field exceeds the lowered inception threshold and thus lead to intermittent or continuous arcing current [112, 116]. This discharge type is also called dry band arcing (Figure 4.13 (d)).

(a)	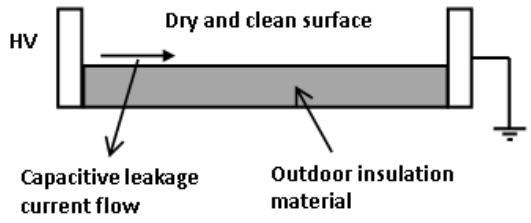	• Initial condition, i.e. dry and clean surface • Non-conductive surface
(b)	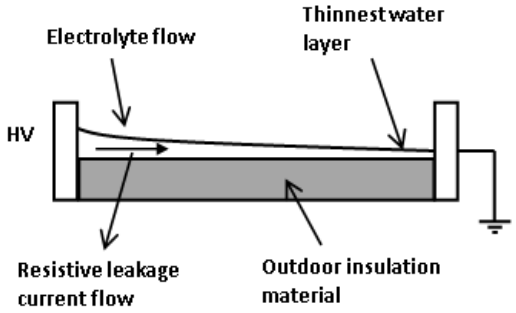	• Wet condition • Conductive surface
(c)	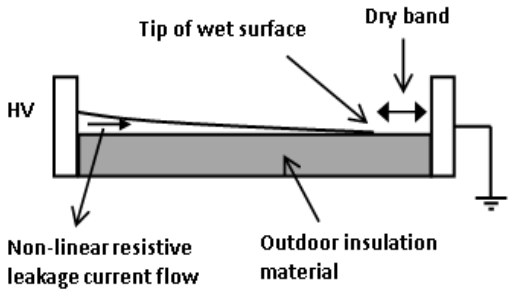	• Formation of dry band due to water evaporation from localised heating • Loss of hydrophobicity • Significant rise of surface resistance at the dry band region • Large non-uniform field at the tip of wet surface
(d)	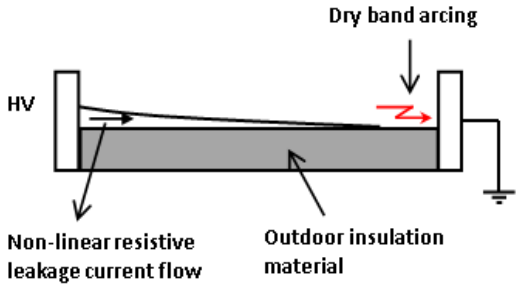	• Dry band arcing • Producing intermittent or continuous arcing current

Figure 4.13: Transition of leakage current phenomena and dry band arcing development (the diagram is amended from [117])

In the case of surface discharges at the oil-pressboard interface, the occurrence of full discharge events are preceded by processes that have been discussed in the previous chapter in Section 3.4.2 and Figure 3.10. In brief, the creation of white marks indicates a drying out process at the oil-pressboard interface and plays an important role leading to the occurrence of the first and subsequent full discharges that follow the white mark channels. The appearance of white marks is a result of moisture vaporisation and generation of gases that push the remaining oil molecules out of the pressboard pores, thus associating the white marks with a gaseous channel. The formation of white marks increases the conductivity of the oil-pressboard interface and the occurrence of full discharge events suggests that the white mark channels experience further increases of conductivity over time due to charge accumulation from continuous PD activity that involves ionisation and polarisation processes.

In general, both dry band arcing and full discharge phenomena are different in terms of the insulation material where such phenomena occur. The former events are at the air-solid insulation interface, whilst the latter occur at the oil-pressboard interface that has much greater dielectric strength. The microscopic geometry of solid materials like silicone rubber for outdoor insulation is not porous compared to the pressboard that is fibrous and porous for the benefit of oil-impregnation in power transformer. Different material properties as well as its surface condition (i.e. surface roughness, porosity, pollution level and etc.) would have different hydrophobic and hydrophilic behaviour [118] which leads to different mechanisms for the presence of water on the solid material. For outdoor insulation, the degree of hydrophobicity can be determined by the contact angle of free water on the insulation surface [118, 119, 120]. On the other hand, the pressboard can be classified as a hydrophilic material due to its ability to hold water in four different states [25, 27], i.e. as absorbed free water, or as free water in capillaries, or as vapour and or as monolayer or polymolecular layers through adsorption on the cellulose walls.

Differences in terms of insulation material for different high voltage applications have ensured that both discharge events are different in terms of the physical and chemical processes that initiate their development. However, they both have similar prior activity, i.e. evaporation of water leading to a dry surface condition. In addition, both discharge events occur at the dry surfaces, i.e. dry band for the outdoor insulation and white mark channels for the oil-pressboard composite insulation. In the case of outdoor

insulation, once the dry band region has developed, as shown in Figure 4.13 (c), the tip of the wet surface plays an important role in the occurrence of the dry band arcing (Figure 4.13 (d)). This tip may work as a water needle and thus, the condition is comparable to the needle-bar at the oil-pressboard interface with white marks that nearly bridged the gap and eventually promoted a full discharge (see Figure 3.10 (d)).

4.7 Summary

Full discharge characteristics have been investigated by means of leakage current measurement using a shunt resistor and RFCT. The characteristics have been studied in terms of the frequency spectra, full discharge streamer initiation and propagation, correlation with the simultaneous voltage and correlation with the PRPD data measured using the commercial PD equipment. Frequency and time domain analysis have suggested that full discharges are due to streamers with corona-like discharge characteristics that propagate, bridging the electrode gap. Such a mechanism leads to the flow of leakage current that contains numerous pulses and a continuous component within a period of half an AC cycle or more. Correlation with the PRPD data has shown the validity of such an event being measured in laboratory using commercial PD equipment although there are certain mismatches due to technical factors and the random phenomena that can occur during the surface discharges. Therefore, identifying and detecting this kind of discharge is an important factor for the future condition monitoring of power transformers. A comparison between dry band arcing for outdoor insulation and full discharge events at the oil-pressboard interface has been made. Both events have similarities, i.e. they are caused by localised heating processes that lead to moisture evaporation and their occurrences occur predominantly on the dry surface.

Chapter 5

Modelling of Surface Discharge at the Oil-pressboard Interface

5.1 Introduction

The inter-phase region of HV transformer comprises composite insulation of oil and cellulose-based pressboard barrier. An empirical study of surface discharge behaviour at the oil-pressboard interface using a needle-bar electrode experiment has been presented in Chapters 3 and 4. This chapter focusses on the study of the physics of the observed surface discharge behaviour by means of computer simulation modelling using charge transport equations. It appears that discharges during the initiation and propagation of streamers are associated to PD events in the dielectric liquid [85]. The streamer initiation voltage of a dielectric liquid under impulse voltages is comparable with PD inception under AC voltages and also demonstrates the same physical processes [85]. The surface discharge model developed in this thesis is based on charge transport continuity equations used by some authors to model streamer development in transformer oil [76, 78, 79] and water [90]. In particular, these equations have been used to predict surface discharge current in air [95]. In this work, charge generation is modelled using field dependent molecular ionisation theory. The charge movement during surface discharge is studied by validating the modelling results with the experimental data. The model has been developed using COMSOL Multiphysics [121], an FEA software package on a 2-D axial symmetry plane by considering the porous structure of pressboard. The consideration of porous structure requires knowledge of the effective value of permittivity of the oil-impregnated pressboard and this has been

estimated on the basis of relative mass density. Before this estimation method is used, it has been firstly validated with the experimental data published in the literature [122].

5.2 Model Representation

A detailed description of the developed model and any assumptions made is described in this section.

5.2.1 Simulation Model Geometry

Solving a 3-D FEA model for this research can become computational cost in terms of the run time and memory usage because it may involve millions of degrees of freedom (related to discrete representation of the field variables) to be solved. By using a 2-D model, the number of degrees of freedom can be reduced down to less than one million. However, imitating the needle-bar configuration used in the surface discharge experiment on 2-D axial symmetry and xy planes (see Figure 5.1) does not represent a needle shape for the HV electrode as can be seen in the 3-D geometry shown in Figure 5.2. Hence, the surface discharge at the oil-pressboard interface is modelled using a 2-D axial symmetry plane as shown in Figure 5.3, so that, the electrode configuration in terms of a 3-D view is as shown in Figure 5.4. The 3-D view illustrates a needle electrode that is pointed and perpendicular to a disc of pressboard surface immersed in mineral oil and surrounded by a ring of ground electrode bar with an inner radius of 30 mm placed on the pressboard disc. This is the best geometry configuration to represent the needle-bar configuration as used for the surface discharge experiment (see Figure 3.1). The assumption is that this configuration would lead to different physics in terms of the streamer initiation and propagation directions due to different electric field profiles, however, the physics of the discharge mechanism is identical.

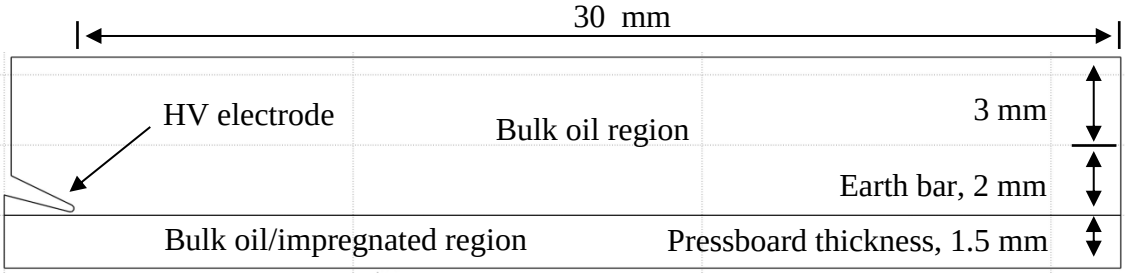

Figure 5.1: Geometry drawn on 2-D axial symmetry and xy planes

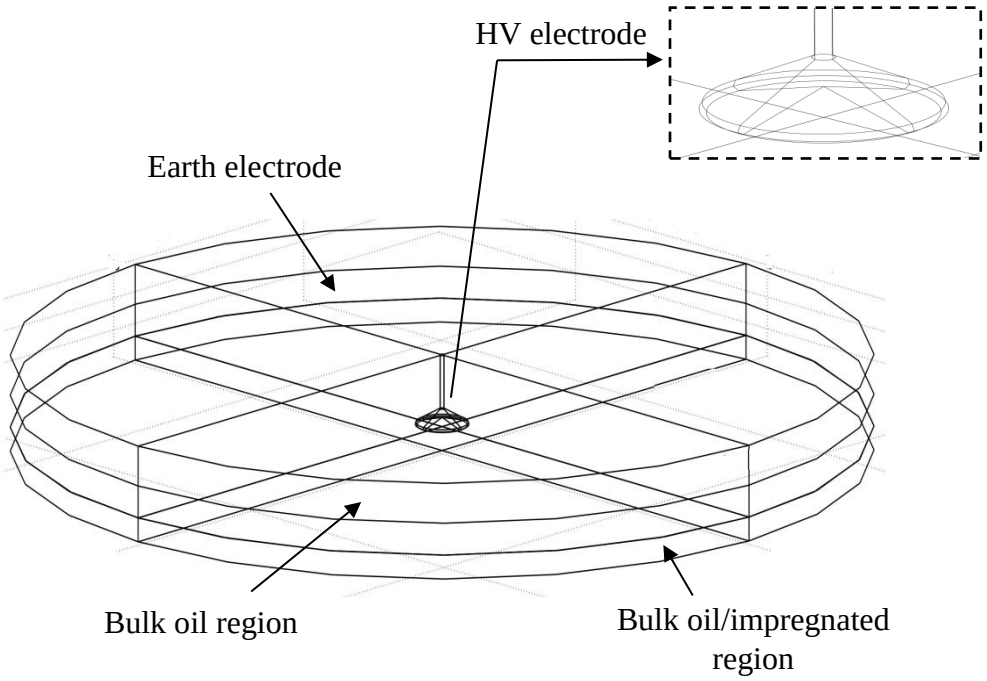

(a) 3-D view based on 2-D axial symmetry geometry

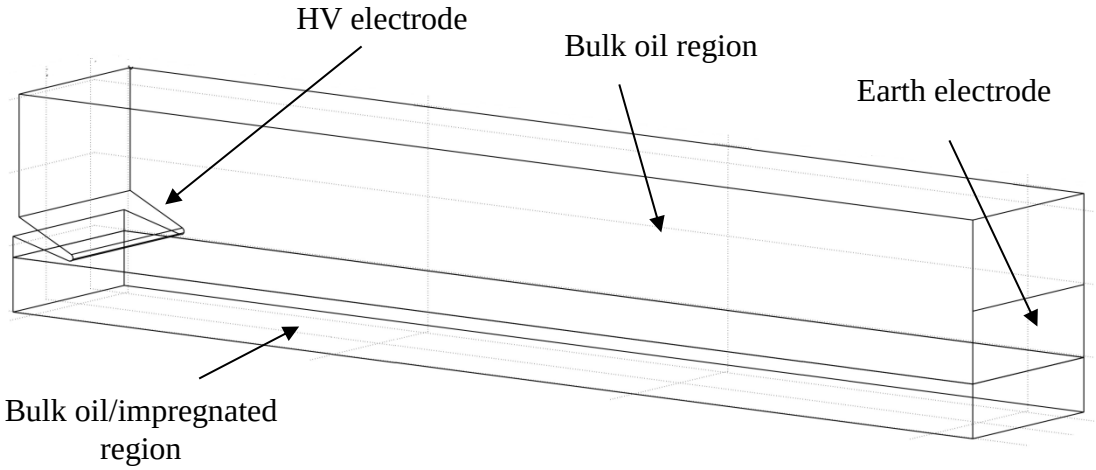

(b) 3-D view based on 2-D xy geometry

Figure 5.2: Unwanted 3-D model geometry converted from the 2-D model in Figure 5.1 based on the axial symmetry and xy geometry concepts

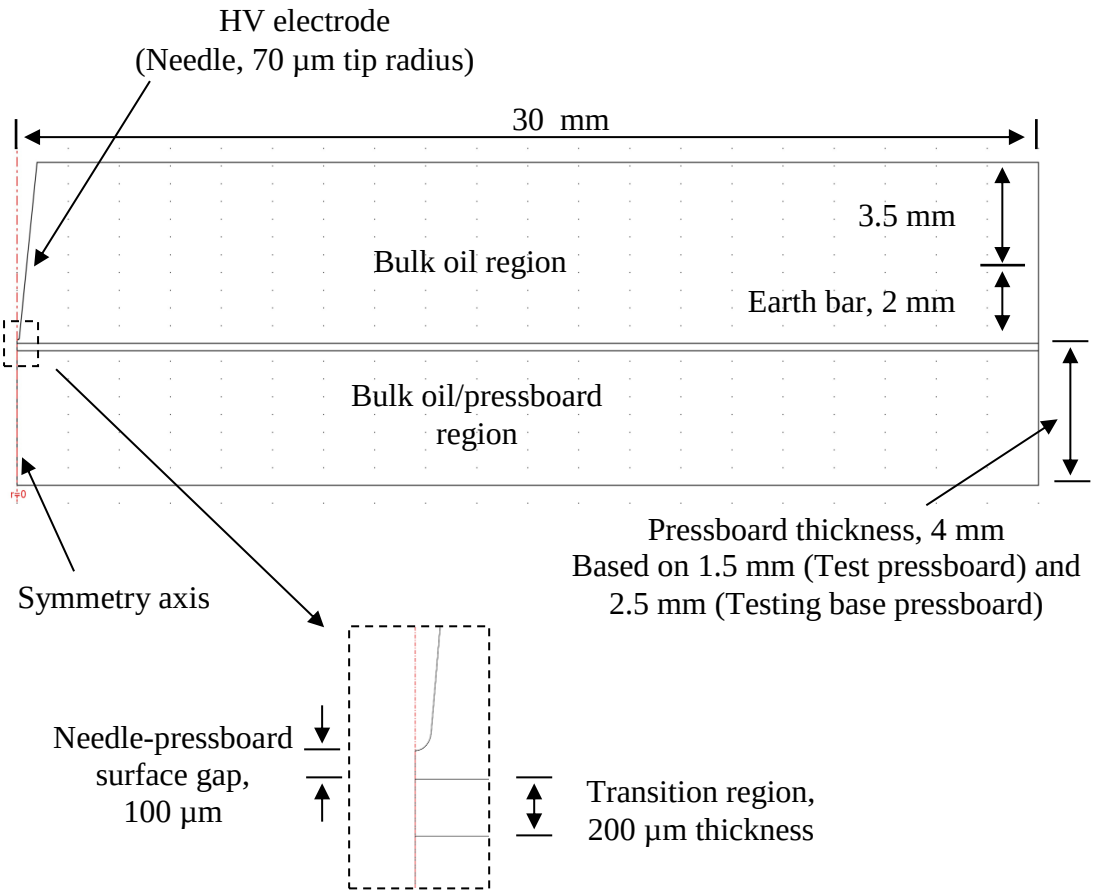

Figure 5.3: Model geometry for surface discharge simulation using the 2-D axial symmetry plane

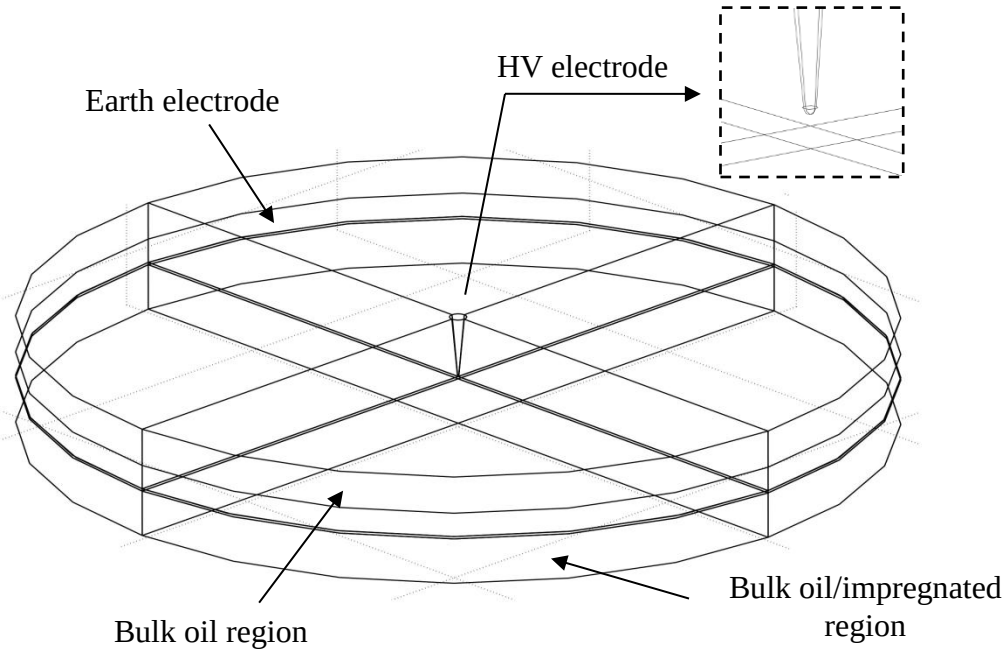

Figure 5.4: 3-D view for the 2-D axial symmetry model in Figure 5.3

Ultimately, a blunt needle tip is an unavoidable condition [123] particularly after long periods of HV application. It is assumed that the effective needle tip radius during the surface discharge experiment is in the range of 70-100 µm, whereby this radius can be observed after about 2-4 hours of HV application for a needle that had a radius of about 1-3 µm prior to voltage application. Examples of needle tips used in this research are shown in Figure 5.5 (a) and (b). The needle is changed when the tip radius is considered to be too blunt and out of shape and this was defined as once the radius is larger than 100 µm as shown in Figure 5.5 (c). This usually occurs after about 7 hours of continuous energisation. Therefore, the nature of the experiment makes it extremely difficult to maintain the needle tip radius over the experiment lifetime. Based upon this condition, for simulation purposes, the needle tip is drawn with a radius of 70 µm and it is assumed that this represents an average condition.

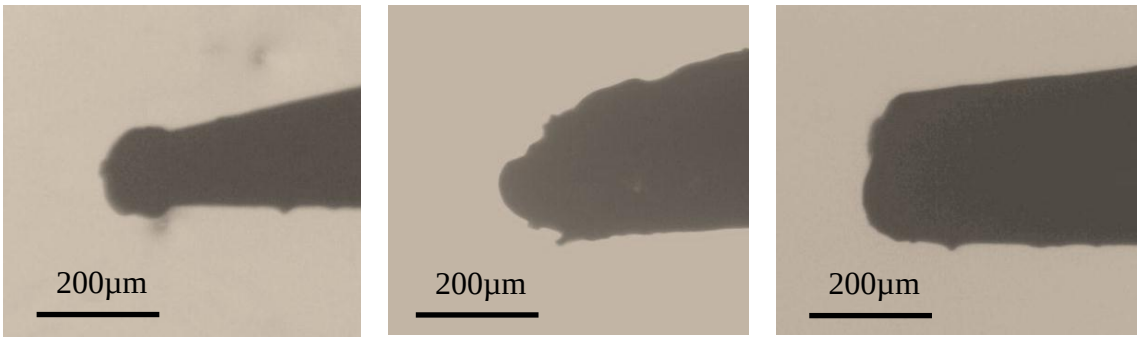

(a) After about 7 hours of experiment – effective tip radius

(b) After more than 35 hours of experiment – effective tip radius

(c) After about 10 hours of experiment – unacceptable blunt condition

Figure 5.5: Details of various blunt conditions of needle tips

The oil-pressboard interface is modelled by considering the physical model shown in Figure 2.15 originally proposed Mitchinson et al [15]. However, the no-slip region which is also called the compact layer in the oil region that is very close to the pressboard surface is neglected in the simulation model. This is due to the fact that this layer is characterised by a thickness of the order of a few ions [70, 71]. To model this layer using finite element analysis (FEA) would prove problematic as very high mesh density would be required to accurately determine the field at this interface. The substantial increase in computational time would not yield benefit in terms of the accuracy of the converged results. Based on the arc and glow discharges at the needle tip and dual colouration phenomenon during full discharges, the needle-bar

configuration in the experiment promotes discharges to occur in the transition region and no-slip region as well as in the boundary layer within the bulk oil region. In order to ensure that in the model the streamer initiates in the boundary layer within the oil region, the needle tip of the simulation model is set at 100 μm from the edge of transition region as illustrated in Figure 5.3. Therefore, the model geometry proposed in this work has three media, i.e. the bulk oil region, a transition region and the bulk oil/pressboard region, whereby the transition region is treated as the porous part of the pressboard so that the streamer can be modelled to propagate through it. On the other hand, the bulk oil/pressboard region is assumed as a perfect insulator, i.e. this region is assigned zero conductivity ($\sigma = 0$).

If the microscopic view of pressboard edge as shown in Figure 2.2 (b) is observed, then the transition region has thickness in the range of 150-300 μm. In the model, the transition region thickness is assumed to be 200 μm. In order to ease the computational cost in terms of the run time and memory usage, the non-homogenous structure of pressboard surface is neglected so that the meshing elements for the simulation model are reduced. The pressboard thickness including the transition region is 4 mm. This represents the tested pressboard (1.5 mm) and the testing base (2.5 mm pressboard).

5.2.2 Governing Equations in Bulk Oil and Transition Regions

In order to model the surface discharge at the oil-pressboard interface which involves streamer propagation in the oil and transition regions, the governing equations for both regions are based on the charge transport continuity equations:

$$\frac{\partial N_p}{\partial t} + \nabla \cdot \left(\overrightarrow{J_{c\_p}}\right) = G_p\left(\left|\vec{E}\right|\right) - N_p N_n K_{rpn} - N_p N_e K_{rpe} \tag{5.1}$$

$$\frac{\partial N_n}{\partial t} - \nabla \cdot \left(\overrightarrow{J_{c\_n}}\right) = \frac{N_e}{\tau_a} - N_p N_n K_{rpn} \tag{5.2}$$

$$\frac{\partial N_e}{\partial t} - \nabla \cdot \left(\overrightarrow{J_{c\_e}}\right) = G_e\left(\left|\vec{E}\right|\right) - N_p N_e K_{rpe} - \frac{N_e}{\tau_a} \tag{5.3}$$

which model the three charge carriers, i.e. positive and negative ions and electrons. Where, N_p, N_n and N_e are the density of positive ions, negative ions and electrons

(mol·m^{-3}) respectively, $\overrightarrow{J_{c\_p}}$, $\overrightarrow{J_{c\_n}}$ and $\overrightarrow{J_{c\_e}}$ are the conduction current density vectors (mol·m^{-2}·s^{-1}) due to the migration of positive ions, negative ions and electrons respectively, K_{rpn} and K_{rpe} are the recombination coefficients (m^3·s^{-1}·mol^{-1}) between positive and negative ions and between positive ions and electrons respectively and τ_a is the time constant (s) for the electron attachment. The terms $G_p(|\vec{E}|)$ and $G_e(|\vec{E}|)$ are the generation rate (mol·m^{-3}·s^{-1}) for positive ions and electrons correspondingly. These equations represent the generation, loss and transport mechanisms of the charge species under the influence of an electric field. Employing the charge transport continuity equations in the transition region represents this particular region as a porous medium of pressboard that allows streamers to propagate through it. To determine the electric field distribution, Equations (5.1)-(5.3) are coupled with Poisson's equation:

$$\nabla \cdot (-\varepsilon_0 \varepsilon_r \vec{E}\,) = (N_p - N_n - N_e) q N_A \tag{5.4}$$

Where ε_0 and ε_r are the permittivity of free space (8.854×10^{-12} F·m^{-1}) and relative permittivity of the material respectively, $\vec{E}$ is the electric field vector (V·m^{-1}), q is the elementary charge (1.6022×10^{-19} C) and N_A is the Avogadro's number (6.023×10^{23} mol^{-1}). Throughout the simulations, the mole unit has been used in the charge transport continuity equations, thus, the terms elementary charge q and Avogadro's number N_A should be employed in the relevant equations. Implementation of this approach allows analysis of any imbalances based on the unit error indications in the COMSOL Multiphysics software. In addition, heat conduction is also considered in the model:

$$\frac{\partial T}{\partial t} = \frac{1}{\rho C_P}\left(k_T \nabla^2 T + \vec{E} \cdot (\overrightarrow{J_{c\_p}} + \overrightarrow{J_{c\_n}} + \overrightarrow{J_{c\_e}}) q N_A\right) \tag{5.5}$$

Where ρ is the mass density (kg·m^{-3}), C_P is the specific heat capacity (J·kg^{-1}·K^{-1}), k_T is the thermal conductivity (W·m^{-1}·K^{-1}) of the material and T is the temperature (K). The first term on the right hand side of Equation (5.5) equates to the heat conduction as a result of thermal diffusivity. The second term on the right hand side of the equation represents the heat source from the electrical power dissipation, Q_v (W·m^{-3}) as a result of conduction current heating from the movement of charge carriers during the partial

discharge under the influence of local electric field. The conduction current density vectors due to positive ions, negative ions and electrons can be expressed as:

$$\overrightarrow{J_{c\_p}} = N_p \mu_p \vec{E}, \qquad \overrightarrow{J_{c\_n}} = N_n \mu_n \vec{E}, \qquad \overrightarrow{J_{c\_e}} = N_e \mu_e \vec{E} \tag{5.6}$$

Where μ_p, μ_n and μ_e are the mobilities ($m^2 \cdot s^{-1} \cdot V^{-1}$) for the positive ions, negative ions and electrons respectively.

It should be noted that the velocity of the fluid (mineral oil) as a result of electric field, i.e. electro-osmosis processes [71, 124] is neglected in the model based upon the very short period of discharge, i.e. nanoseconds to microseconds. It is therefore assumed that the bulk oil is stationary over the transition region. The diffusivity of the charge carriers for both regions are also not considered as this is an insignificant effect compared to the influence of the conductivity leading to a conduction current or migration current. Hence, technically, the model only considers the conduction current as depicted in Equations (5.1)-(5.3).

The role of electric field dependent molecular ionisation in streamer propagation in dielectric liquid like transformer oil has been qualitatively discussed in the literature [87, 125, 126, 127]. Recent validation work using the COMSOL Multiphysics Simulation package [78, 79] has shown that field dependent molecular ionisation plays a dominant role in pre-breakdown streamer development in transformer oil. In this research, the charge generation rates $G_p(|\vec{E}|)$ and $G_e(|\vec{E}|)$ are modelled based on the Zener model [86] that causes the field dependent molecular ionisation mechanism and eventually contribute to partial discharges at the oil-pressboard interface. The Zener model is:

$$G_F(|\vec{E}|) = \frac{qN_0 a|\vec{E}|}{h} exp\left(-\frac{\pi^2 m^* a \Delta^2}{qh^2|\vec{E}|}\right) \tag{5.7}$$

Where $G_F(|\vec{E}|)$ is the charge generation rate based on the Zener model ($mol \cdot m^{-3} \cdot s^{-1}$), N_0 is the density of the ionisable species ($mol \cdot m^{-3}$), a is the molecular separation distance (m), h is the Planck's constant (6.626×10^{-34} J·s), m^* is the effective electron mass (kg)

and Δ is the molecular ionisation energy (J). Based on the mechanism of field dependent molecular ionisation, it is assumed that a free electron and a positive ion are extracted from a neutral molecule as a result of a sufficiently high electric field. Hence, the terms of charge generation in Equations (5.1) and (5.3) are:

$$G_p(|\vec{E}|) = G_e(|\vec{E}|) = G_F(|\vec{E}|) \tag{5.8}$$

5.2.3 Governing Equations in Bulk Oil/Pressboard Region

With the assumption that the bulk oil/pressboard region is a perfect insulator, the charge transport equations are not applicable in the modelling of this region. Hence, the current through the bulk oil/pressboard region is only a displacement current, i.e. conduction current in this particular region is equal to zero. The governing equations for this region are:

$$\nabla \cdot (-\varepsilon_0 \varepsilon_r \vec{E}\,) = 0 \tag{5.9}$$

$$\frac{\partial T}{\partial t} = \frac{1}{\rho C_P}(k_T \nabla^2 T) \tag{5.10}$$

5.2.4 Boundary Conditions

In the COMSOL Multiphysics package [121], the charge transport continuity equations (Equations (5.1)-(5.3)) can be solved using the "Convection and Diffusion" application mode, Poisson's equations (Equations (5.4) and (5.9)) are associated with the "Electrostatics" application mode and the heat conduction equations (Equations (5.5) and (5.10)) are solved using the "Heat Transfer by Conduction" application mode. This section discusses in detail the boundary conditions imposed for each governing equation based on the boundaries labelled in Figure 5.6. Table 5.1 summarises the boundary conditions for each application mode.

As a consequence of the exclusion of the "Convection and Diffusion" application mode in the bulk oil/pressboard region boundaries 2 and 7 are not applicable for this particular application mode within the model. Since the diffusivity of the charge carriers is

neglected and only conduction current is accounted, the boundary conditions at the electrodes, i.e. outer boundary 3 for HV electrode and outer boundary 9 for ground electrode are set to zero normal diffusive flux:

$$\hat{n} \cdot (-D_i \nabla N_i) = 0 \tag{5.11}$$

Where D is the diffusion coefficient ($m^2 \cdot s^{-1}$), i is either p, n or e and $\hat{n}$ is the unit vector normal to the boundary. With the assumption that free charge carriers migrations through the outer boundaries 4 and 8 are extremely small in magnitude and can be considered negligible compared to the electrode boundaries, both outer boundaries are set to zero normal flux:

$$\hat{n} \cdot \vec{F_i} = 0 \tag{5.12}$$

Where $\vec{F_i}$ is the total flux density ($mol \cdot m^{-2} \cdot s^{-1}$) for each charge carrier. Based on the boundary conditions in Equations (5.11) and (5.12), the simulation model works as such that the conduction currents are only permitted to flow in and out from the system through the electrodes. Consequently, in the "Electrostatics" application mode, the outer boundaries 4, 7 and 8 are set to zero normal electric displacement field:

$$\hat{n} \cdot \vec{D} = 0 \tag{5.13}$$

Where $\vec{D}$ is the electric displacement field ($C \cdot m^{-2}$).

The model is developed to study the partial discharge mechanism in terms of the movement of free charge carriers by validating the simulation results with the values obtained experimentally under AC voltage application. Based on the short period of a partial discharge event, i.e. nanoseconds to microseconds, the variation in applied AC voltage within that timescale is assumed to be negligible. Therefore, a DC voltage V_{app} is set to the boundary of needle electrode (boundary 3).

In the case of "Heat Transfer by Conduction" application mode, each of the outer boundaries is set to zero normal thermal diffusive flux:

$$-\hat{n} \cdot (-k_T \nabla T) = 0 \tag{5.14}$$

as such the system is said to be adiabatic, i.e. no heat exchange occurring with the environment of the system within the short timescale of interest for the simulation model.

In order to investigate the partial discharge mechanism with streamer propagation in the transition region, the normal flux components for both the "Convection and Diffusion" and "Electrostatics" application modes have to be continuous across the boundary. Hence, the interior boundary 5 for both application modes are set to zero normal flux difference between the two media i.e. bulk oil region and transition region. A similar boundary setting is also applied to the interior boundary 5 for the "Heat Transfer by Conduction" application mode to ensure heat conduction also occurs in the transition region.

In addition, to ensure the continuity of the normal current component due to the free charge carriers across the boundary between the transition region and bulk oil/pressboard region, the internal boundary 6 must be able to support a net surface charge. The continuity equation for the surface charge density N_s (mol·m^{-2}) can be expressed as the difference in normal total conduction currents between both sides of the interface:

$$\begin{aligned} \frac{\partial N_s}{\partial t} &= \hat{n} \cdot \left(\overrightarrow{J_{c\_trans}} - \overrightarrow{J_{c\_oil/pb}}\right) \\ &= \hat{n} \cdot \overrightarrow{J_{c\_trans}} \\ &= \hat{n} \cdot (\overrightarrow{J_{c\_p}} + \overrightarrow{J_{c\_n}} + \overrightarrow{J_{c\_e}})\vec{E} \end{aligned} \tag{5.15}$$

Where $\frac{\partial N_s}{\partial t}$ is the time derivative of the surface charge density (mol·m^{-2}·s^{-1}), $\overrightarrow{J_{c\_trans}}$ and $\overrightarrow{J_{c\_oil/pb}}$ are the total conduction current density vectors (mol·m^{-2}·s^{-1}) in the transition region and bulk oil/pressboard region correspondingly. Since the bulk oil/pressboard region is modelled as a perfect insulator, the term of conduction current in this region is omitted. Modelling surface charge is done by integrating Equation (5.8) over time using the "Weak Form Boundary" application mode in the COMSOL Multiphysics software [121].

Consequently, the surface charge density N_s is set as the condition for the interior boundary 6 of the "Electrostatics" application mode. On the other hand, by adopting the conditional boundary condition as in [59] to avoid inherent error in COMSOL Multiphysics software, the condition of the interior boundary 6 for each free charge carriers of the "Convection and Diffusion" application mode is set to:

$$\hat{n} \cdot \overrightarrow{F_p} = \begin{cases} 0 & if \quad \hat{n} \cdot \vec{E} < 0 \\ \hat{n} \cdot \overrightarrow{J_{c\_p}} & if \quad \hat{n} \cdot \vec{E} \geq 0 \end{cases} \tag{5.16}$$

$$\hat{n} \cdot \overrightarrow{F_n} = \begin{cases} \hat{n} \cdot \overrightarrow{J_{c\_n}} & if \quad \hat{n} \cdot \vec{E} \leq 0 \\ 0 & if \quad \hat{n} \cdot \vec{E} > 0 \end{cases} \tag{5.17}$$

$$\hat{n} \cdot \overrightarrow{F_e} = \begin{cases} \hat{n} \cdot \overrightarrow{J_{c\_e}} & if \quad \hat{n} \cdot \vec{E} \leq 0 \\ 0 & if \quad \hat{n} \cdot \vec{E} > 0 \end{cases} \tag{5.18}$$

Surface charges may have low ability to move in response to the electric field due to trapping mechanisms at the oil-pressboard interface. Hence, if the surface charge N_s as a result of positive and negative ions and electrons attached to the interior boundary 6 is assumed to have only one value of mobility, the electrical power dissipation on the surface, Q_s ($W \cdot m^{-2}$) caused by the conduction of surface charges at the boundary can be expressed as:

$$\begin{aligned} Q_s &= \vec{E} \cdot \left(N_s \mu_s \vec{E}\right) q N_A \\ &= \vec{E} \cdot \left(\overrightarrow{J_{c\_s}}\right) q N_A \end{aligned} \tag{5.19}$$

Where μ_s is the surface charge mobility ($m^2 \cdot s^{-1} \cdot V^{-1}$) and $\overrightarrow{J_{c\_s}}$ is the surface conduction current density ($mol \cdot m^{-1} \cdot s^{-1}$).

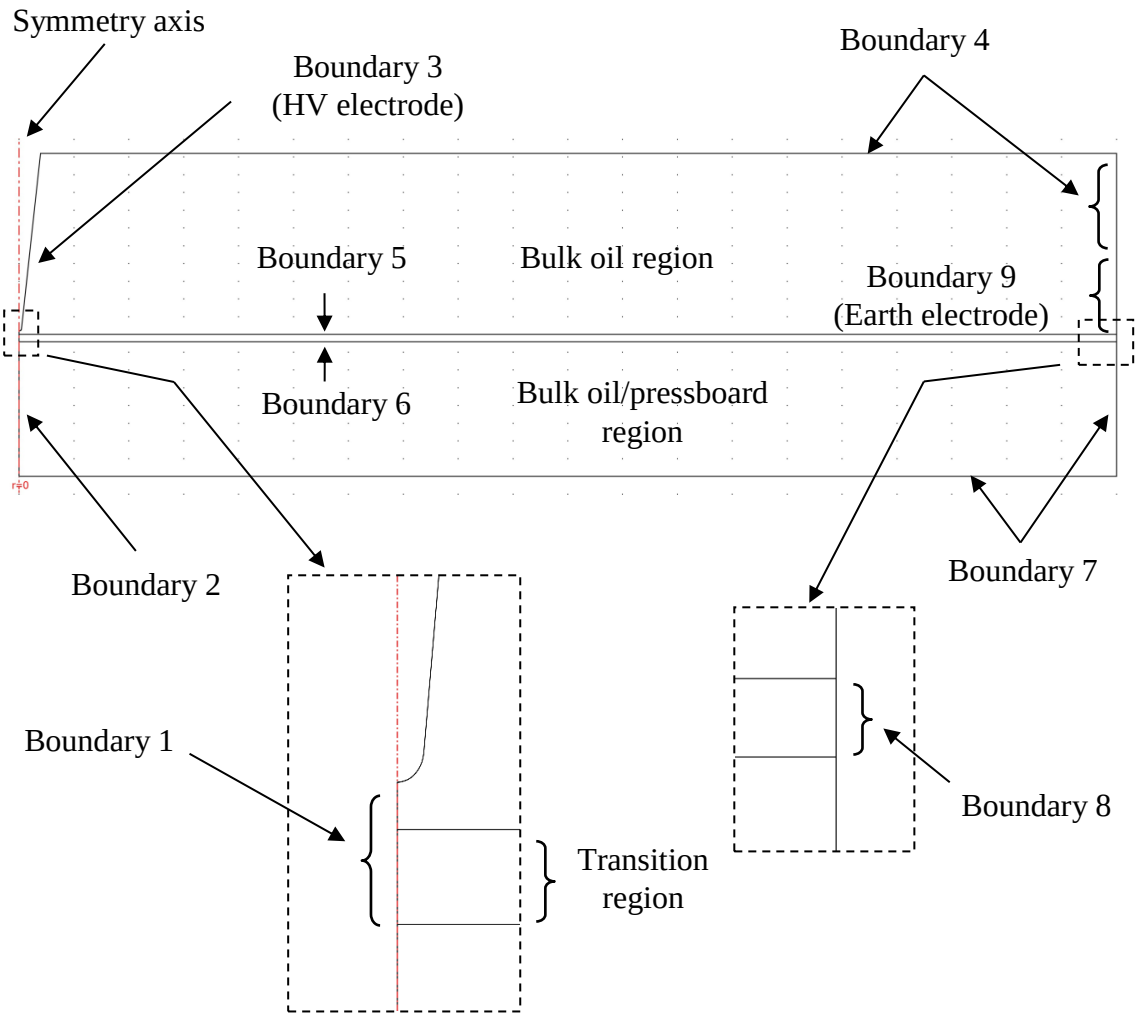

Figure 5.6: Boundary numbers for the surface discharge model geometry

Table 5.1: Boundary conditions with reference to Figure 5.6 for the model of surface discharge at the oil-pressboard interface

Application Mode	Convection and Diffusion $(N_{i=p,n,e})$	Electrostatics (V)	Heat Transfer by Conduction (T)
Boundary 1 (symmetry axis)	Axial symmetry $r = 0$	Axial symmetry $r = 0$	Axial symmetry $r = 0$
Boundary 2 (symmetry axis)	NA		
Boundary 3 (Outer)	Convective flux $\hat{n} \cdot (-D_i \nabla N_i) = 0$	Electric potential $V = V_{app}$	Thermal insulation $-\hat{n} \cdot (-k_T \nabla T) = 0$
Boundary 4 (Outer)	Insulation/Symmetry $\hat{n} \cdot \vec{F_i} = 0$ Where, $\vec{F_i} = -D_i \nabla N_i + \vec{J_i}$	Zero charge/ Symmetry $\hat{n} \cdot \vec{D} = 0$ Where, $\vec{D} = \varepsilon_0 \varepsilon_r \vec{E}$	
Boundary 5 (Interior)	Continuity $\hat{n} \cdot (\overrightarrow{F_1} - \overrightarrow{F_2}) = 0$	Continuity $\hat{n} \cdot (\overrightarrow{D_1} - \overrightarrow{D_2}) = 0$	Continuity $\hat{n} \cdot (\overrightarrow{Q_1} - \overrightarrow{Q_2}) = 0$ Where, $\vec{Q} = -k_T \nabla T$
Boundary 6 (Interior)	Flux $\hat{n} \cdot \vec{F_i} = F_0$ Refer Equation (5.16)-(5.18) for details.	Surface charge $\hat{n} \cdot (\overrightarrow{D_1} - \overrightarrow{D_2}) = N_s q N_A$ Refer Equation (5.15) for details.	Heat flux discontinuity $\hat{n} \cdot (\overrightarrow{Q_1} - \overrightarrow{Q_2}) = \vec{E} \cdot (\overrightarrow{J_{c\_s}}) q N_A$ Refer Equation (5.19) for details.
Boundary 7 (Outer)	NA	Zero charge/ Symmetry $\hat{n} \cdot \vec{D} = 0$	Thermal insulation $-\hat{n} \cdot (-k_T \nabla T) = 0$
Boundary 8 (Outer)	Insulation/Symmetry $\hat{n} \cdot \vec{F_i} = 0$		
Boundary 9 (Outer)	Convective flux $\hat{n} \cdot (-D_i \nabla N_i) = 0$	Ground $V = 0$	

5.2.5 Model Parameters

In practice, the pressboard porosity reflects the permittivity values due to oil and moisture penetration and absorption during impregnation process that leads to a complex composite insulation system. By introducing in the model the transition region, where the pressboard density is very much lower compared to the bulk region and thus, promotes a layer comprising of a mixture of oil molecules, cellulose pressboard, and other species such as water, it is necessary to determine the effective relative permittivity of the transition region for simulation purposes. The permittivity of the transition region ε_{trans} is estimated using the relative mass density of pressboard X_{pb_trans}, oil X_{oil_trans} and water X_{water_trans} in the transition region as follows:

$$\varepsilon_{trans} = X_{pb\_trans}\varepsilon_{pb} + X_{oil\_trans}\varepsilon_{oil} + X_{water\_trans}\varepsilon_{water} \tag{5.20}$$

Where ε_{pb} , ε_{oil} , ε_{water} are relative permittivity of pressboard, oil and water respectively. In order to confirm the validity of Equation (5.20), the equation has been tested and compared with the empirical data of permittivity of oil-impregnated pressboard as affected by moisture from published results in the literature [122]. For this purpose, a similar relative mass density concept used in the transition region is also applied to the bulk oil/pressboard region and for the whole oil-impregnated pressboard. Therefore, the effective relative permittivity for both media can be expressed as follows:

$$\varepsilon_{oil/pb} = X_{pb\_oil/pb}\varepsilon_{pb} + X_{oil\_oil/pb}\varepsilon_{oil} + X_{water\_oil/pb}\varepsilon_{water} \tag{5.21}$$

$$\varepsilon_{T} = X_{oil/pb}\varepsilon_{oil/pb} + X_{trans}\varepsilon_{trans} \tag{5.22}$$

Where $X_{pb\_oil/pb}$, $X_{oil\_oil/pb}$ and $X_{water\_oil/pb}$ are relative mass density of pressboard, oil and water in the bulk oil/pressboard region respectively, $X_{oil/pb}$ and X_{trans} are the relative mass density of the bulk oil/pressboard and transition regions with respect to the whole oil-impregnated pressboard correspondingly and $\varepsilon_{oil/pb}$ and ε_{T} are the relative permittivity of the bulk oil/pressboard region and whole oil-impregnated pressboard respectively.

In the literature [122], the size of the pressboard samples was 70 mm × 70 mm with 5 mm thickness and conformed to the BS 231:1950 Type II standard [128] whereby the mass density is in the range of 900-1150 kg·m^{-3}. If the pressboard mass density is 900 kg·m^{-3}, hence the dry pressboard sample mass is 22.1 g.

It is assumed that the impregnation process leads to the presence of water in the transition region which will grow exponentially with respect to the total weight of water in the pressboard reaching a saturation level so that additional moisture is in the oil/pressboard bulk region. This assumption is important for curve fitting between the model and experimental results. Oil-impregnated pressboard is considered to have four different moisture conditions as used in this research, i.e. dry (less than 0.5%), 3%, 6% and 9% so that a similar assumed percentage of effective weight of water in both the transition and bulk oil/pressboard regions can be used afterwards for simulation purposes. In order to work out the unknown density of oil and pressboard within the transition region, it is necessary to assume the thickness of the transition and bulk oil/pressboard regions and the volume ratio between pressboard and composite oil/water in both regions.

Figure 5.7 shows the estimated permittivity for the transition and bulk oil/pressboard regions as well as the whole oil-impregnated pressboard, i.e. transition region plus bulk/oil region. The permittivity values are determined based on the oil mass density ρ_{oil} of 880 kg·m^{-3}, water mass density ρ_{water} of 1000 kg·m^{-3}, pressboard permittivity ε_{pb} of 4, oil permittivity ε_{oil} of 2.2 and water permittivity ε_{water} of 80, 200 µm thickness of each side, i.e. upper and lower sides of the pressboard that anticipated as the transition region and volume ratio of 2 : 8 between pressboard and composite oil/water in the transition region and vice versa in the bulk oil/pressboard region (8 : 2 ratio). As depicted in Figure 5.7, moisture content in the pressboard plays important role to the permittivity of each pressboard region. The permittivity of the transition region tends to increase significantly as the moisture content is around 6%. On the other hand, the permittivity of the bulk oil/pressboard regions increases linearly with the moisture level. Both characteristics contribute to the effective permittivity profile of the whole oil-impregnated pressboard.

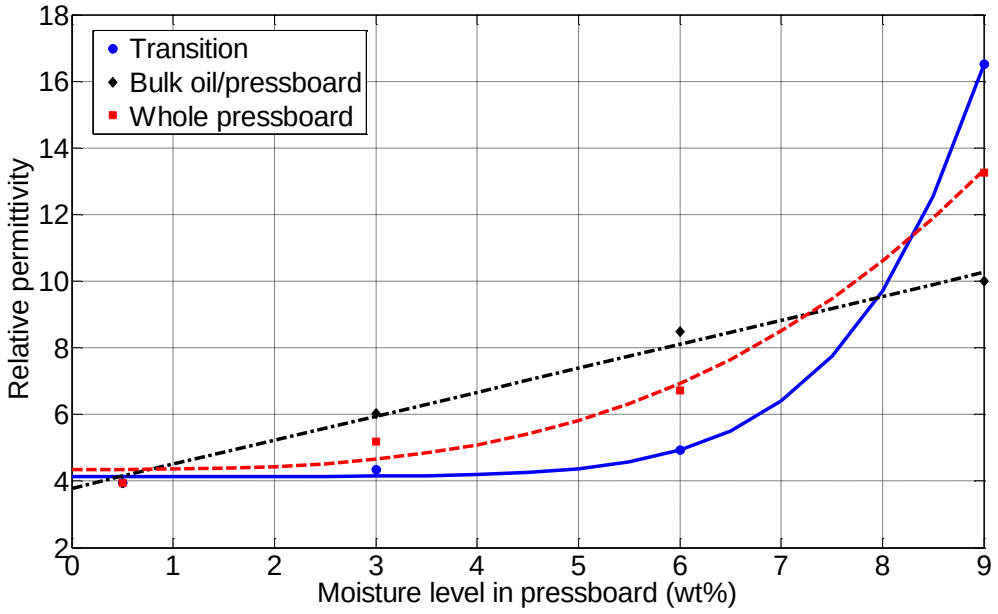

Figure 5.7: Relative permittivity based on the relative density estimation

Figure 5.8 compares the calculated and measured permittivity of the whole oil-impregnated pressboard. The figure shows a close agreement between the calculated and measured values. Such a close correlation confirms that it is reasonable to use Equation (5.20) and (5.21) to calculate the permittivity at the transition and bulk oil/pressboard regions. In the case of 1.5 mm thick pressboard used in the surface discharge experiment with dimension of 100 mm × 100 mm and pressboard mass density ρ_{pb} of 1400 kg·m^{-3}, the estimated permittivity values of the transition and bulk oil/pressboard regions are given in Table 5.2.

As in the case of permittivity, the penetration of oil and moisture into the porous pressboard may also influence the conductivity values. However, the use of relative density would cause the effective conductivity to be overestimated even when ultra-pure water conductivity σ_{water} of 50 µS·m^{-1} [129] is used in conjunction with the pressboard conductivity σ_{pb} of 0.05 pS·m^{-1} [74, 130], oil conductivity σ_{oil} of 0.5 pS·m^{-1} [74, 130]. For instance, by using the relative density, the conductivity for a 3% moisture pressboard is in the order of 1×10^{-7} S·m^{-1}. This is too large compared to the 4% moisture pressboard reported in [93] which is still in the order of $1\text{x}10^{-12}$ S·m^{-1}. Therefore, the conductivity in the transition region is assumed to be similar to the oil conductivity. This assumption also reflects the mobility of the free charge carriers.

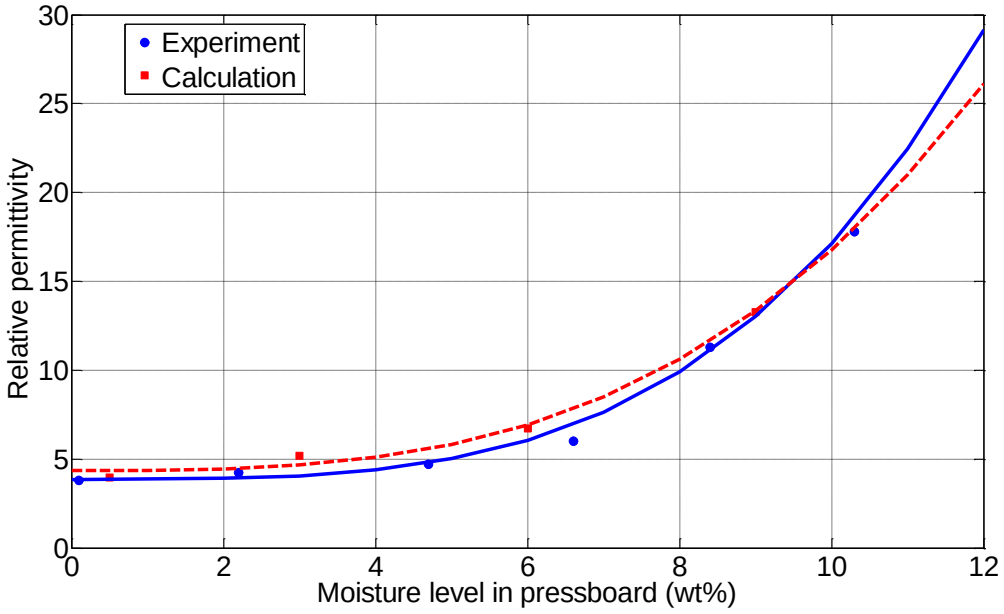

Figure 5.8: Comparison of the whole oil-impregnated pressboard permittivity between the experimental data from Table 1 in [122] and calculated values using the relative mass density estimation

Table 5.2: Relative permittivity calculated using the relative mass density estimation for simulation purposes

Region	Symbol	Relative permittivity			
		dry	3%	6%	9%
Transition	ε_{trans}	3.3	3.5	3.7	8.6
Bulk oil/pressboard	$\varepsilon_{oil/pb}$	4.2	7.0	10.3	12.3

All parameters in the transition and bulk oil/pressboard regions that relate to the thermal equation (Equation (5.5) and (5.10)), i.e. the specific heat capacity C_P and thermal conductivity k_T are estimated using the relative mass density concept. The recombination coefficients, K_{rpn} and K_{rpe} for both the bulk oil and transition regions are determined using Langevin's equation [88] and can be expressed as follows:

$$K_{rpn} = K_{rpe} = \frac{q}{\varepsilon_0 \varepsilon_r}(\mu_p + \mu_n)N_A \tag{5.23}$$

With reference to Equation (5.23), the coefficient value for recombination between positive ions and electrons K_{rpe} also uses the similar term with the coefficient rate of

positive and negative ion recombination K_{rpn}. This is also assumed in other models [75, 78, 79, 90] due to overestimation problems when electron mobility is used instead of negative ion mobility.

All parameters and their respective values used in the simulation are given in Appendix A. Table A.1 provides the general parameters and their corresponding values, whilst Tables A.2, A.3 and A.4 summarise the parameters and their relevant values specified in the bulk oil, transition and bulk oil/pressboard regions respectively for validation with the experimental result. The value of electron attachment time constant τ_a and molecular ionisation energy Δ have been obtained through curve fitting with the experimental data.

As for the surface charge mobility in Equation (5.19), the model uses the ion mobility in the pressboard region previously used in [74], i.e. ten times lower than the ion mobility in oil.

5.3 Simulation Results

This section summarises the simulation results obtained. The model has allowed study of the discharge mechanisms occurring within the transition region. This study gives insight into white mark generation as well as field molecular ionisation and electron attachment mechanisms that ultimately influence the properties of the conduction current.

5.3.1 Comparison with Experimental Data

The surface discharge behaviour at the oil-pressboard interface is studied by validating the simulation result with the experimental data by means of surface discharge current pulse. The simulation result is validated with the experimental result of surface discharge on a dry pressboard determined around the positive peak of applied AC voltage. Based on the short period of current pulse, any AC voltage variation is neglected (Section 5.2.4), a positive DC voltage V_{app} of $30\sqrt{2}$ was applied in the model. The surface discharge model was solved over a time range of 3 μs. The simulation run time to solve that time range was about 3 hours. The current pulse obtained from the

2-D axial symmetry model was calculated by surface integral of the sum of conduction current density $\overrightarrow{J_c}$ and displacement current density $\overrightarrow{J_d}$ at the earth electrode as follows:

$$I = \int_A \hat{n} \cdot \left[\overrightarrow{J_c}(qN_A) + \overrightarrow{J_d}\right] dA \tag{5.24}$$

$$I = \int_{z1}^{z2} \hat{n} \cdot \left[\overrightarrow{J_c}(qN_A) + \overrightarrow{J_d}\right] (2\pi r) dz \tag{5.25}$$

In COMSOL, Equation (5.25) is solved using the Boundary Integration Variables. Both the conduction current density $\overrightarrow{J_c}$ and displacement current density $\overrightarrow{J_d}$ can be expressed as follows:

$$\overrightarrow{J_c} = \left(N_p\mu_p + N_n\mu_n + N_e\mu_e\right)\vec{E} \tag{5.26}$$

$$\overrightarrow{J_d} = -\frac{\partial}{\partial t}\left(\varepsilon_0\varepsilon_r\vec{E}\right) \tag{5.27}$$

Figure 5.9 (a) shows the comparison between the experimental data and the simulated current pulse. The experimental current pulse is a filtered signal using a zero-phase low pass filter [131] to remove noise. The oscillations of the measured current are probably due to stray inductance and capacitance within the measurement circuit. It can be noticed that the magnitude of modelled current pulse is around 0.21 mA, which is greater than the measured current pulse (i.e. about 0.16 mA). The model appears to have a good agreement with the experimental pulse in terms of the rising front. However, the simulated current decays at a faster rate compared to the decaying tail of the experimental current pulse. It is worthwhile noting that the first overshoot in the simulation result at around 0.03 mA is due to the application of step voltage with rise time of 20 ns. This represents the first PD event in the model which occurs in the oil region (100 μm gap between the needle tip and the pressboard surface) before the current started to decay and eventually has a DC current profile. It is also important to note, as depicted in Figure 5.9 (b), the total charge injected into the system demonstrates close correlation between the experiment and simulation. The current pulse leads to approximately 100 pC of charges being injected into the system. The injected charge was calculated by time integration of current pulse waveforms.

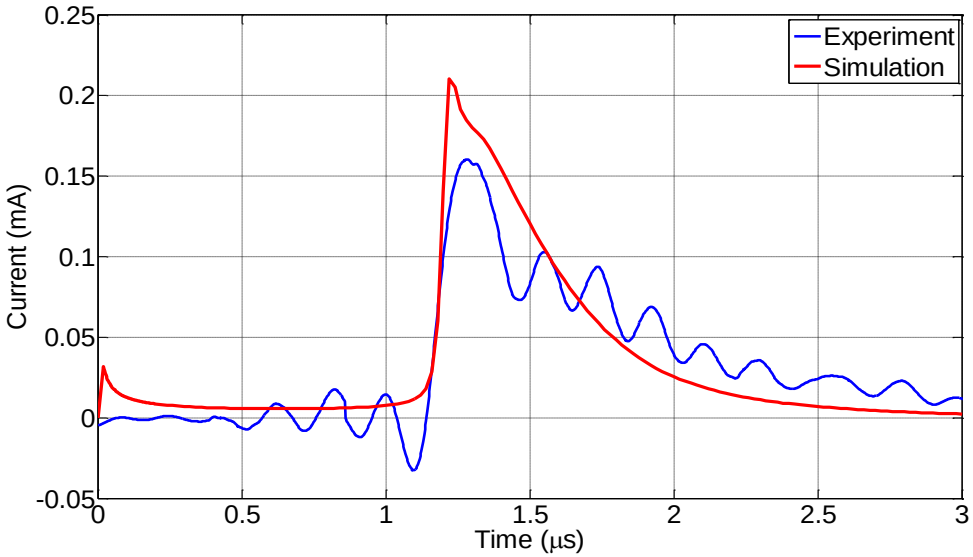

(a) Surface discharge current pulse

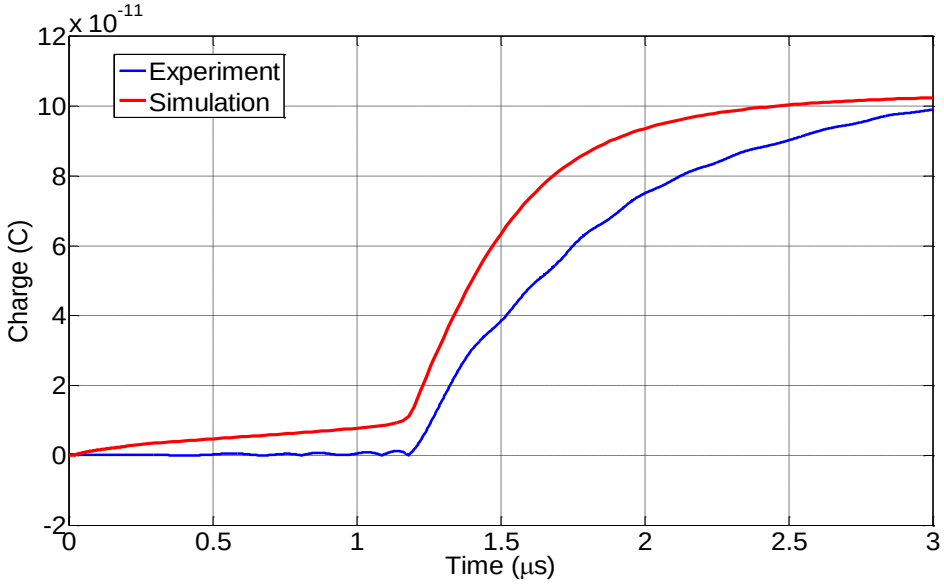

(b) Variation of injected charge into the system

Figure 5.9: Comparison between experimental and simulation results of surface discharge at the oil-pressboard interface

Simulation results shown in Figure 5.9 are based on the data given in Appendix A. The validation work was conducted by varying two parameters, i.e. the molecular ionisation energy and the electron attachment time constant. The value of molecular ionisation energy is important to control the overshoot of the simulated pulse current. It is inversely proportional to the magnitude of the peak current. Increasing the value of molecular ionisation energy would not cause significant changes to the rising front of the pulse current. However, if the value is too high, no streamer development can be

obtained. This is due to the exponential term of the Zener equation. On the other hand, the value of electron attachment time constant is important when modelling the decaying tail of the current pulse. It has a proportional relationship with the decaying time of the current pulse. It should be noted that, increasing the attachment time to increase the decay time would also increase the peak of the pulse current pulse. The simulated discharge current waveform contributes to the amount of charges injected into the system. Hence, both parameters were determined by considering the simulated current pulse as well as the total amount of charges injected into the system.

5.3.2 Discussion on the Surface Discharge Behaviour

The behaviour of surface discharge at the oil-pressboard interface is discussed based on three different directions of streamer propagation, i.e. (1) streamer propagation in the oil region along the symmetry axial line from the needle tip, (2) streamer distribution with radial direction along boundary 5 (interface between oil and pressboard) and (3) streamer within the transition region based on the distance from the interception point between boundary 5 and symmetry axis. Appendix B illustrates the simulated streamer propagation by demonstrating the surface plots of electric field distribution over time. The analysis of the surface discharge behaviour is by correlating the temporal dynamic profiles for electric field, charge carrier density, net space charge density and temperature associated with the streamer for the different stages marked on the simulated surface discharge current shown in Figure 5.10.

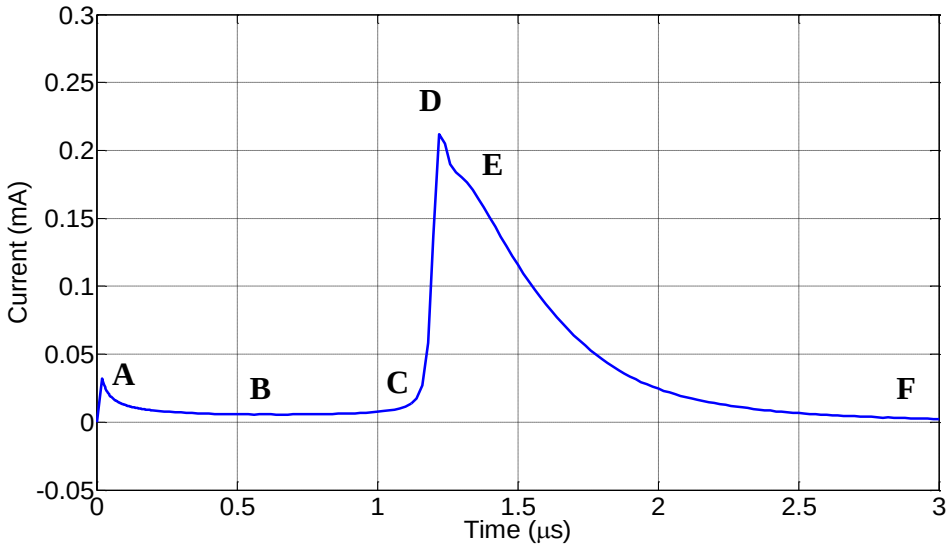

Figure 5.10: Simulated surface discharge current waveform

(1) Streamer in the oil region

Figure 5.11 shows the electric field distribution along the symmetry axis from the needle tip in the bulk oil region, at the oil-pressboard interface line (boundary 5) and in the transition region. As can be seen in the figure, as time progresses, the peaks of electric field are distributed further away from the needle tip. It should be noted that the peaks in the oil region represent the maximum value of electric field in the spatial domain of the system, which is at the vicinity of streamer tip. On the other hand, as the streamer touches the pressboard surface and propagates along the pressboard surface as well as into the transition region, the peaks of the electric field profile along the symmetry axis do not give the maximum electric field in the spatial domain of the system. This is due to the fact that the streamer is shifted due to permittivity mismatch between the oil and transition region. The diversion of electric field distribution due to permittivity mismatch between two different materials has been discussed by some authors [51, 80] that consider the solid dielectric as a perfect insulator. Based upon the shifting of streamer propagation obtained from the simulation, the rest of the discussions in this section are based on the three different directions of the streamer. Therefore, Figures 5.12-5.16 demonstrate the density distribution of net space charge and charge carriers and the distribution of temperature in the oil region before the streamer reaches the pressboard surface.

With respect to the temporal dynamic profiles shown in Figures 5.11-5.16, the first curve at 0.02 μs represents the behaviour that leads to the first peak of discharge current (stage A) as step input of DC voltage is applied. As the voltage becomes constant, the first current pulse decays gradually and seems constant at a certain level (from stage A to B: 0.02-0.5 μs) before starting to increase again gradually (from stage B to C: 0.5-1.1 μs) to cause the second pulse current which is of interest. During this period of time, the electric field peaks decrease gradually and are almost constant before they started to increase back gradually as shown in Figure 5.11. It is important to note that the electric field profile is a superposition effect from the density of net space charge distribution within the 2-D axial symmetry model system. However, during the period from stage A to C, the density of net space charge distribution shown in Figure 5.12 is sufficient to give good correlation between the net charge density and peaks of electric field profile. The net space charge distribution shows the dominant role of positive ions in enhancing the new electric field distribution as time progresses. The generation of positive ions is

caused by the electric field dependent molecular ionisation mechanism. Eventually, the new enhanced electric field leads to the field dependent molecular ionisation to occur further away from the needle tip. It is worthwhile to note that based on the electric field distribution, the velocity of streamer propagation during the period from stage A to C is in the range of 0.02-0.2 km·s^{-1}. This subsonic range of streamer velocity can be correlated to the 1st mode streamer that occurs during streamer initiations [66, 132, 133]. Figure 5.16 shows that the temperature variation within the streamer is less affected during the corresponding period.

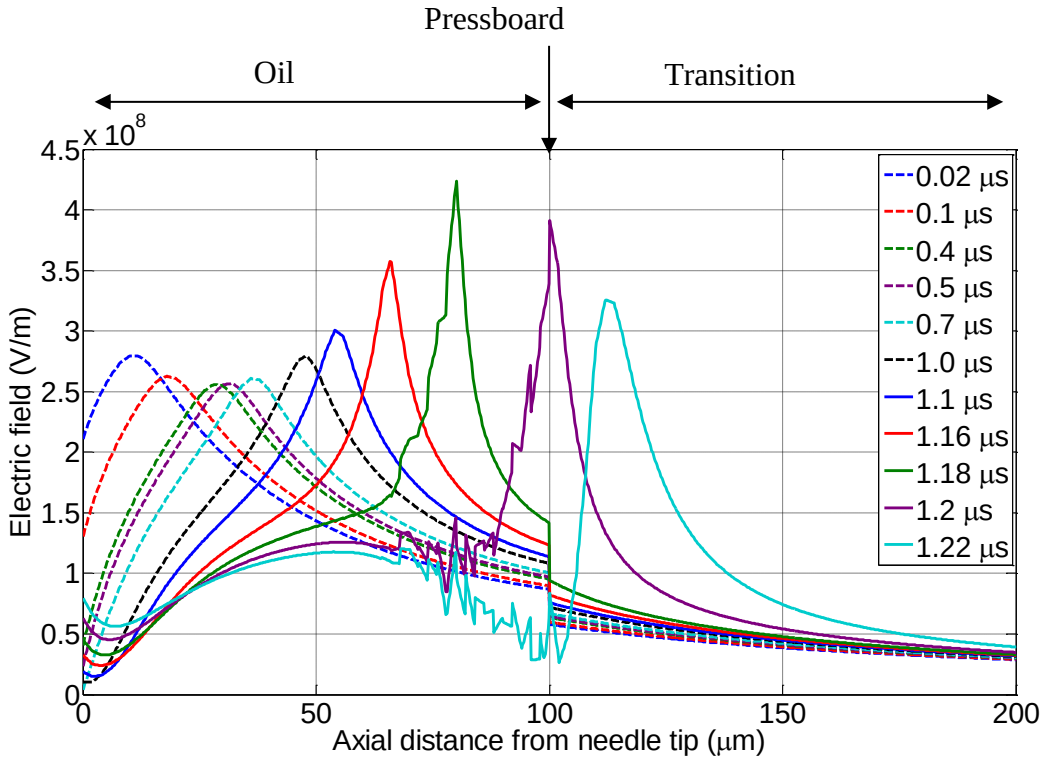

Figure 5.11: Electric field distribution along the symmetry axis

It appears that the net charge density is dominated by positive ions with density that is approximately 10 times higher than its counterpart charge carriers. This is caused by the generation of positive ions at the area close to the needle tip from the field dependent molecular ionisation mechanism and they move away from the needle electrode that is similar in polarity at a slow velocity as depicted in Figure 5.13. The negative ions and electrons on the other hand, are attracted toward the needle electrode that has opposite polarity as can be seen in Figures 5.14 and 5.15. The electrons move toward the needle electrode at a faster velocity compared to the positive ions based on the following relationship:

$$v_i = \mu_i \vec{E} \tag{5.28}$$

Where v_i and μ_i are velocity ($m \cdot s^{-1}$) and mobility ($m^2 \cdot s^{-1} \cdot V^{-1}$) of each charge carrier respectively. At the same time, the electron attachment mechanism causes the reduction of electron density to generate slow negative ions within the system.

From 1.1 μs to 1.18 μs (with reference to Figure 5.10 from stage C to a certain point before stage D of the simulated current pulse), the streamer propagates at a higher velocity within the distance of 50 μm from the pressboard surface before it touches the pressboard surface. This can be seen from the electric field distribution shown in Figure 5.11 whereby the peaks of the electric field curve increase significantly and move a further distance during the time interval. Such profiles of electric field are caused by multiplication of positive ions at the edge of the streamer as a result of field dependent molecular ionisation mechanism as shown in the net space charge profile (Figure 5.12). There is also significant rise in the electron density as shown in Figure 5.15 that moves toward the needle electrode at a higher velocity than the velocity of positive ion moving away from the needle electrode. However, as demonstrated in Figure 5.14, the electron attachment process does not lead to fast multiplication in the density of negative ions although an increment is noticeable. This suggests that the attachment process has less effect in streamer propagation that leads to the rising front of current pulse. During the mentioned time range, as the pulse current amplitude increases, there is also a significant rise in the temperature.

As demonstrated in the electric field distribution shown in Figure 5.11, the streamer touches the pressboard at the time of 1.2 μs. With respect to the electric field distribution, changes in the streamer velocity within the distance of 50 μm from the pressboard surface until it touches the surface have been calculated and the velocity increases from 0.2 $km \cdot s^{-1}$ to 1 $km \cdot s^{-1}$. This suggests that the streamer changes from the 1st mode to the 2nd mode [66, 67] as it moves into contact with the pressboard surface. This result shows an agreement with the experimental results published in [53, 54, 55, 56] that 2nd mode streamer propagates along an oil-pressboard interface (i.e. in the oil region close to the pressboard surface) at a voltage level of 50% breakdown probability or less under impulse voltages. It should be noted that this kind of streamer propagation is not observed if no pressboard is placed in the simulation model. In fact, the only

profile that has been observed is similar to those simulated over 0.02-0.5 μs. This indicates the important role of permittivity mismatch between the oil and pressboard in modifying the charge generation process particularly over the area that is close to the pressboard surface. This area can be associated to the free-oil boundary layer that is next to the pressboard surface as shown in the diagram of the physical model of the oil-pressboard interface (Figure 2.15).

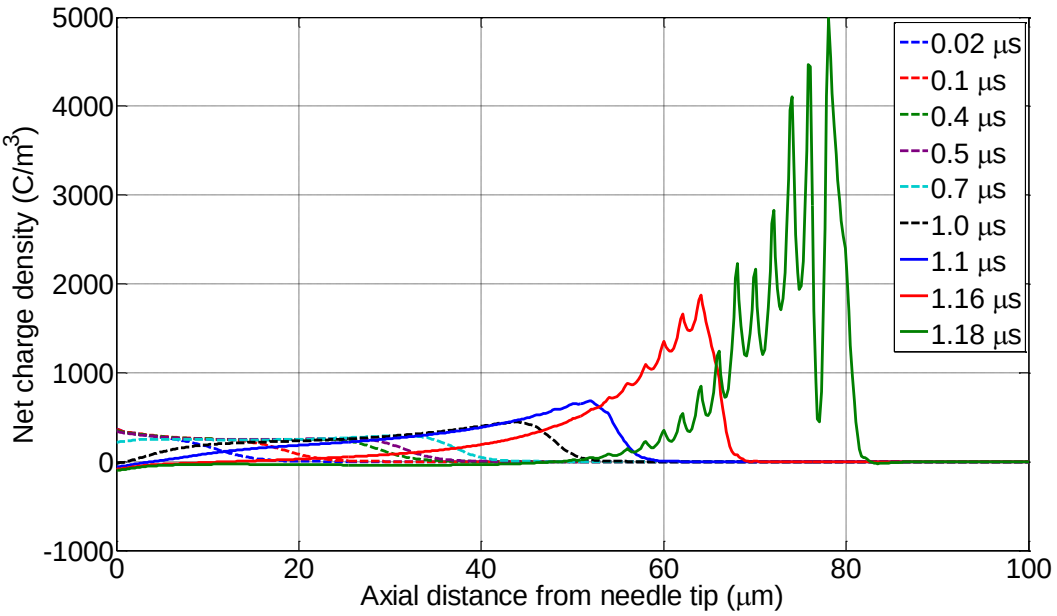

Figure 5.12: Net space charge density distribution along the symmetry axis

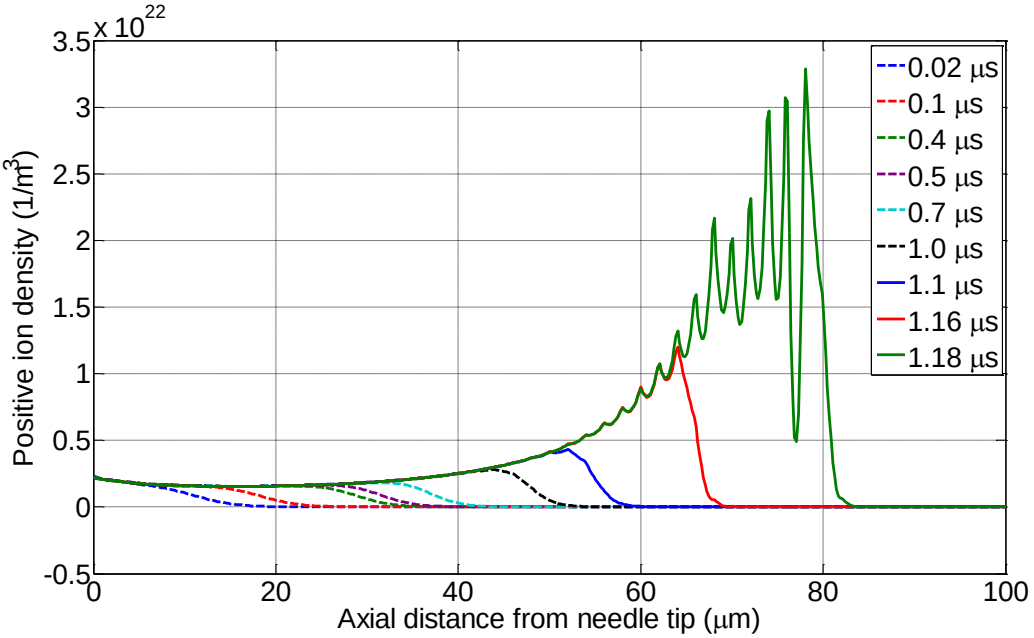

Figure 5.13: Positive ion density distribution along the symmetry axis

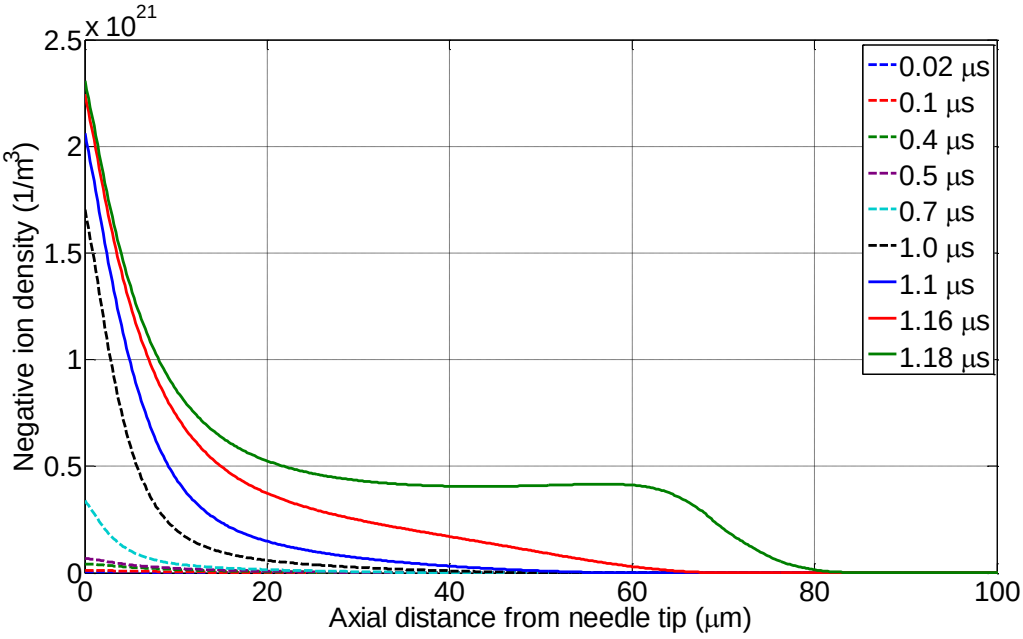

Figure 5.14: Negative ion density distribution along the symmetry axis

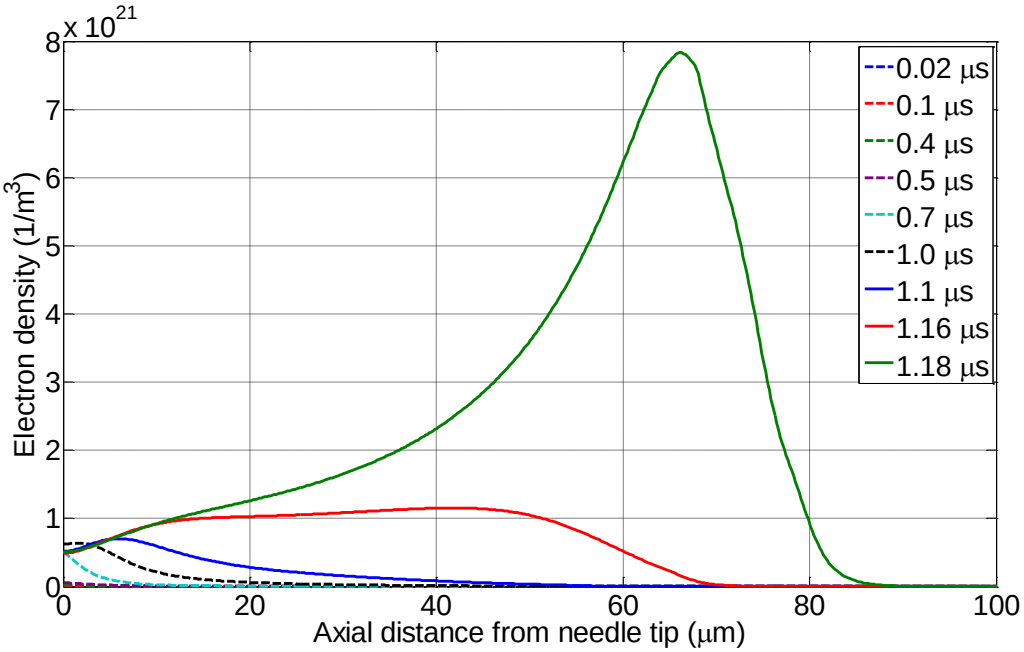

Figure 5.15: Electron density distribution along the symmetry axis

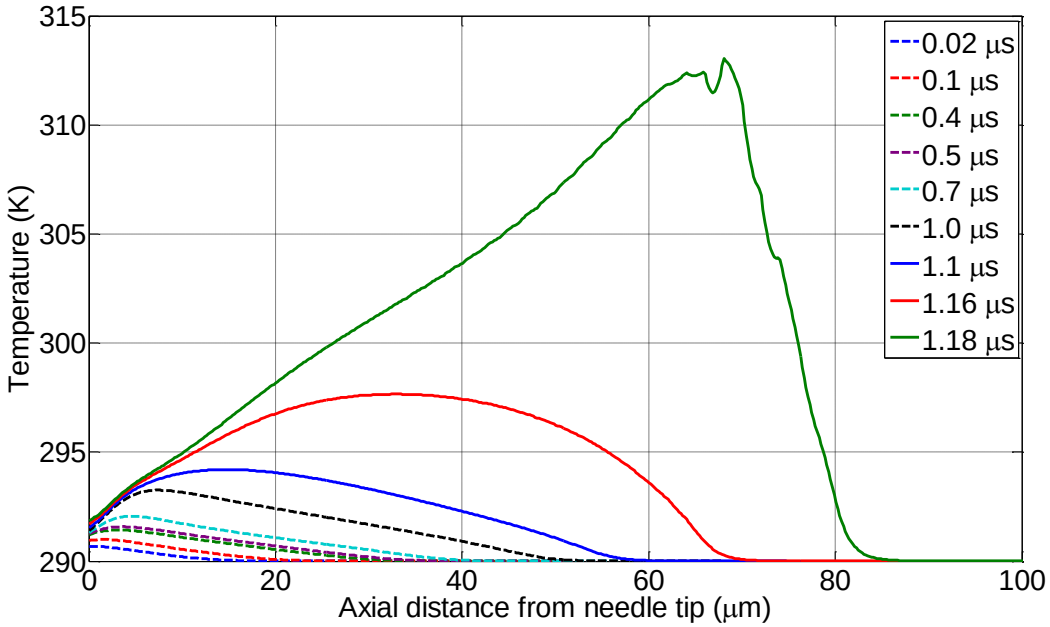

Figure 5.16: Temperature distribution along the symmetry axis

It should be highlighted that the large oscillations in the positive ion density (see Figure 5.13) which also reflect the results of net space charge density (see Figure 5.12) are caused by the maximum size of mesh element used in the simulation, i.e. 2 μm in the regions where the streamer propagates. A mesh sensitivity study by introducing boundary mesh at the regions with large oscillations has shown that, reducing the size of mesh element would reduce the oscillations (see Figure 5.17). The mesh sensitivity study has been undertaken using the similar parameters given in Appendix A. This includes the two parameters that were used in the validation work with the experimental results, i.e. the molecular ionisation energy and the electron attachment time constant. It appears that varying the mesh size without changing the parameter values leads to reductions in the accuracy of the solution (see Figure 5.18). This suggests that, in order to maintain the accuracy of the solution by obtaining a good correlation between the simulation and experimental data, reducing the mesh size should also be accompanied with different values of parameters.

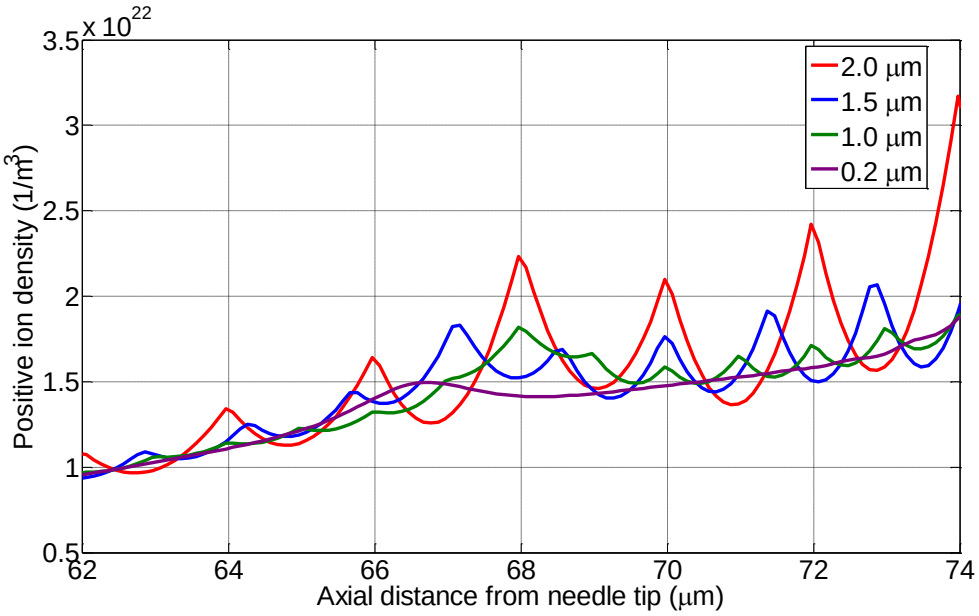

Figure 5.17: Positive ion density distribution along the symmetry axis based on different sizes of mesh element

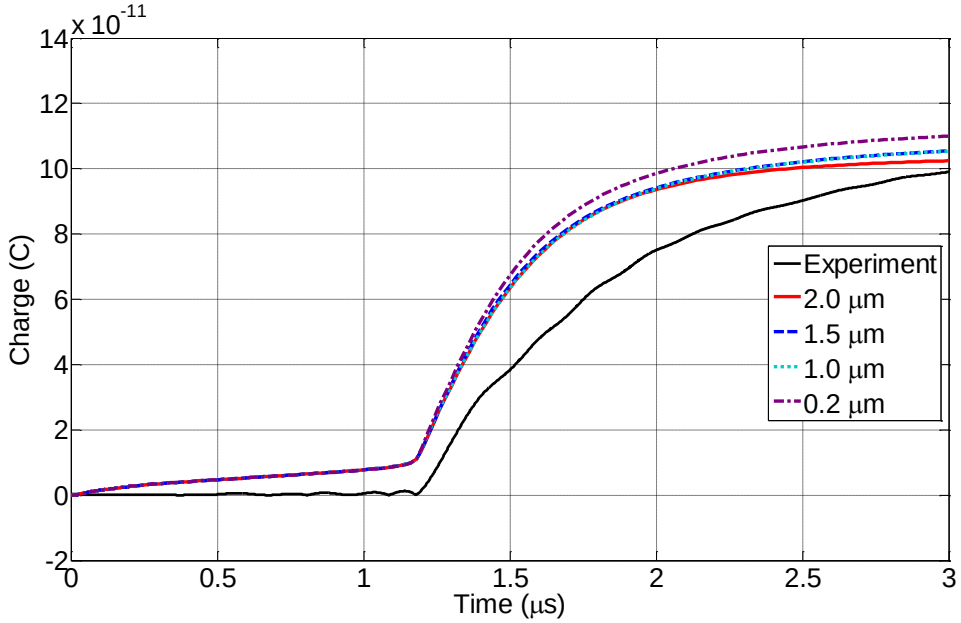

Figure 5.18: Comparison between experimental and simulation results of injected charge based on different sizes of mesh element

(2) Streamer on the pressboard surface (boundary 5)

The surface discharge behaviour on the pressboard surface is discussed in this section based on the temporal dynamic profiles shown in Figures 5.19-5.24. As mentioned earlier and shown in Figure 5.11, the streamer reaches the pressboard surface within 1.2 μs. At this time, the electric field is altered and distributed in a radial direction along the pressboard surface. Such behaviour causes the maximum electric field within the system to occur along the pressboard surface (within 5 μm of radial direction from the symmetry axis) as depicted in Figure 5.19. It is worth noting that through the simulation period of 3 μs, the highest magnitude of maximum electric field within the system is obtained at the moment the streamer touches the pressboard surface. This is due to the role of positive ions over other charge carriers on the pressboard surface due to their multiplication from the field dependent molecular ionisation mechanism and the electron attachment process that leads to the generation of slow negative ions. This can be seen from the profile of net space charge density as shown in Figure 5.20.

As time progresses from 1.2 μs to 1.22 μs (from a certain point after stage C to stage D of the simulated current pulse), the streamer propagates into the transition region as well as along the pressboard surface suggesting streamer branches have been created. Such branches lead to the influence of a constructive superposition effect on the electric field within the system and thus, cause the peak of the current pulse (stage D) as shown in Figure 5.10. Streamer propagation in the transition region is discussed later. On the other hand, the extension of the field dependent molecular ionisation mechanism in the streamer branch on the pressboard surface as depicted in Figure 5.19 is a result of the net space charge density as shown in Figure 5.20. During this period of time, there is a significant rise in the amount of positive ions in a radial direction further away from the symmetry axis as shown in Figure 5.21. The rise in the density of negative ions and electrons in Figures 5.22 and 5.23 is a result of electron attachment and field dependent molecular ionisation mechanisms.

The temporal profiles of electric field shown in Figure 5.19 from 1.22 μs to 3.0 μs (from stage D to stage F of the modelled current pulse) demonstrate the stopping length of the streamer branch on the pressboard surface. The streamer branch on the pressboard surface stopped at approximately 12 μm in radial direction from the symmetry axis based on the reduction trend in the peak of electric field profile on the same spot. Such

a reduction is due to a destructive superposition effect from the net space charge distribution within the system. It appears that the destructive superposition effect is primarily caused by differences of polarity in the net space charge density along the pressboard surface, as depicted in Figure 5.20.

With reference to the immediate decrease of the peak of current pulse in Figure 5.10 (from stage D to E: 1.22-1.3 μs), a sudden decrease in the peak of electric field to a value that is less than 2×10^{8} $V\cdot m^{-1}$ can be seen in Figure 5.19. It is important to note that due to exponential term in the Zener model (Equation (5.7)) and based on the parameter values given in Appendix A (Tables A.2 and A3), the field dependent molecular ionisation mechanism will effectively take place if the electric field is around 2.5×10^{8} $V\cdot m^{-1}$. Hence, it appears that the streamer tends to stall from the time of 1.22 μs as a result of the destructive superposition effect discussed previously. Consequently, considering the gradual reduction in the positive ion density and significant changes in the density of negative ions (increase) and electrons (decrease) shown in Figures 5.21-5.23, the electron attachment mechanism starts to prevail from stage E to F in the surface discharge behaviour. This suggests the role of the electron attachment mechanism is the dominant factor in the decaying tail of current pulse due to the replacement of fast electrons with slow negative ions in which both charge carriers move towards the needle electrode that has the opposite polarity.

The temporal dynamic profiles of net space charge density shown in Figure 5.20 demonstrate accumulation of negative polarity charge carriers ahead the streamer. This behaviour is caused by the streamer extinction mechanism from the time of 1.22 μs to 3.0 μs (from stage D to stage F of current pulse), whereby there is no further enhancement in the electric field as a result of destructive superposition effect. This leads to no further generation of positive ions and electrons during this period as depicted in Figures 5.21 and 5.23 respectively. Consequently, recombination between positive and negative ions and between positive ions and electrons cause a gradual reduction in the density of positive ions. The reduction in electric field also causes a reduction in the velocity of the charge carriers. In order to explain the profile of negative ions shown in Figure 5.22, two steps of mechanism can be hypothesised. First, the reductions in velocity cause the positive ions to accumulate at the point where the streamer has stopped rather than move toward the earth electrode and also cause a slower movement of electrons toward the needle electrode. Reductions in velocity

might also cause competition for electrons to drift between the two sources of positive polarity i.e. the needle electrode and the accumulated positive ions on the pressboard surface for recombination. This would enhance the electron attachment mechanism so that there is a gradual accumulation of negative ions on the pressboard surface as time progresses from 1.22 μs to 1.7 μs before the negative ions started to reduce until 3.0 μs due to domination of the recombination process, as illustrated in Figure 5.22.

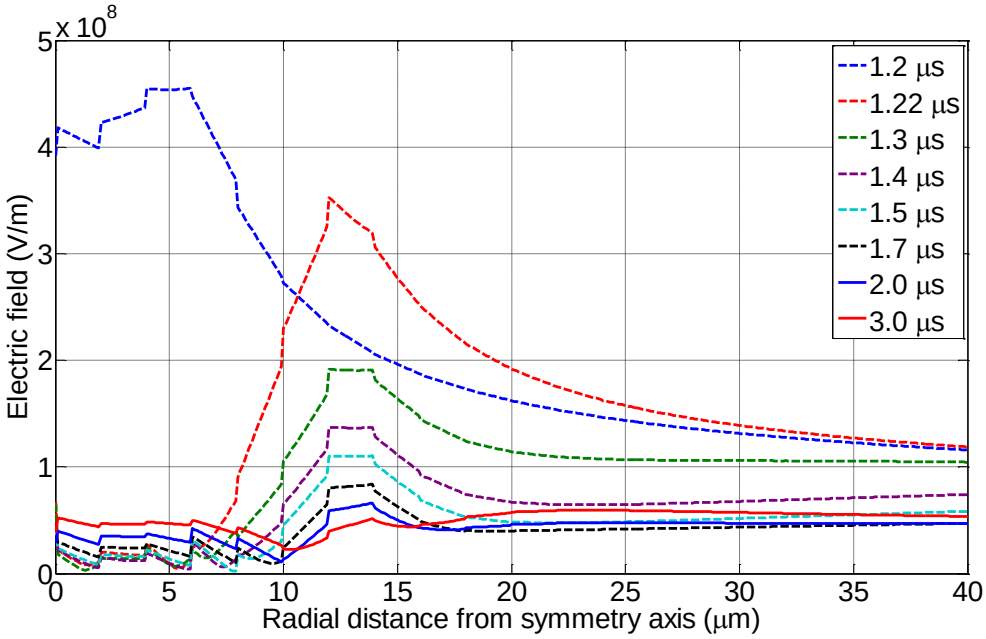

Figure 5.19: Electric field distribution along boundary 5

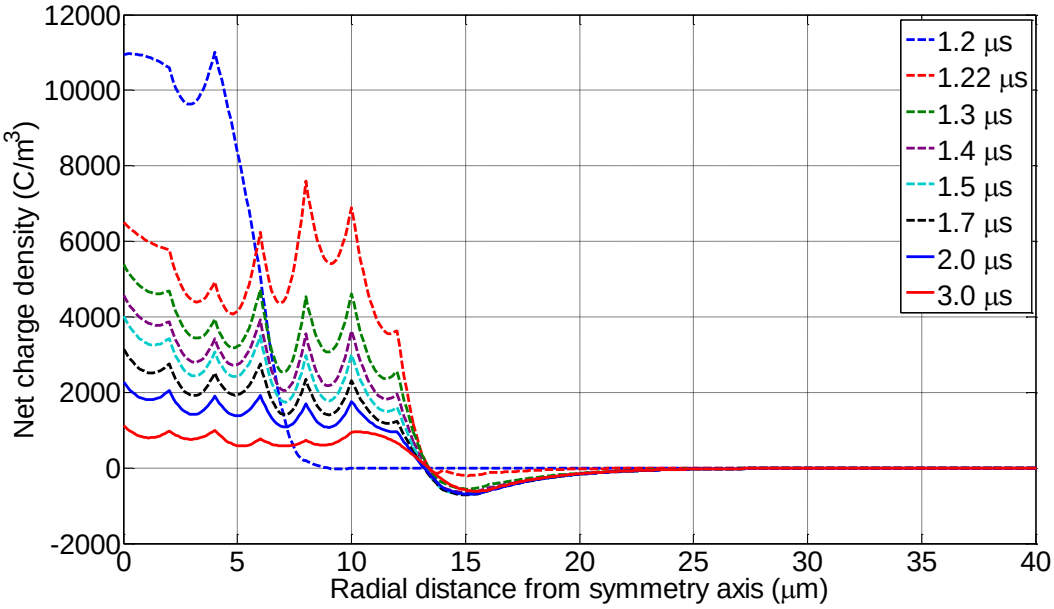

Figure 5.20: Net space charge density distribution along boundary 5

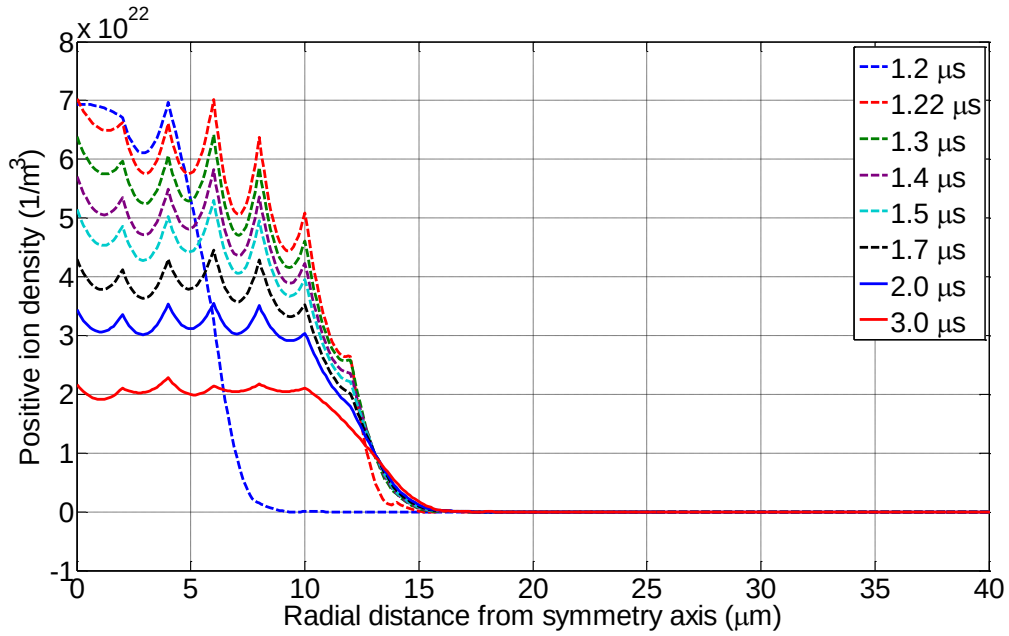

Figure 5.21: Positive ion density distribution along boundary 5

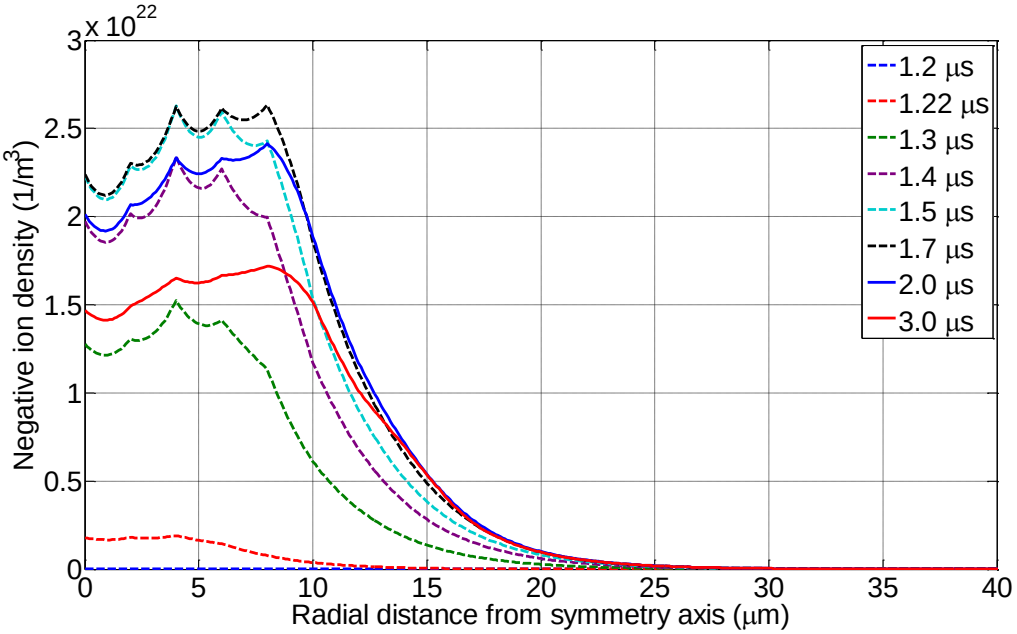

Figure 5.22: Negative ion density distribution along boundary 5

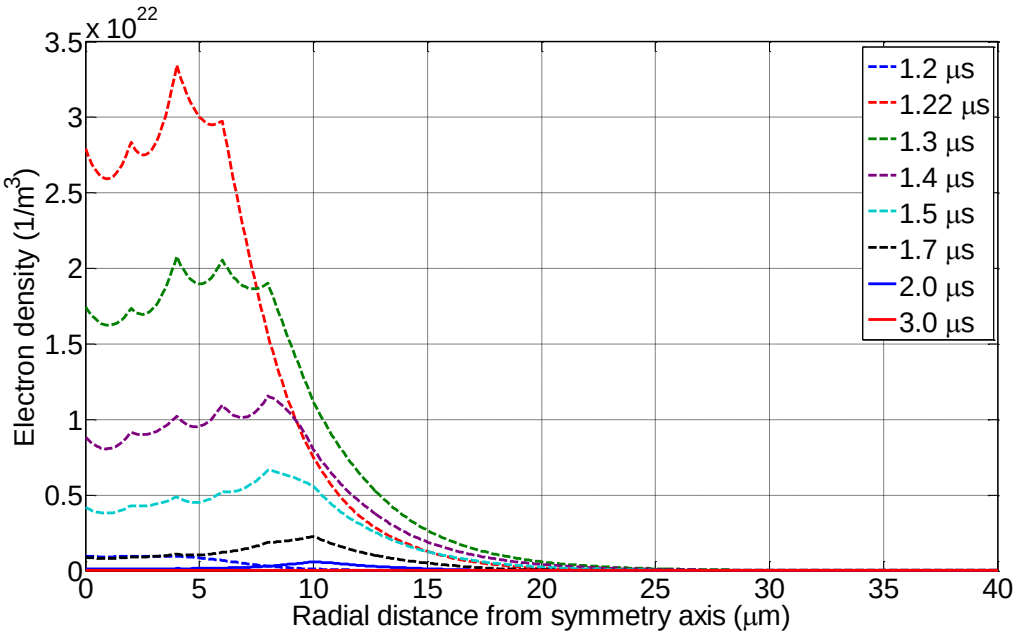

Figure 5.23: Electron density distribution along boundary 5

Figure 5.24 shows the simulation results of temperature distribution along the pressboard surface. It can be noticed that the hottest spot at a particular time appears at the tip of streamer along the pressboard surface. Figure 5.25 (a) shows the variation of temperature at the hottest spot on the pressboard surface. The results indicate that streamer branch on the pressboard surface causes significant increase in the temperature at that particular spot. The temperature increases significantly up to about 650 K within 0.2 μs. Then, the temperature increases gradually to approximately 697 K before it decreases gradually to about 650 K. These magnitudes are beyond the temperature that may cause carbonisation of cellulose through dehydration and pyrolysis processes (less than 500 K) [134]. Therefore, the simulated temperatures of the hottest spot on pressboard surface provide a reasonable argument behind the formation white and black marks during the surface discharge experiment as a result of drying out and ionisation processes. It appears that concentration of high temperature over a long period of surface discharges would enhance the carbonisation of cellulose pressboard particularly at the vicinity of needle tip as depicted in Figure 3.8.

In order to aid further understanding on the temperature variation at the hottest spot with respect to time, it is necessary to correlate the temperature variation with the dissipated energy from the generated space charges. The temperature variations are solved using Equation (5.5) whereby, the electrical power dissipation term is

proportional with the rate of temperature variation. By neglecting the thermal conduction term to simplify the solution and performing time integration on Equation (5.5), the cumulative energy density as a result of electrical power dissipation from the generated charges is determined and shown in Figure 5.25 (b). Correlation between Figures 5.25 (a) and (b) suggests that the significant growth of energy dissipation causes the temperature to increase substantially to a certain magnitude. The moment when the energy increases steadily, the temperature starts to decrease gradually. This gradual decrease is caused by the thermal dispersion in the system which is governed by the thermal conductive term in the thermal equation (Equation (5.5)).

It should be noted that the hottest spot on the pressboard surface occupies a very small volume of the transition region. For instance, the hottest spot with the temperature value of 697 K (at the time of 1.7 μs) occupies approximately 3.77×10^{-22} m^3 of the transition region. With reference to Figure 5.25 (a), the spot experienced a temperature increase of 407 K. Based on the specific heat capacity and mass density of the transition region given in Table A.3 (see Appendix A), the simulated energy injected into the volume of the hottest spot is approximately 2.65×10^{-13} J. If the calculation is made using the simplified cumulative energy shown in Figure 5.25 (b), the simulated energy injected into the hottest spot volume is 3.17×10^{-13} J. A higher value is expected because the simplified cumulative energy was determined by neglecting the thermal conduction term that accounts for the thermal dispersion in the system.

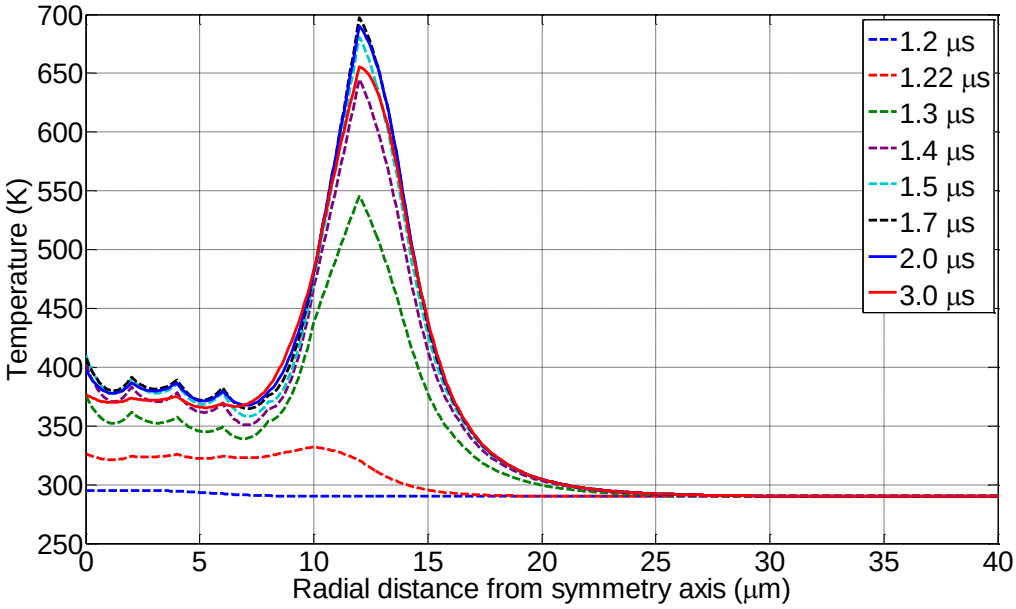

Figure 5.24: Temperature distribution along boundary 5

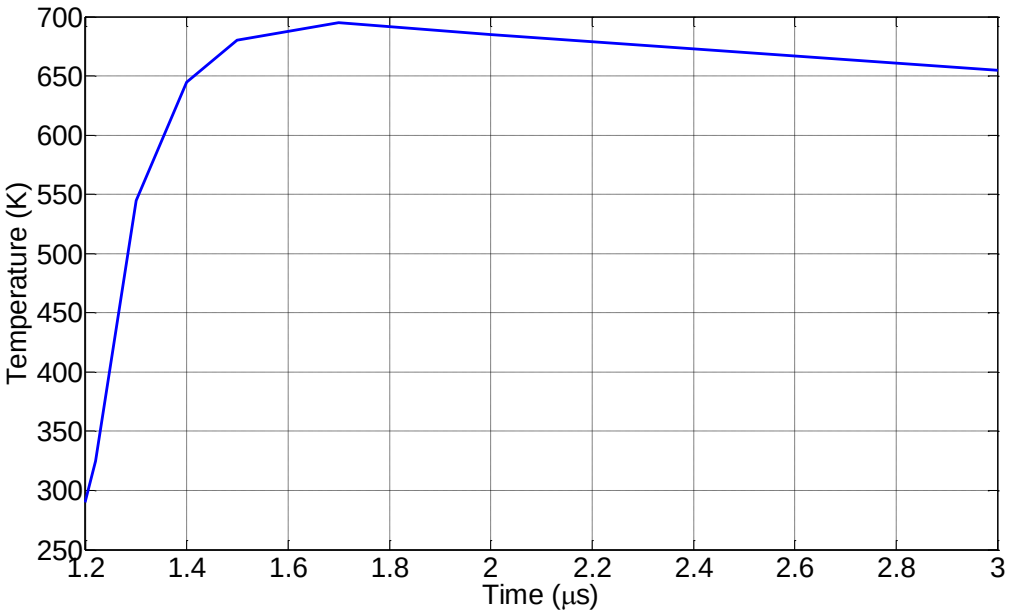

(a) Variation of temperature at the hottest spot with respect to Figure 5.24

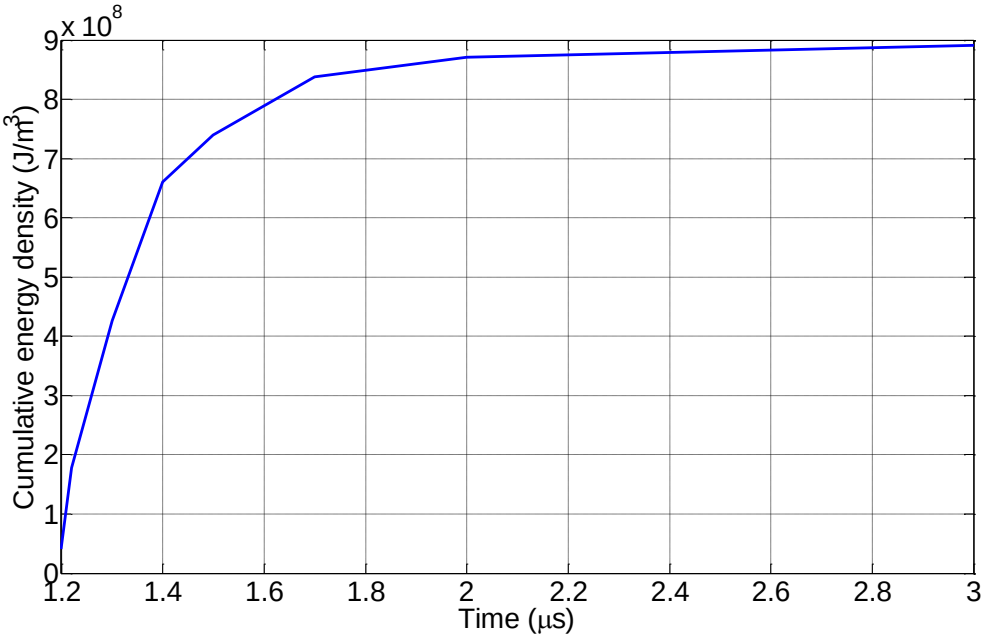

(b) Cumulative energy density calculated from the electrical power dissipation term in Equation (5.5)

Figure 5.25: Relationship between temperature variation and energy density at the streamer tip on pressboard surface

(3) Streamer in the transition region

The simulated surface discharge current pulse shown in Figure 5.10 is also a result of streamer propagation within the transition region. Thus, the behaviour of surface discharge at the oil-pressboard interface is discussed based on the temporal dynamic profiles shown in Figures 5.26-5.31 that have been simulated for the transition region. The results are plotted over time from 1.22 μs to 3.0 μs. This time frame corresponds to the moment the streamer enters the transition region until the end of simulation period, from stage D to stage F of current pulse. It is important to note that each result is based on the distance from the interception point between boundary 5 and symmetry axis. This distance does not have a fixed angle because the streamer does not propagate in a straight line as time progresses. It may shift direction over time as illustrated in the results presented in Appendix B. Therefore, for analysis purposes, each result that corresponds to a particular time was obtained based on the distance from the interception point between boundary 5 and symmetry axis to the point where electric field is at its maximum magnitude. It should be highlighted that the results presented in Appendix B suggest that the 2-D axial symmetry model leads to a 'ring-like' structure streamer tip in which the 'ring-like' structure is increasing in size as it propagates toward the earth bar. This infers that model simplification from 3-D to 2-D axial symmetry does change the physics of the streamer propagation.

Figure 5.26 shows the temporal dynamic profiles of the electric field corresponding to streamer propagation in the transition region. The gradual decrease in the peaks of electric field profile is a result of the superposition effect of space charge as shown in Figure 5.27. During this period, there is not much change in the density of positive ions at the vicinity of streamer tip as shown in Figure 5.28. On the other hand, the amounts of negative ions are increasing (Figure 5.29) and vice versa for the electrons (Figure 5.30). This is similar to the case of the streamer branch on the pressboard surface, confirming the important role of the electron attachment mechanism during the decaying period of the surface discharge current pulse particularly from stage E to F.

Again, similar to the case of pressboard surface, the cumulative energy dissipated from space charge in the streamer leads to temperature rise. Figure 5.31 shows that at the time of 1.7 μs, the temperature in the transition region increases up to about 450 K. This temperature magnitude is greater than the boiling point of water (373 K). It should

be noted that the thermal parameters in the transition region consider the mixing of oil, water and cellulose pressboard. Hence, this result reasonably suggests that streamer propagation inside the transition region is capable of leading to the evaporation of moisture. The result supports the hypothesis of a drying out process during surface discharges at the oil-pressboard interface is caused evaporation of moisture. Over time, temperature in the transition region increases above the boiling temperature of mineral oil, i.e. approximately 500 K. This signifies the generation of other gases as a result of oil vaporisation. Eventually, gas expansion from the vaporisation of water and oil pushes oil out of the pores of the cellulose pressboard and creates white marks. Therefore, based on the simulation result, energy from a partial discharge event at the oil-pressboard interface will clearly lead to thermal degradation on the pressboard surface.

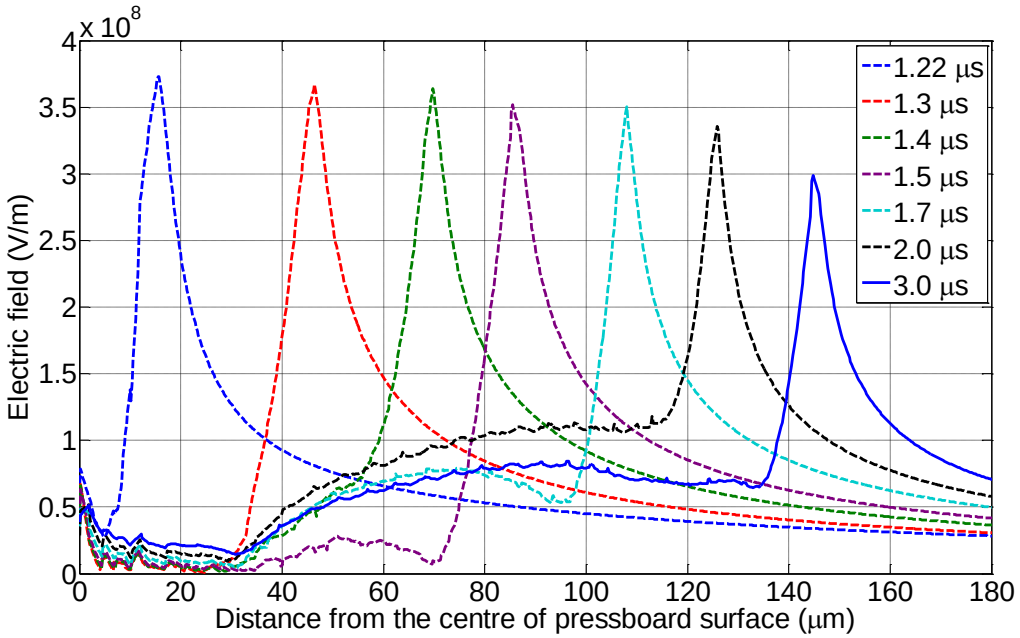

Figure 5.26: Electric field distribution in transition region

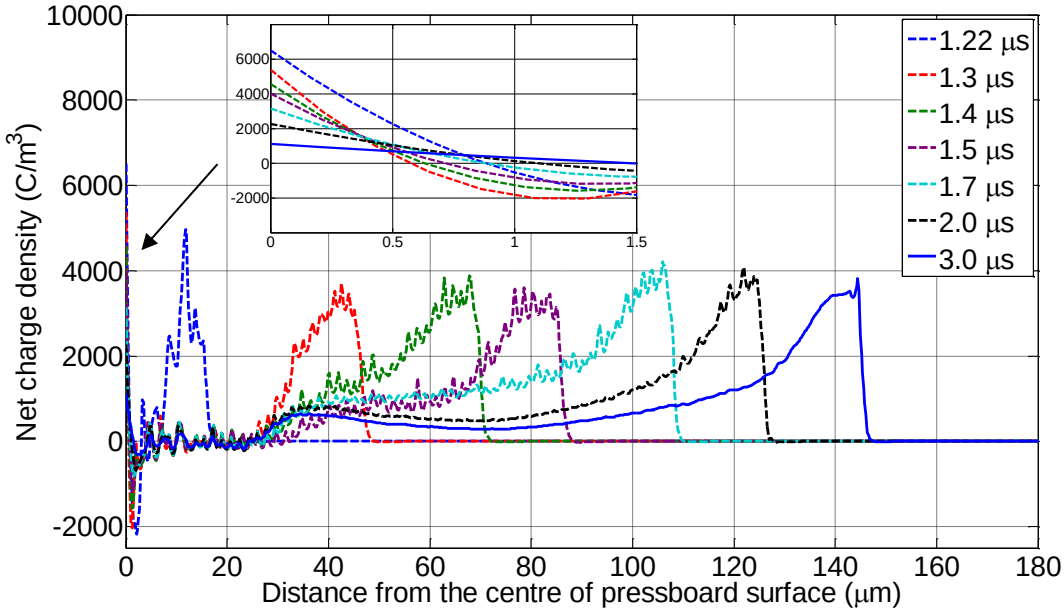

Figure 5.27: Net space charge density distribution in transition region

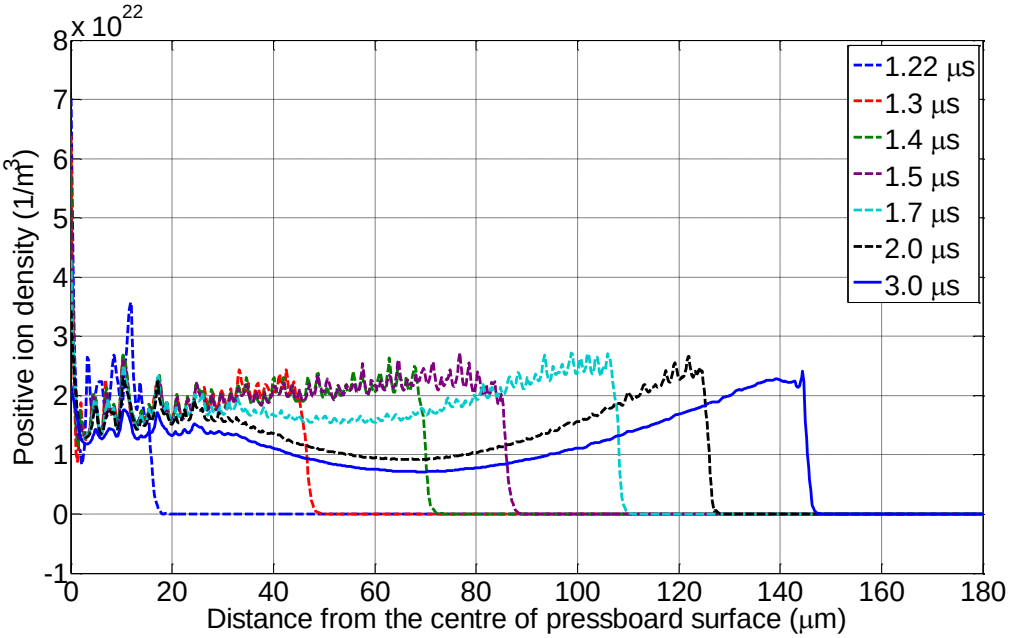

Figure 5.28: Positive ion density distribution in transition region

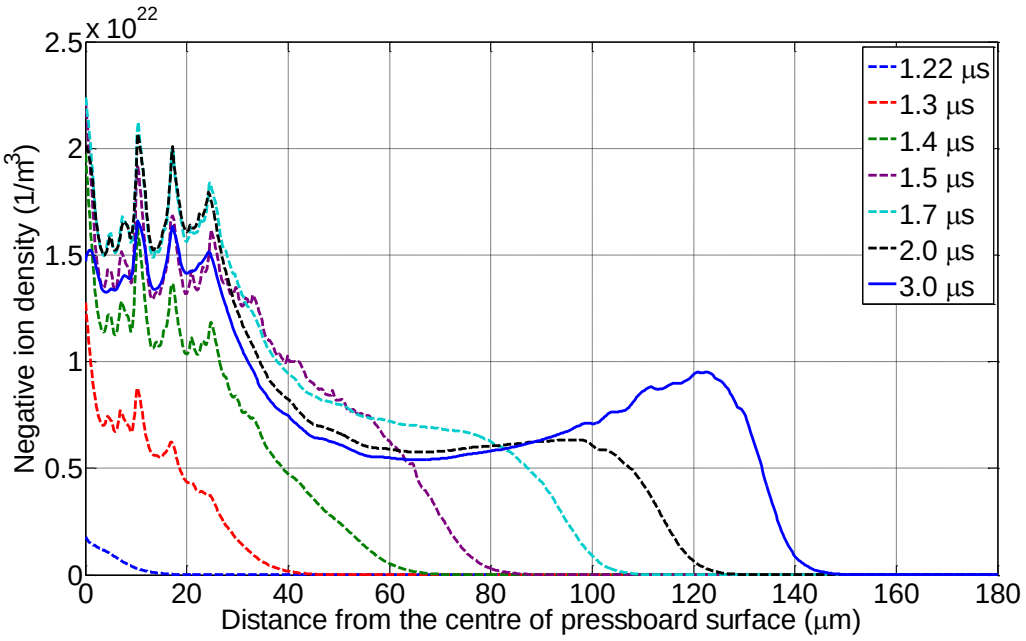

Figure 5.29: Negative ion density distribution in transition region

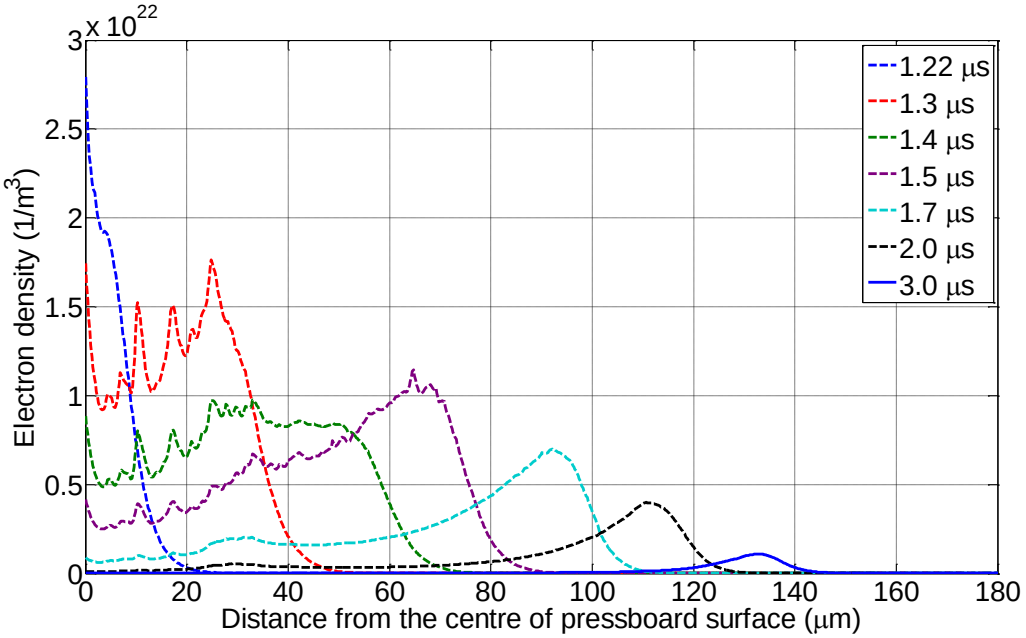

Figure 5.30: Electron density distribution in transition region

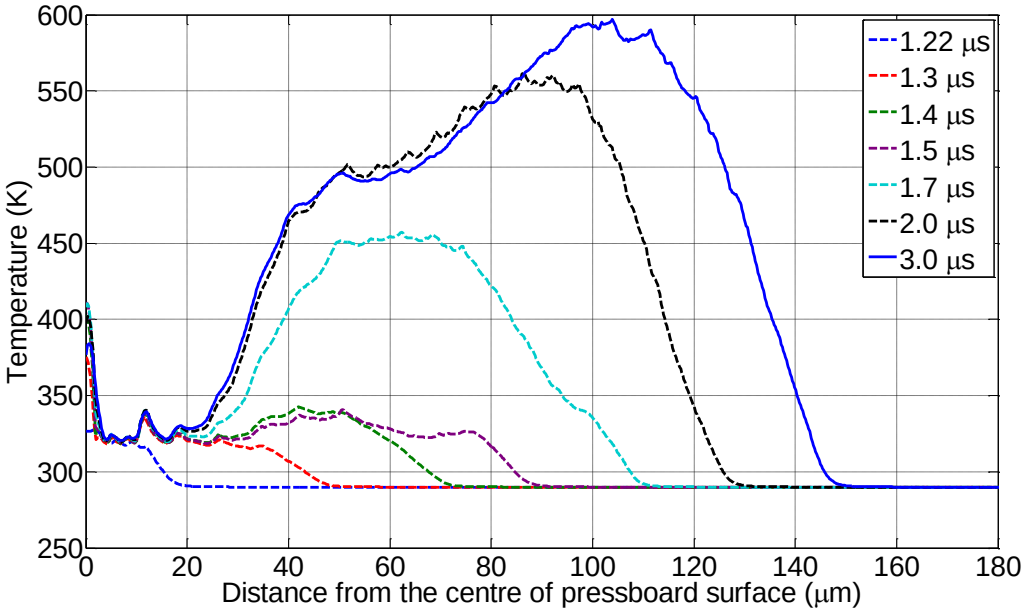

Figure 5.31: Temperature distribution in transition region

5.3.3 Analysis of the Influence of Permittivity

Analysis of the influence of permittivity setting in the model has been undertaken to study its effect on the magnitude of discharge current pulses. These findings can be qualitatively correlated with the partial discharge magnitude observed in the surface discharge experiment for different moisture levels in pressboard. No quantitative validation with experimental data is conducted which requires parametric study of certain variables from the charge generation and recombination terms in the charge transport equations (Equation (5.1)-(5.3)). These include the density of the ionisable species, molecular ionisation energy, recombination coefficients, electron attachment time constant, mobility of charge carriers and etc. Therefore, this study has been conducted by using similar parameters given in Appendix A (Tables A.1-A.4) except the permittivity values for the transition and bulk oil/pressboard regions. The permittivity values for both regions are based on those calculated previously for different moisture levels in pressboard (see Table 5.2). However, due to issues with timely convergence, the simulated current pulse for pressboard containing 9% moisture level was determined using molecular ionisation potential of 6.7 eV. This is due to a high permittivity value at the transition region as a result of a large mass density of water within this particular region will cause a high permittivity mismatch with the oil permittivity and eventually leads to a discontinuity effect at the interface. Such

discontinuity effect is due to choice of parameters where increasing water content in the transition region is neglected. Therefore, it is reasonable to decrease the ionisation potential as moisture level increases although this has only been done for the case of 9% moisture level in this study.

Table 5.3 shows the peak values of surface discharge current pulse based on the different permittivity levels determined earlier for different moisture levels in pressboard (see Table 5.2). It can be noticed that the magnitude of the peak current increases as the moisture content in the pressboard increases. This result demonstrates a qualitative agreement with the PD data shown in Figures 3.11-3.14 whereby the magnitude of apparent charge around the peak of positive cycle increases as the moisture level increases, although no significant difference is observed between the PD data for the dry and 3% moisture pressboards (Figures 3.11 and 3.12).

Table 5.3: Magnitude of peak current of the simulated surface discharge current pulse for different moisture levels within pressboard with respect to permittivity values in Table 5.2

Moisture levels within pressboard	Dry (< 0.5%)	3%	6%	9%
Peak Current	0.21 mA	0.46 mA	0.8 mA	3.85 mA

5.4 Summary

A model has been developed using an FEA software package to study the behaviour of surface discharge at the oil-pressboard interface at the positive half cycle of AC voltage. The surface discharge behaviour was investigated by validating the simulation results against experimental data of surface discharge current pulse. The simulation result has shown that a field dependent molecular ionisation mechanism plays an important role in the streamer propagation during the period of the rising front of the current pulse. On the other hand, an electron attachment process is essential during the period of the decaying tail of the current pulse.

A parametric study of two parameters, i.e. the molecular ionisation energy and the electron attachment time constant has been undertaken as part of the validation work. The first parameter which is available in the Zener model (Equation (5.7)) is important to control the overshoot of a current pulse. It is inversely proportional in relation to the magnitude of the peak current. Although no significant variation can be noticed with the rising front of the current pulse when changing the value of ionisation potential, there will not be any streamer development if the value of the ionisation potential is too high. This is due to the exponential term of the Zener equation. Hence, this supports the importance of the Zener model during the period of the rising front of the current pulse. On the other hand, the role of the second parameter is clearly important when modelling the decaying tail of the current pulse. It has a proportional relationship with the decaying time of the current pulse. However, the drawback is that this will also increase the peak of the current pulse when increasing the attachment time to increase the decay time. Both parameters were also determined by considering the total amount of charges injected into the system.

The consideration of pressboard as a porous material in the model and the use of relative mass density to estimate the effective permittivity for simulation purposes have confirmed the hypotheses about the localised nature observed in the experiment of surface discharge at the oil-pressboard interface. These include the development of white marks on the pressboard surface and the formation of carbonised marks that predominantly appear on the pressboard surface at the vicinity of needle tip. The simulation results have associated both degradation marks on pressboard surface with high energy of long periods of partial discharge event that leads to thermal degradation at the oil-pressboard interface. Permittivity mismatch has been found to play an important role in the electric field distribution at the oil-pressboard interface, which has been reported earlier [51, 59, 80]. Such conditions at the oil-pressboard interface of the model have led to 2nd mode streamer to be observed before the streamer reaches the pressboard surface. This streamer propagation mode is in agreement with experimental observations published in [53, 54, 55, 56] that 2nd mode streamer propagates along an oil-pressboard interface (i.e. in the oil region close to the pressboard surface) at a voltage level of 50% breakdown probability or less under impulse voltages. Studies based on 2-D axial symmetry have allowed the key features of the surface discharge behaviour at the oil-pressboard interface to be modelled and validated using experimental measurements.

Chapter 6

Conclusions and Further Work

6.1 Conclusions

A surface discharge experiment using a needle-bar configuration has been developed to study the behaviour of surface discharge at the oil-pressboard interface. The experiment was conducted in an oil bath under a long duration AC electrical stress as such modelling surface discharge activity within a power transformer without a loading current and assuming the discharge started at the interface. Four different pressboard samples, i.e. dry pressboard (less than 0.5 %) and pressboard conditioned to 3 %, 6 % and 9 % moisture content have been tested to increase understanding on the behaviour of surface discharge at the oil-pressboard interface. An OMICRON Mtronix PD measurement system (MPD 600) has been used to monitor and record the PD data of important events during the surface discharge experiment. In addition, two types of current transducer have been used to measure the leakage currents due to full discharge events. Full discharge is defined as a rare discharge event (usually visible in the form of arcs) that temporarily bridges the HV electrode and the earth at the oil-pressboard without resulting in a complete electrical breakdown.

The experimental work presented in this thesis contributes to a further understanding on the surface discharge behaviour at the oil-pressboard interface. This is important to the development of condition monitoring strategies for large power transformers and to allow a prognostic study of their lifespan. For that purpose, a chronological process in the surface discharge that limited to the occurrence of a first full discharge event has been recognised. This process offers a systematic approach to correlate the significant

surface discharge activities with the respective PRPD data. The process highlights four degradation stages during the surface discharge at the oil-pressboard interface in which it starts with arcing discharge or glow activity at the needle tip (the early stage of surface discharge). Then, there is a formation of white marks that propagate towards the earth electrode with rare occurrence and very low light intensity of arcing or glow discharge at the needle tip. The white marks have been suggested in the literature as well as in this research to result from local drying and evaporation processes of moisture and more volatile element of the mineral oil. Next, as the white marks nearly reach the earth bar, repetitive bluish arcing occurs at the earth bar to bridge between the earth and the white marks which can continue for a few seconds or minutes. Finally, there is a full discharge that temporarily bridges the needle tip and the earth bar. Significant differences in the PRPD data have been observed among the stages, thus providing useful information on the degradation behaviour during surface discharge at the oil-pressboard interface.

Another contribution to the field of condition monitoring of power transformers has been made by analysing the experimental results based on different moisture levels within the pressboard. The different moisture levels have been observed to play an important role on the PD activity of certain processes. The PRPD data have shown that the moisture level in the pressboard is proportional with the severity of PD activity at the early stage of surface discharge. In terms of duration of the white marks development up to the occurrence of a first full discharge, an unexpected behaviour has been observed. While dry pressboard is very robust and time to full discharge is significant (much longer time has been recorded), for the case of wet pressboard, as the moisture increases, the duration increases. This can be explained with excessive presence of moisture at the interface requiring more heat energy from PD activities to evaporate the moisture during the process of white mark growth.

Throughout the research, as the white marks develop about half way across the gap from the needle tip, reduction in PD activity can be observed before it starts to increase again due to the occurrence of arc events at the earth electrode that bridge the white marks. The decreasing trend in PRPD data observed in this work is an important finding whereby traditional evaluation is not a reliable condition monitoring measure of health. This finding is qualitatively agree with a survey on a failed transformer reported in the literature [8] and supports the suggestion by CIGRE WG 12.18 [6] to revise the usual

practice in condition monitoring to associate a decreasing trend or the absence of an increasing trend as a healthy condition. The finding can also be regarded as a key indicator of white mark propagation and ultimately there is surface discharging at the oil-pressboard interface.

In order to understand the characteristics of the full discharge events, investigations have been undertaken by means of leakage current measurement using a shunt resistor and RFCT along with a commercial PD measuring equipment. A non-standard frequency bandwidth setting (15 MHz ± 750 kHz) has been used due to poor frequency integration for multiple pulses event from the full discharges when the frequency is set to compliance with the IEC 60270. In this work, the characteristics of a full discharge event have been studied in terms of time and frequency domains. Based on both analyses, the full discharge event is a corona-like discharge that propagates bridging electrode gap without causing electrical breakdown (i.e. without tripping the protection system). The leakage current waveform contains multiple pulses superimposed with small continuous currents. Physically, a full discharge is characterised as a weakly luminous streamer with partial illumination bridging the electrode gap but do not cause to electrical breakdown. Although these characteristics are similar to non-breakdown events reported in the literature as a result of positive streamer in bulk oil (due to the breakdown voltage of negative polarity being twice as high as the positive polarity), the full discharges at the oil-pressboard interface have no relationship with the voltage polarity. Their occurrences are dominated by accumulated charges on the pressboard surface that gradually move along the white marks on the pressboard under prolonged AC voltage stress until these charges are high enough to cause a full discharge at a certain voltage threshold near peak value at either polarity.

It should be noted that the random occurrence of full discharges infers that the PD measurement system must be able to detect and identify the full discharges for condition monitoring purposes. In order to confirm this, the leakage current results from full discharge events measured via the RFCT have been compared with the commercial PD measurement system (Mtronix equipment). The results are correlated, although there are certain mismatches due to technical factors and the random phenomena that can occur during the surface discharges. This promotes value added knowledge for the condition monitoring of surface discharge at the oil-pressboard interface by identifying and detecting a full discharge event. This work also includes

comparison between dry band arcing occurs at the outdoor insulation and full discharges at the oil-pressboard interface. It appears that both events have similarities whereby they both involve by localised heating process that leads to water vaporisation and they occur mainly on a dry surface.

The work presented in this thesis has also made a significant contribution to the development of a computational simulation model of surface discharge at the oil-pressboard interface. A 2-D axial symmetry model has been developed using COMSOL Multiphysics, an FEA software package and then validated with the measured current pulse to study the mechanism of surface discharge at the oil-pressboard interface. More importantly, the model is developed by considering the pressboard as a porous material based on the physical model of oil-pressboard interface proposed previously [15]. The region that is considered porous in this work is the one recognised as a transition region, near the pressboard surface where there is mingling of oil molecules, cellulose fibre and other species such as water. Prior to the computational simulation of the surface discharge, the permittivity value in the transition region has been modelled using relative mass density between oil, pressboard and water and good agreement has been obtained with the data from the literature [122].

In general, the surface discharge simulation results show that the field dependent molecular ionisation mechanism plays an important role in the streamer propagation at the oil-pressboard interface during the period of a rising front of the current pulse. On the other hand, electron attachment is dominant during the period of the decaying tail of the current pulse. Besides predicting the surface current pulse, the proposed model has also successfully used the thermal properties of oil, pressboard and water to explain the development of white marks on the pressboard surface and the formation of black marks that predominantly appear on the pressboard surface in the vicinity of the needle tip due to surface discharge activity. The results suggest that degradation marks are due to energy over long periods of partial discharge events that lead to thermal degradation at the oil-pressboard interface. There is also an agreement with the literature in terms of streamer velocity (2^{nd} mode) at the oil-pressboard interface, with a value of 1 $km \cdot s^{-1}$ being predicted.

6.2 Further Work

For further work, experiments on the effects of surface discharge at the oil-pressboard under lightning or/and switching impulse waveforms should be performed. Comparison can be made for creepage discharge due to impulse voltages before a surface discharge is initiated and after the surface discharge is initiated based on the surface discharge process at the oil-pressboard that has been recognised as shown in Figure 3.10. An initial expectation from this experiment is the lowering of the impulse withstand capability. However, the findings from this work would be useful to further characterise the degradation behaviour as a result of surface discharges, in addition to the points that have been discussed in this work.

Experiments of surface discharge at the oil-pressboard interface can also be performed by taking advantage of the concept of a 2-D axial symmetry. With respect to this, for instance, electrode configuration as shown in Figure 5.2 (a) can be used. There is no possibility that experimentally the streamer will propagate in a ring-like manner due to random behaviour of discharge occurrences and the non-uniformity condition (surface structure and contamination) at the oil-pressboard interface. However, this will give insight for the modelling work and further justify assumptions made in order to obtain a working model.

In this work, the pressboard is modelled to have two different permittivity values within it, i.e. in the transition region and bulk oil/pressboard region. Thus, the whole composite of oil-pressboard is modelled to have step permittivity change from one to another (bulk oil region → transition region → oil/pressboard bulk region). Therefore, for further work, the effects of providing a smooth transition in the pressboard permittivity should be studied. This is not necessarily by modelling the permittivity as an exponential function in the pressboard because this maybe increases the non-linear condition to the model. Thus, alternatively, this can be performed geometry wise by introducing multiple regions in the pressboard with different permittivity values for each region in which this is expected better in terms of model stability.

Further computational work to study the surface discharge behaviour due to negative streamer should also be considered. In the literature, negative streamers that develop to breakdown have also been modelled using the Zener theory. However, a higher voltage

is required to initiate a negative streamer. This explains the lack of the use of Zener theory alone in initiating a negative streamer to study the surface discharge behaviour under much lower voltage that creates much lower electric fields. Hence, to model PD events due to a negative streamer might require another theory preceding the field dependent molecular ionisation mechanism (Zener theory).

Appendix A

Model Parameters

Table A.1: General parameter values used in the model

Parameter	Symbol	Value
Permittivity of free space	ε_0	8.854×10^{-12} F·m^{-1}
Elementary charge	q	1.6022×10^{-19} C
Avogadro's number	N_A	6.023×10^{23} mol^{-1}
Planck's constant	h	6.626×10^{-34} J·s

Table A.2: Parameter values specified in the bulk oil region

Parameter	Symbol	Value
Relative permittivity of transformer oil	ε_{oil}	2.2
Positive ion mobility	μ_p	1×10^{-9} $m^2 \cdot s^{-1} \cdot V^{-1}$
Negative ion mobility	μ_n	1×10^{-9} $m^2 \cdot s^{-1} \cdot V^{-1}$
Electron mobility	μ_e	1×10^{-4} $m^2 \cdot s^{-1} \cdot V^{-1}$
Ion-ion recombination coefficient	K_{rpn}	9.908×10^{6} $m^3 \cdot s^{-1} \cdot mol^{-1}$
Ion-electron recombination coefficient	K_{rpe}	9.908×10^{6} $m^3 \cdot s^{-1} \cdot mol^{-1}$
Electron attachment time constant	τ_a	1.55×10^{-7} s
Density of ionisable species	N_0	0.16603 $mol \cdot m^{-3}$
Molecular separation distance	a	3×10^{-10} m
Effective electron mass	m^*	$0.1\times m_e = 9.11\times10^{-32}$ kg
Molecular ionisation energy	Δ	1.14×10^{-18} J (i.e. 7.12 eV)
Specific heat capacity of transformer oil	C_{P_oil}	1870 $J \cdot kg^{-1} \cdot K^{-1}$
Thermal conductivity of transformer oil	k_{T_oil}	0.13 $W \cdot m^{-1} \cdot K^{-1}$
Mass density of transformer oil	ρ_{oil}	880 $kg \cdot m^{-3}$

Table A.3: Parameter values specified in the transition region

Parameter	Symbol	Value
Relative permittivity of transition region	ε_{trans}	3.3
Positive ion mobility	μ_p	1×10^{-9} $m^2 \cdot s^{-1} \cdot V^{-1}$
Negative ion mobility	μ_n	1×10^{-9} $m^2 \cdot s^{-1} \cdot V^{-1}$
Electron mobility	μ_e	1×10^{-4} $m^2 \cdot s^{-1} \cdot V^{-1}$
Ion-ion recombination coefficient	K_{rpn}	6.605×10^{6} $m^3 \cdot s^{-1} \cdot mol^{-1}$
Ion-electron recombination coefficient	K_{rpe}	6.605×10^{6} $m^3 \cdot s^{-1} \cdot mol^{-1}$
Electron attachment time constant	τ_a	1.55×10^{-7} s
Density of ionisable species	N_0	0.16603 $mol \cdot m^{-3}$
Molecular separation distance	a	3×10^{-10} m
Effective electron mass	m^*	$0.1\times m_e = 9.11\times10^{-32}$ kg
Molecular ionisation energy	Δ	1.14×10^{-18} J (i.e. 7.12 eV)
Specific heat capacity of transition region	C_{P_trans}	1753.6 $J \cdot kg^{-1} \cdot K^{-1}$
Thermal conductivity of transition region	k_{T_trans}	0.15 $W \cdot m^{-1} \cdot K^{-1}$
Mass density of transition region	ρ_{trans}	984.88 $kg \cdot m^{-3}$

Table A.4: Parameter values specified in the bulk oil/pressboard region

Parameter	Symbol	Value
Relative permittivity of bulk oil/pressboard region	$\varepsilon_{oil/pb}$	4.2
Specific heat capacity of bulk oil/pressboard region	$C_{P\_oil/pb}$	1476.3 $J \cdot kg^{-1} \cdot K^{-1}$
Thermal conductivity of bulk oil/pressboard region	$k_{T\_oil/pb}$	0.17 $W \cdot m^{-1} \cdot K^{-1}$
Mass density of bulk oil/pressboard region	$\rho_{oil/pb}$	1296.82 $kg \cdot m^{-3}$

Appendix B

Snapshots of Electric Field Distribution

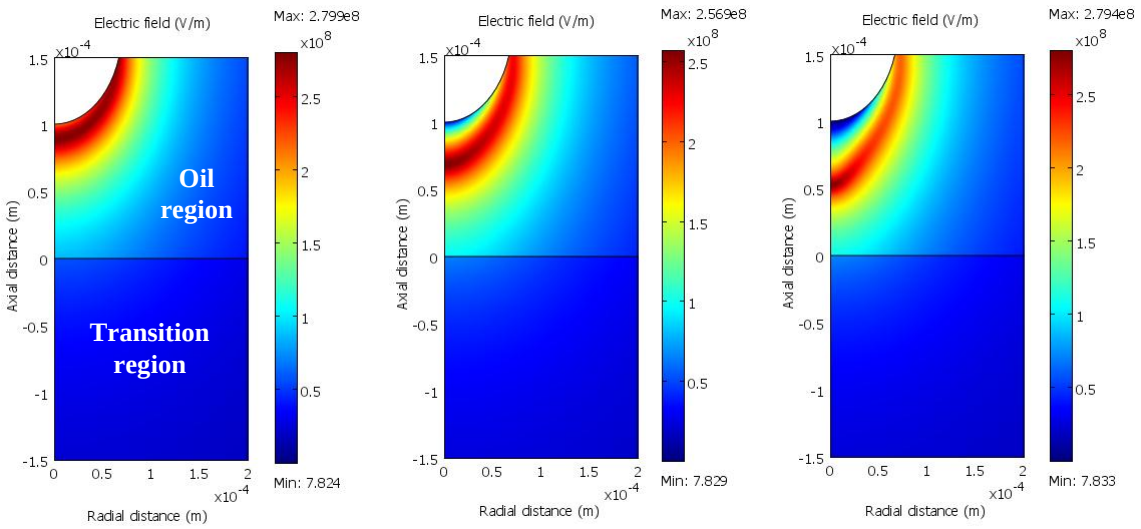

t=0.02 μs t=0.5 μs t=1.0 μs

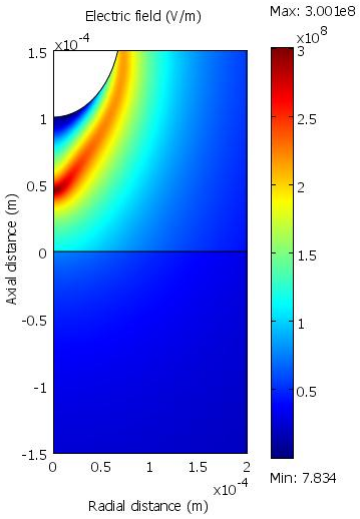

t=1.1 µs

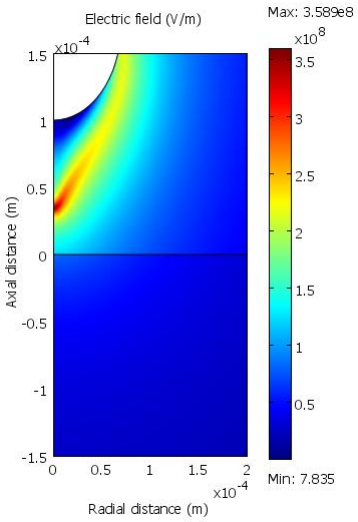

t=1.16 µs

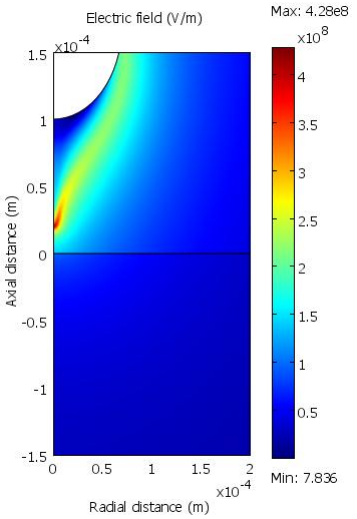

t=1.18 µs

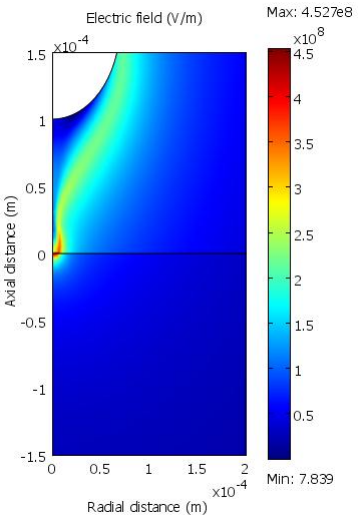

t=1.2 µs

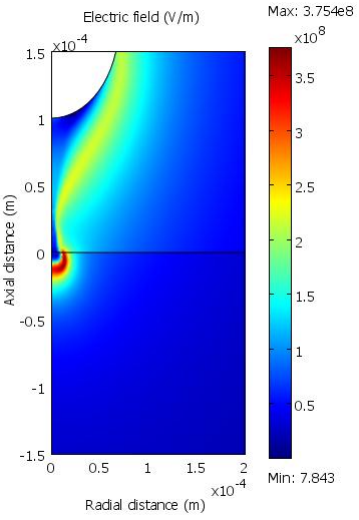

t=1.22 µs

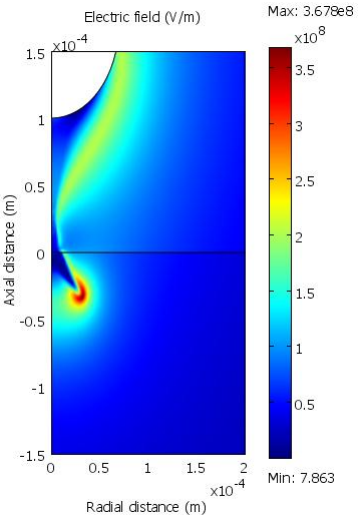

t=1.3 µs

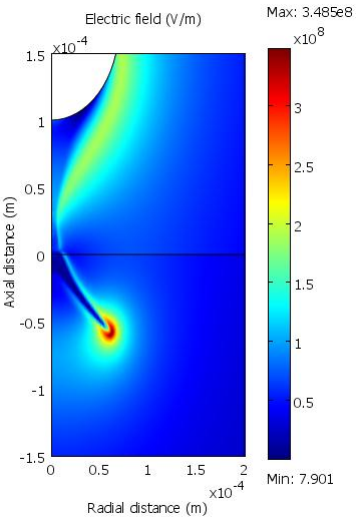

t=1.5 µs

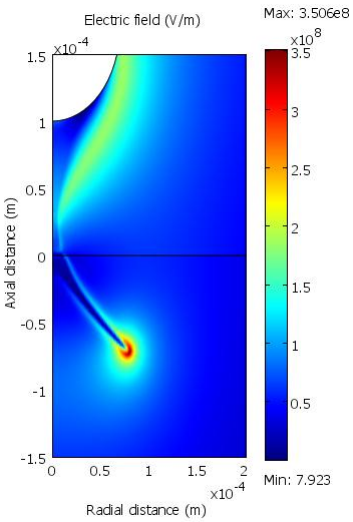

t=1.7 µs

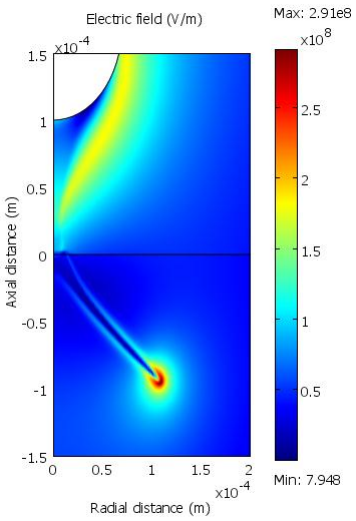

t=3.0 µs

Appendix C

List of Publications

C.1 Refereed Conference Papers

The following papers have been peer reviewed and presented at International Conferences:

1. H. Zainuddin, P.M. Mitchinson and P.L. Lewin, "A method for the measurement of leakage current due to surface discharge at the oil-pressboard interface," in *IEEE 2011 Electrical Insulation Conference*, Annapolis, Maryland, USA, 5-8 June 2011, pp. 41-44.

2. H. Zainuddin, P.M. Mitchinson and P.L. Lewin, "Investigation on the surface discharge phenomenon at the oil-pressboard interface," in *17th IEEE International Conference on Dielectric Liquids*, Trondheim, Norway, 26-30 June 2011.

3. H. Zainuddin, P.L. Lewin and P.M. Mitchinson, "Modeling the inter-phase region of high voltage transformers," in *17th IEEE International Conference on Dielectric Liquids*, Trondheim, Norway, 26-30 June 2011.

4. H. Zainuddin, P.L. Lewin and P.M. Mitchinson, "Characteristics of leakage current during surface disharge at the oil-pressboard interface," in *2012 IEEE Conference on Electrical Insulation and Dielectric Phenomena*, Montreal, Canada, 14-17 October 2012, pp. 483-486.

5. H. Zainuddin, P.L. Lewin and P.M. Mitchinson, "Partial discharge characteristics of surface tracking on oil-impregnated pressboard under AC voltages," in *IEEE 2013 International Conference on Solid Dielectrics*, Bologna, Italy, 30 June - 4 July 2013, pp. 1016-1019.

C.2 Peer Reviewed Journal Papers

The following papers were under production at the point of submission of the thesis:

1. H. Zainuddin, P.L. Lewin and P.M. Mitchinson, "Degradation behaviour during creepage discharge at the oil-pressboard interface under AC voltage," intended for submission to IEEE Transactions on Dielectrics and Electrical Insulation.

2. H. Zainuddin, P.L. Lewin and P.M. Mitchinson, "Towards full discharge events as value added information for condition monitoring of surface discharge at the oil-pressboard interface," intended for submission to IEEE Transactions on Dielectrics and Electrical Insulation.

3 H. Zainuddin and P.L. Lewin, "Numerical modelling of surface discharge at the oil-pressboard interface with experimental validation," intended for submission to IEEE Transactions on Dielectrics and Electrical Insulation.

References

[1] D. J. Allen and A. White, "Transformer design for high reliability," in *Second International Conference on the Reliability of Transmission and Distribution Equipment*, Coventry, UK, 29-31 March 1995, pp. 66-72.

[2] V. Sokolov, Z. Berler, and V. Rashkes, "Effective methods of assessment of insulation system conditions in power transformers: a view based on practical experience," in *Proceedings of the Electrical Insulation Conference and Electrical Manufacturing & Coil Winding Conference*, Cincinnati, Ohio, USA, 1999, pp. 659-667.

[3] V. Sokolov, "Failure statistics. Transformer and bushings design review. Typical failure modes and failure causes. What can be learned from post mortem inspection," in *Fifth AVO New Zealand International Technical Conference*, Methven, New Zealand, 2006.

[4] S. V. Kulkarni and S. A. Khaparde, *Transformer Engineering Design and Practice*, CRC Press, 2004.

[5] R. Mohamed, "Partial discharge signal propagation, modelling and estimation in high voltage transformer windings," PhD thesis, University of Southampton, 2010.

[6] CIGRE Working Group 12.18: Life Management of Transformers, "Guidelines for life management techniques for power transformers," Draft Final Report Rev. 2, 22 June 2002.

[7] C. Bengtsson, "Status and trends in transformer monitoring," *IEEE Transactions on Power Delivery*, vol. 11, pp. 1379-1384, 1996.

[8] J. A. Lapworth and A. Wilson, "Transformer internal over-voltages caused by remote energisation," in *IEEE PES PowerAfrica 2007 Conference and Exposition*, Johannesburg, South Africa, 16-20 July 2007.

[9] P. M. Mitchinson, "Surface tracking in the inter-phase region of large transformers," PhD thesis, University of Southampton, 2008.

[10] H. Gui and Z. De-Yi, "Surface discharge characteristics of impregnated pressboard under AC voltages," in *Proceedings of the 3rd International Conference on Properties and Applications of Dielectric Materials*, Tokyo, Japan, 8-12 July 1991, pp. 313-316.

[11] V. Sokolov, "Understanding failure modes of transformers," in *Proceedings of the Euro TechCon*, 2005, pp. 43-65.

[12] P. M. Mitchinson, P. L. Lewin, G. Chen, and P. N. Jarman, "A new approach to the study of surface discharge on the oil-pressboard interface," in *IEEE International Conference on Dielectric Liquids (ICDL)*, Futuroscope-Chasseneuil, France, 30 June - 3 July 2008.

[13] E. Kuffel, W. S. Zaengl, and J. Kuffel, *High Voltage Engineering: Fundamentals*, 2nd ed., Butterworth-Heinemann, 2000.

[14] D. Linhjell, L. Lundgaard, and G. Berg, "Streamer propagation under impulse voltage in long point-plane oil gaps," *IEEE Transactions on Dielectrics and Electrical Insulation*, vol. 1, pp. 447-458, 1994.

[15] P. M. Mitchinson, P. L. Lewin, B. D. Strawbridge, and P. Jarman, "Tracking and surface discharge at the oil-pressboard interface," *IEEE Electrical Insulation Magazine*, vol. 26, pp. 35-41, March/April 2010.

[16] A. K. Lokhanin, G. Y. Shneider, V. V. Sokolov, and V. M. Chornogotsky, "Internal insulation failure mechanisms of HV equipment under service conditions," in *CIGRE Report 15-201*, 2002.

[17] V. Sokolov, "Transformer condition-based ranking," in *Fifth AVO New Zealand International Technical Conference*, Methven, New Zealand, 2006.

[18] M. J. Heathcote, *J & P Transformer Book*, 12th ed., Butterworth-Heinemann, 1998.

[19] R. Bartnikas (editor), *Engineering Dielectrics, Volume 3: Electrical Insulating Liquids*, American Society for Testing and Materials, 1994.

[20] J. Bidlack, M. Malone, and B. Russel, "Molecular structure and component integration of secondary cell walls in plants," *Proc. Okla. Acad. Sci.*, vol. 72, pp. 51-56, 1992.

[21] M. C. Silva, et al., "Characterization of three non-product materials from a bleached eucalyptus kraft pulp mill, in view of valorising them as a source of cellulose fibres," *Industrial Crops and Products*, vol. 27, pp. 288-295, 2008.

[22] K. Giese, "The effects of cellulose insulation quality on electrical intrinsic strength," *IEEE Electrical Insulation Magazine*, vol. 10, pp. 38-42, September/October 1994.

[23] Y. Suzuki and M. Takagi, "Oil impregnation in transformer boards (2) theoretical analysis of changes in impregnation depth," *IEEE Transactions on Electrical Insulation*, vol. EI-19, pp. 344-349, 1984.

[24] BS EN 60814:1998, IEC 60814:1997, "Insulating liquids. Oil-impregnated paper and pressboard. Determination of water by automatic coulometric Karl Fischer titration"

[25] Y. Du, M. Zahn, B. C. Lesieutre, A. V. Mamishev, and S. R. Lindgren, "Moisture equilibrium in transformer paper-oil systems," *IEEE Electrical Insulation Magazine*, vol. 15, pp. 11-20, January/February 1999.

[26] L. E. Lundgaard, W. Hansen, D. Linhjell, and T. J. Painter, "Aging of oil-impregnated paper in power transformers," *IEEE Transactions on Power Delivery,* vol. 19, pp. 230-239, 2004.

[27] V. G. Arakelian and I. Fofana, "Water in oil-filled high-voltage equipment part I: states, solubility, and equilibrium in insulating materials," *IEEE Electrical Insulation Magazine,* vol. 23, pp. 15-27, July/August 2007.

[28] Y. Du, A. V. Mamishev, B. C. Lesieutre, M. Zahn, and S. H. Kang, "Moisture solubility for differently conditioned transformer oils," *IEEE Transactions on Dielectrics and Electrical Insulation,* vol. 8, pp. 805-811, 2001.

[29] V. V. Sokolov and B. V. Vanin, "Experience with in-field assessment of water contamination of large power transformers," in *Proceedings of EPRI Substation Equipment Diagnostic Conference VII,* New Orleans, LA, USA, 1999.

[30] A. M. Emsley and G. C. Stevens, "Review of chemical indicators of degradation of cellulosic electrical paper insulation in oil-filled transformers," *IEE Proceedings - Science, Measurement and Technology,* vol. 141, pp. 324-334, 1994.

[31] P. M. Mitchinson, I. L. Hosier, P. L. Lewin, A. S. Vaughan, G. C. Chen, and P. Jarman, "An experiment to evaluate the benefits of processing aged transformer oil," in *Conference Record of the 2006 IEEE International Symposium on Electrical Insulation,* Toronto, Canada, 11-14 June 2006, pp. 89-92.

[32] J. Bouchard, M. Methot, and B. Jordan, "The effects of ionizing radiation on the cellulose of woodfree paper," *Cellulose,* vol. 13, pp. 601-610, 2006.

[33] H. Z. Ding and Z. D. Wang, "On the degradation evolution equations of cellulose," *Cellulose,* vol. 15, pp. 205-224, 2008.

[34] A. J. Kachler and I. Hohlein, "Aging of cellulose at transformer service temperatures. Part 1: Influence of type of oil and air on the degree of polymerization of pressboard, dissolved gases, and furanic compounds in oil," *IEEE Electrical Insulation Magazine,* vol. 21, pp. 15-21, March/April 2005.

[35] I. Hohlein and A. J. Kachler, "Aging of cellulose at transformer service temperatures. Part 2: Influence of moisture and temperature on degree of polymerization and formation of furanic compounds in free-breathing systems," *IEEE Electrical Insulation Magazine,* vol. 21, pp. 20-24, September/October 2005.

[36] F. Shafizadeh and Y. L. Fu, "Pyrolysis of cellulose," *Carbohydrate Research,* vol. 29, pp. 113-122, 1973.

[37] J. Dai, Z. D. Wang, and P. Jarman, "Creepage discharge on insulation barriers in aged power transformers," *IEEE Transactions on Dielectrics and Electrical Insulation,* vol. 17, pp. 1327-1335, 2010.

[38] W. Wang, B. Bao, J. Xu, and C. Li, "Creepage discharge performance for high moisture pressboard," in *2011 Annual Report Conference on Electrical Inslation*

and Dielectric Phenomena (CEIDP), Cancun, Mexico, 16-19 October 2011, pp. 480-483.

[39] D. W. Crofts, "The static electrification phenomena in power transformers," *IEEE Transactions on Electrical Insulation*, vol. 23, pp. 137-146, 1988.

[40] L. Peyraque, A. Beroual, and F. Buret, "Static electrification of pressboard/oil interface and transient phenomena," *IEEE Transactions on Dielectrics and Electrical Insulation*, vol. 5, pp. 443-449, 1998.

[41] T. V. Oommen, "Static electrification properties of transformer oil," *IEEE Transactions on Electrical Insulation*, vol. 23, pp. 123-128, 1988.

[42] P. K. Poovamma, R. Jagadish, and K. Dwarakanath, "Investigation on static electrification characteristics of transformer oil," *Journal of Electrostatics*, vol. 33, pp. 1-14, 1994.

[43] J. Zhang and L. J. Cao, "The study on flow electrification of oil-cellulose insulating system in large power transformer," in *Proceedings of 1995 International Conference on Energy Management and Power Delivery*, 21-23 November 1995, pp. 416-421.

[44] G. Touchard, P. O. Grimaud, H. Romat, and O. Moreau, "Flow electrification in power transformers. Explanation of the wall-current measurements," *IEEE Transactions on Dielectrics and Electrical Insulation*, vol. 1, pp. 728-733, 1994.

[45] V. V. Sokolov and B. V. Vanin, "Evaluation of power transformer insulation through measurement of dielectric characteristics," in *Proceedings of the 63rd Annual International Conference of Doble Clients*, 1996.

[46] X. Wang and Z. D. Wang, "Particle effect on breakdown voltage of mineral and ester based transformer oils," in *2008 Annual Report Conference on Electrical Insulation and Dielectric Phenomena*, Quebec, Canada, 26-29 October 2008, pp. 598-602.

[47] T. V. Oommen, C. C. Claiborne, and J. T. Mullen, "Biodegradable electrical insulation fluids," in *Proceedings of the Electrical Insulation Conference and Electrical Manufacturing & Coil Winding Conference*, Rosemont, USA, 22-25 September 1997, pp. 465-468.

[48] S. J. Fitton, "Surface discharges within oil insulated apparatus," in *IEE Colloquium on An Engineering Review of Liquid Insulation*, London, UK, 7 January 1997, pp. 6/1-6/2.

[49] L. Kebbabi and A. Beroual, "Influence of the properties of materials and the hydrostatic pressure on creepage discharge characteristics over solid/liquid interfaces," in *2003 Annual Report Conference on Electrical Insulation and Dielectric Phenomena*, 19-23 October 2003, pp. 293-296.

[50] L. Kebbabi and A. Beroual, "Optical and electrical characterization of creeping discharges over solid/liquid interfaces under lightning impulse voltage," *IEEE Transactions on Dielectrics and Electrical Insulation*, vol. 13, pp. 565-571, 2006.

[51] R. J. Taylor, "Effect of permittivity matching on the flashover of solid/liquid interfaces," *Proceedings of the IEE,* vol. 124, pp. 899-904, 1977.

[52] M. U. Anker, "Effect of test geometry, permittivity matching and metal particles on the flashover voltage of oil/solid interfaces," *IEEE Transactions on Power Apparatus and Systems,* vol. PAS-102, pp. 3796-3802, 1983.

[53] O. Lesaint and G. Massala, "Transition to fast streamers in mineral oil in the presence of insulating solids," in *Conference Record of the 1996 IEEE International Symposium on Electrical Insulation,* Montreal, Canada, 16-19 June 1996, pp. 737-740.

[54] G. Massala and O. Lesaint, "Positive streamer propagation in large oil gaps: electrical properties of streamers," *IEEE Transactions on Dielectrics and Electrical Insulation,* vol. 5, pp. 371-381, 1998.

[55] L. Lundgaard, D. Linhjell, G. Berg, and S. Sigmond, "Propagation of positive and negative streamers in oil with and without pressboard interfaces," *IEEE Transactions on Dielectrics and Electrical Insulation,* vol. 5, pp. 388-395, 1998.

[56] R. Liu, A. Jaksts, and T. Bengtsson, "Streamer propagation in composite oil/cellulose insulation under LI voltages," in *Conference Record of the 2000 IEEE International Symposium on Electrical Insulation,* Anaheim, CA, USA, 2000, pp. 426-430.

[57] Y. Nakao, H. Itoh, Y. Sakai, and H. Tagashira, "Studies of impulse creepage discharge in transformer oil," *IEEE Transactions on Electrical Insulation,* vol. 26, pp. 732-738, 1991.

[58] P. Atten and A. Saker, "Streamer propagation over a liquid/solid interface," *IEEE Transactions on Electrical Insulation,* vol. 28, pp. 230-242, 1993.

[59] J.-W. G. Hwang, "Elucidating the mechanism behind pre-breakdown phenomena in transformer oil systems," PhD thesis, Massachusetts Institute of Technology, 2010.

[60] IEEE C57.113-1991, "IEEE guide for partial discharge measurement in liquid-filled power transformers and shunt reactors"

[61] CIGRE Working Group D1.33: High Voltage Testing and Measuring Techniques, "Guide for partial discharge measurements in compliance to IEC 60270," 2008.

[62] J. Dai, Z. D. Wang, and P. Jarman, "Moisture and ageing effect on the creepage discharge characteristics at the oil/transformer-board interface under divergent field," in *2008 Annual Report Conference on Electrical Insulation and Dielectric Phenomena,* Quebec, Canada, 26-29 October 2008, pp. 662-665.

[63] C. Vincent, N. G. Trinh, R. Olivier, and J. Aubin, "Behavior of an oil-paper interface in presence of carbon particle contamination," in *Conference Record of the 1994 IEEE International Symposium on Electrical Insulation,* Pittsburgh, PA, USA, 5-8 June 1994, pp. 534-537.

[64] R. Liu and A. Jaksts, "Breakdown processes in transformer insulation under LI voltages," in *IEEE International Conference on Dielectric Liquids (ICDL)*, 26 June - 1 July 2005, pp. 75-78.

[65] C. Tang, G. Chen, M. Fu, and R. Liao, "Space charge behaviour in multi-layer oil-paper insulation under different DC voltages and temperatures," *IEEE Transactions on Dielectrics and Electrical Insulation*, vol. 17, pp. 775-784, 2010.

[66] R. E. Hebner, *Measurements of electrical breakdown in liquids*, Plenum Press, New York, pp. 519-537, 1988.

[67] O. Lesaint and G. Massala, "Positive streamer propagation in large oil gaps: Experimental characterization of propagation modes," *IEEE Transactions on Dielectrics and Electrical Insulation*, vol. 5, pp. 360-370, 1998.

[68] BS EN 60112:2003, "Methods for the determination of the proof and the comparative tracking indices of solid insulating materials"

[69] BS EN 60270:2001, IEC 60270:2001, "High-voltage test techniques - Partial discharge measurements"

[70] A. W. Adamson, *Physical Chemistry of Surfaces*, 4th ed., John Wiley & Sons, Inc., 1982.

[71] P. H. Rieger, *Electrochemistry*, Prentice-Hall International, Inc., 1987.

[72] O. Moreau, G. Artana, H. Romat, and G. Touchard, "A contribution to modelling and experimental studies of flow electrification in transformers," in *Conference Record of the ICDL'96, 12th International Conference on Conduction and Breakdown in Dielectric Liquids*, Roma, Italy, 15-19 July 1996, pp. 405-410.

[73] O. Moreau, P. Plion, and G. Touchard, "Modelling of flow electrification in a 3D computational fluid dynamics software: Application to power transformers," in *1995 Annual Report Conference on Electrical Insulation and Dielectric Phenomena*, Virginia Beach, VA, USA, 22-25 October 1995, pp. 424-427.

[74] J. M. Cabaleiro, T. Paillat, O. Moreau, and G. Touchard, "Modelling of static development and dynamic behaviour of the electrical double layer at oil-pressboard interface," in *2009 Electrostatics Joint Conference*, Boston, USA, 16-18 June 2009.

[75] F. M. O'Sullivan, "A model for the initiation and propagation of electrical streamers in transformer oil and transformer oil based nanofluids," PhD thesis, Massachusetts Institute of Technology, 2007.

[76] F. O'Sullivan, J. G. Hwang, M. Zahn, O. Hjortstam, L. Pettersson, and B. Peter, "A model for the initiation and propagation of positive streamers in transformer oil," in *Conference Record of the 2008 IEEE International Symposium on Electrical Insulation (ISEI 2008)*, Vancouver, Canada, 9-12 June 2008, pp. 210-214.

[77] J. Jadidian, J. G. Hwang, M. Zahn, N. Lavesson, O. Widlund, and K. Borg, "Streamer initiation and propagation in transformer oil under positive and negative impulse voltages," in *IEEE Pulsed Power Conference*, Chicago, USA, 19-23 June 2011, pp. 251-256.

[78] J. G. Hwang, M. Zahn, and L. A. A. Pettersson, "Mechanisms behind positive streamers and their distinct propagation modes in tansformer oil," *IEEE Transactions on Dielectrics and Electrical Insulation*, vol. 19, pp. 162-174, 2012.

[79] J. Jadidian, M. Zahn, N. Lavesson, O. Widlund, and K. Borg, "Effects of impulse voltage polarity, peak amplitude and rise time on streamers initiated from a needle electrode in transformer oil," *IEEE Transactions on Plasma Science*, vol. 40, pp. 909-918, 2012.

[80] J. Jadidian, M. Zahn, N. Lavesson, O. Widlund, and K. Borg, "Surface flashover breakdown mechanisms on liquid immersed dielectrics," *Applied Physics Letters*, vol. 100, 2012.

[81] U. Gafvert, A. Jaksts, C. Tornkvist, and L. Walfridsson, "Electrical field distribution in transformer oil," *IEEE Transactions on Electrical Insulation*, vol. 27, pp. 647-660, 1992.

[82] U. Gafvert, O. Hjortstam, Y. Serdyuk, C. Tornkvist, and L. Walfridsson, "Modeling and measurements of electric fields in composite oil/cellulose insulation," in *2006 Annual Report Conference on Electrical Insulation and Dielectric Phenomena*, Kansas City, USA, 15-18 October 2006, pp. 154-157.

[83] L. Onsager, "Deviation from Ohm's law in a weak electrolytes," *The Journal of Chemical Physics*, vol. 2, pp. 599-615, 1934.

[84] F. O'Sullivan, et al., "Modeling the effect of ionic dissociation on charge transport in transformer oil," in *2006 Annual Report Conference on Electrical Insulation and Dielectric Phenomena*, Kansas City, USA, 15-18 October 2006, pp. 756-759.

[85] E. O. Forster, "Partial discharge and streamers in liquid dielectrics. The significance of the inception voltage," *IEEE Transactions on Electrical Insulation*, vol. 28, pp. 941-946, 1993.

[86] C. Zener, "A theory of the electrical breakdown of solid dielectrics," *Proceedings of the Royal Society of London. Series A*, vol. 145, pp. 523-529, 1934.

[87] J. C. Devins, S. J. Rzad, and R. J. Schwabe, "Breakdown and prebreakdown phenomena in liquids," *Journal of Applied Physics*, vol. 52, pp. 4531-4545, 1981.

[88] W. F. Schmidt, *Liquid State Electronics of Insulating Liquids*, CRC Press, 1997.

[89] W. F. Schmidt, "Electron mobility in nonpolar liquids: the effect of molecular structure, temperature, and electric field " *Canadian Journal of Chemistry*, vol. 55, pp. 2197-2210, 1977.

[90] J. Qian, R. P. Joshi, E. Schamiloglu, J. Gaudet, J. R. Woodworth, and J. Lehr, "Analysis of polarity effects in the electrical breakdown of liquids," *Journal of Physics D: Applied Physics,* vol. 39, pp. 359-369, 2006.

[91] H. Z. Ding, Z. D. Wang, and P. Jarman, "On electrical stresses at wedge-shaped oil gaps in power transformers with application to surface discharge and breakdown," in *IEEE International Conference on Dielectric Liquids (ICDL)*, Futuroscope-Chasseneuil, France, 30 June - 3 July 2008.

[92] A. P. Washabaugh and M. Zahn, "A chemical reaction-based boundary condition flow electrification," *IEEE Transactions on Dielectrics and Electrical Insulation,* vol. 4, pp. 688-709, 1997.

[93] C. Ekanayake, S. M. Gubanski, A. Graczkowski, and K. Walczak, "Frequency response of oil impregnated pressboard and paper samples for estimating moisture in transformer insulation," *IEEE Transactions on Power Delivery,* vol. 21, pp. 1309-1317, 2006.

[94] T. N. Tran, "Surface discharge dynamics: theory, experiment and simulation," PhD thesis, University of Southampton, 2010.

[95] T. N. Tran, I. O. Golosnoy, P. L. Lewin, and G. E. Georghiou, "Numerical modelling of negative discharges in air with experimental validation," *Journal of Physics D: Applied Physics,* vol. 44, pp. 1-15, 2011.

[96] S. Kumara, Y. V. Serdyuk, and S. M. Gubanski, "Charging of polymeric surfaces by positive impulse corona," *IEEE Transactions on Dielectrics and Electrical Insulation,* vol. 16, pp. 726-733, 2009.

[97] *Omicron Mtronix MPD 600*. Available: http://www.omicron.at/en/

[98] BS EN 60641-2:2004, "Pressboard and presspaper for electrical purposes - Part 2: Methods of tests"

[99] P. Rain and O. Lesaint, "Prebreakdown phenomena in mineral oil under step and ac voltage in large-gap divergent fields," *IEEE Transactions on Dielectrics and Electrical Insulation,* vol. 1, pp. 692-701, 1994.

[100] O. Lesaint, A. Saker, P. Gournay, R. Tobazeon, J. Aubin, and M. Mailhot, "Streamer propagation and breakdown under ac voltage in very large oil gaps," *IEEE Transactions on Dielectrics and Electrical Insulation,* vol. 5, pp. 351-359, 1998.

[101] K. Temmen, "Evaluation of surface changes in flat cavities due to ageing by means of phase-angle resolved partial discharge measurement," *Journal of Physics D: Applied Physics,* vol. 33, pp. 603-608, 2000.

[102] *Tektronix Digital Phosphor Oscilloscopes*. Available: http://www2.tek.com/cmswpt/psdetails.lotr?ct=PS&cs=psu&ci=18210&lc=EN

[103] I. M. Culbert, H. Dhirani, and B. K. Gupta, "On-line measurement of partial discharges on large motors in a generating station," in *Proceedings of the*

Electrical Insulation Conference and Electrical Manufacturing & Coil Winding Conference, Cincinnati, USA, 2001, pp. 537-540.

[104] Y. Tian, P. L. Lewin, A. E. Davies, S. G. Swingler, S. J. Sutton, and G. M. Hathaway, "Comparison of on-line partial discharge detection methods for HV cable joints," *IEEE Transactions on Dielectrics and Electrical Insulation,* vol. 9, pp. 604-615, 2002.

[105] L. Hao and P. L. Lewin, "Partial discharge source discrimination using a support vector machine," *IEEE Transactions on Dielectrics and Electrical Insulation,* vol. 17, pp. 189-197, 2010.

[106] P. Rain, C. Boisdon, O. Lesaint, and R. Tobazeon, "Behavior of streamers under divergent ac fields in transformer oils at large gaps," *IEEE Transactions on Dielectrics and Electrical Insulation,* vol. 26, pp. 715-725, 1991.

[107] M. A. M. Piah, A. Darus, and A. Hassan, "Electrical tracking performance of LLDPE-natural rubber blends by employing combination of leakage current level and rate of carbon track propagation," *IEEE Transactions on Dielectrics and Electrical Insulation,* vol. 12, pp. 1259-1265, 2005.

[108] S. Kumagai, X. Wang, and N. Yoshimura, "Solid residue formation of RTV silicone rubber due to dry-band arcing and thermal decomposition," *IEEE Transactions on Dielectrics and Electrical Insulation,* vol. 5, pp. 281-289, 1998.

[109] L. H. Meyer, S. H. Jayaram, and E. A. Cherney, "Correlation of damage, dry band arcing energy and temperature in inclined plane testing of silicone rubber for outdoor insulation," *IEEE Transactions on Dielectrics and Electrical Insulation,* vol. 11, pp. 424-432, 2004.

[110] B. Shi, G. Karady, Q. Huang, and M. Tuominen, "Experimental studies of the characteristics of dry band arcing on ADSS fiber optic cables," *IEEE Transactions on Power Delivery,* vol. 19, pp. 1936-1940, 2004.

[111] M. A. R. M. Fernando and S. M. Gubanski, "Leakage current patterns on contaminated polymeric surfaces," *IEEE Transactions on Dielectrics and Electrical Insulation,* vol. 6, pp. 688-694, 1999.

[112] T. Suda, "Frequency characteristics of leakage current waveforms of an artificially polluted suspension insulator," *IEEE Transactions on Dielectrics and Electrical Insulation,* vol. 8, pp. 705-709, 2001.

[113] K. L. Chrzan and F. Moro, "Concentrated discharges and dry bands on polluted outdoor insulation," *IEEE Transactions on Power Delivery,* vol. 22, pp. 466-471, 2007.

[114] Waluyo, P. M. Pakpahan, and Suwarno, "Study on the electrical equivalent circuit models of polluted outdoor insulators," in *8th International Conference on Properties and Application of Dielectric Materials*, June 2006, pp. 546-549.

[115] M. A. R. M. Fernando, J. Lambrecht, and S. Gubanski, "Modelling non-linear leakage currents on artificially polluted polymeric surfaces," in *1998 Annual*

Report Conference on Electrical Insulation and Dielectric Phenomena, Atlanta, USA, 25-28 October 1998, pp. 52-55.

[116] M. A. M. Piah, A. Darus, and A. Hassan, "Leakage current and surface discharge phenomena: Effect on tracking and morphological properties of LLDPE-natural rubber compounds," in *Proceedings of the 7th International Conference on Properties and Applications of Dielectric Materials*, Nagoya, Japan, 1-5 June 2003, pp. 347-350.

[117] M. A. M. Piah, "Leakage current and surface tracking characterization of new natural rubber-based material for high voltage insulation," PhD thesis, Universiti Teknologi Malaysia, 2004.

[118] S. M. Gubanski and A. E. Vlastos, "Wettability of naturally aged silicone and EPDM composite insulators," *IEEE Transactions on Power Delivery,* vol. 5, pp. 1527-1535, 1990.

[119] S. H. Kim, E. A. Cherney, and R. Hackam, "The loss and recovery of hydrophobicity of RTV silicone rubber insulator coatings," *IEEE Transactions on Power Delivery,* vol. 5, pp. 1491-1500, 1990.

[120] R. S. Gorur, J. W. Chang, and O. G. Amburgey, "Surface hydrophobicity of polymers used for outdoor insulation," *IEEE Transactions on Power Delivery,* vol. 5, pp. 1923-1933, 1990.

[121] COMSOL AB., *COMSOL Multiphysics Modeling Guide*, 2008.

[122] R. T. Rushall, "Dielectric properties of oil-soaked pressboard as affected by water," *Proceedings of the IEE - Part IIA: Insulating Materials,* vol. 100, pp. 81-88, 1953.

[123] D. J. Swaffield, P. L. Lewin, G. Chen, and S. G. Swingler, "Partial discharge characterization of streamers in liquid nitrogen under applied AC voltages," *IEEE Transactions on Dielectrics and Electrical Insulation,* vol. 15, pp. 635-646, 2008.

[124] M. Pribyl and K. Adamiak, "Numerical models for AC electro-osmotic micropumps," in *2008 IEEE Industry Applications Annual Meeting (IAS '08)*, Edmonton, Alta, Canada, 5-9 October 2008, pp. 1-8.

[125] S. Sakamoto and H. Yamada, "Optical study of conduction and breakdown in dielectric liquids," *IEEE Transactions on Electrical Insulation,* vol. EI-15, pp. 171-181, 1980.

[126] W. G. Chadband, "On variations in the propagation of positive discharges between transformer oil and silicone fluids," *Journal of Physics D: Applied Physics*, vol. 13, pp. 1299-1307, 1980.

[127] W. G. Chadband, "The ubiquitous positive streamer," *IEEE Transactions on Electrical Insulation,* vol. 23, pp. 697-706, 1988.

[128] "Discussion on 'The electrolytic analogue in the design of high voltage power transformers'," *Proceedings of the IEE - Part A: Power Engineering,* vol. 102, pp. 89-93, 1955.

[129] C. Exley and J. D. Birchall, "Hydroxyaluminosilicate formation in solutions of low total aluminum concentration," *Polyhedron,* vol. 11, pp. 1901-1907, 1992.

[130] T. K. Saha and P. Purkait, "Understanding the impacts of moisture and thermal ageing on transformer's insulation by dielectric response and molecular weight measurements," *IEEE Transactions on Dielectrics and Electrical Insulation,* vol. 15, pp. 568-582, 2008.

[131] P. L. Lewin, T. N. Tran, D. J. Swaffield, and J. K. Hallstrom, "Zero-phase filtering for lightning impulse evaluation: A K-factor filter for the revision of IEC60060-1 and -2," *IEEE Transactions on Power Delivery,* vol. 23, pp. 3-12, 2008.

[132] P. Gournay and O. Lesaint, "A study of the inception of positive streamers in cyclohexane and pentane," *Journal of Physics D: Applied Physics,* vol. 26, pp. 1966-1974, 1993.

[133] L. Costeanu and O. Lesaint, "On mechanisms involved in the propagation of subsonic positive streamers in cyclohexane," in *Proceedings of IEEE 14th International Conference on Dielectric Liquids (ICDL 2002),* 7-12 July 2002, pp. 143-146.

[134] D. F. Arseneau, "Competitive reactions in the thermal decomposition of cellulose," *Canadian Journal of Chemistry,* vol. 49, pp. 632-638, 1971.